

# **NASA Contractor Report 178256**

## **Validation of SAM II and SAGE Satellite Data**

(NASA-CR-178256) VALIDATION OF SAM 2 AND  
SAGE SATELLITE Final Report (Institute for  
Atmospheric Optics and Remote) 146 p

CSCL U+A

N87-21429

G3/46 Unclas 43591

**G.S. Kent, P.-H. Wang, U.O. Farrukh, and G.K. Yue**

**Institute for Atmospheric Optics and Remote Sensing**

**101 Research Drive, Hampton, Virginia 23666-1340**

**Contract NAS1-17032**

**April 1987**



National Aeronautics and  
Space Administration

**Langley Research Center**  
Hampton, Virginia 23665-5225

## **FOREWORD**

The Science and Technology Corporation (STC) is pleased to submit the final report on NASA Contract NASI-17032. We are also pleased to acknowledge the assistance of M. P. McCormick, L. R. McMaster, and W. P. Chu of NASA, Langley Research Center, who provided many useful discussions on the various aspects of this work.

## TABLE OF CONTENTS

FOREWORD . . . . .	i
LIST OF FIGURES . . . . .	vii
LIST OF TABLES . . . . .	xi
1. INTRODUCTION . . . . .	1
1.1 Background . . . . .	1
1.2 SAM II and SAGE I Satellite Measurements . . . . .	1
1.3 Tasks and Organization of Report . . . . .	5
2. TASK 1--INVESTIGATE THE GLOBAL CLIMATOLOGY OF TROPOSPHERIC AND STRATOSPHERIC AEROSOLS, AND STRATOSPHERIC O <sub>3</sub> AND NO <sub>2</sub> INCLUDING SPATIAL AND TEMPORAL VARIABILITY . . . . .	7
2.1 Production of Zonal Mean Plots and Tables for SAGE I Data (SAGE I, Reference Publication ) . . . . .	7
2.2 Production of SAGE I Aerosol Optical Depth Maps and Zonal Mean Extinction Plots (includes work carried out under Task Area 8) . . . . .	7
2.3 Ozone Climatology . . . . .	18
2.4 Identification of Calibration Orbits . . . . .	27
2.5 Production of a 16 mm Movie Film of SAM II Data . . . . .	29
2.6 Comparison of SAGE I and SAM II Data . . . . .	33
2.7 Polar Stratospheric Cloud Studies . . . . .	35
2.8 Study of Aerosol Concentrations Near the North Polar Vortex (includes work carried out under Task Area 7) . . . . .	36
2.9 Tropospheric Aerosol Climatology . . . . .	37
2.10 The Aging Process of Aerosol Particles in the Stratosphere . . . . .	43
3. TASK 2--TO INVESTIGATE THE CORRELATION OF STRATOSPHERIC AEROSOLS, O <sub>3</sub> AND NO <sub>2</sub> , WITH EACH OTHER AND VARIOUS METEOROLOGICAL PARAMETERS . . . . .	47
3.1 Correlation Between Aerosol Optical Properties and 30 mb Pressure Height (includes work carried out under Task Area 7) . . . . .	45
3.1.1 Introduction . . . . .	45
3.1.2 Approach . . . . .	46
3.1.3 Results and discussion . . . . .	46
3.1.4 Remarks . . . . .	55

**PRECEDING PAGE BLANK NOT FILMED**

4. TASK 3--TO INVESTIGATE THE INJECTION OF VOLCANIC MATERIAL INTO THE STRATOSPHERE, INCLUDING GLOBAL LOADING AND TRANSPORT (includes work carried out under Task Area 8) . . . . .	65
4.1 Volcanic Loading and Transport . . . . .	65
5. TASK 4--TO INVESTIGATE STRATOSPHERIC PLANETARY WAVES AND THEIR EFFECT ON TRANSPORT OF AEROSOLS, O <sub>3</sub> AND NO <sub>2</sub> . . . . .	65
5.1 Aerosol Extinction and Temperature Changes Associated with Planetary Waves . . . . .	67
5.2 Variations of Aerosol, O <sub>3</sub> and NO <sub>2</sub> Concentrations During Stratospheric Warmings . . . . .	67
5.3 Ozone and Temperature Changes and Associated Fluxes During the Mid-February 1981 Stratospheric Warming . . . . .	68
5.3.1 Introduction . . . . .	68
5.3.2 Data and approach . . . . .	70
5.3.3 Results and discussion . . . . .	72
5.3.3.1 Synoptical meteorology of the high latitude stratosphere for the middle February 1981 warming . . . . .	74
5.3.3.2 Evolution of the planetary waves . . . . .	79
5.3.3.3 Horizontal ozone and temperature transports by planetary waves . . . . .	86
5.3.3.4 Phase relationships between the eddy fields . . . . .	92
5.3.4 Summary . . . . .	95
6. TASK 5--TO INVESTIGATE THE FORMATION AND EVOLUTION OF AEROSOLS INCLUDING THE STUDY OF PHYSICAL AND CHEMICAL PROCESSES . . . . .	101
6.1 Post-Volcanic Decay Rates . . . . .	101
6.1.1 Introduction . . . . .	101
6.1.2 Derivation of empirical function and fitting to theoretical curves . . . . .	102
6.1.3 Fitting to experimental data . . . . .	104
6.1.4 Comparison with other observations and conclusions . .	111
7. TASK 6--TO INVESTIGATE THE DETERMINATION OF STRATOSPHERIC MOLECULAR AND AEROSOL OPTICAL PROPERTIES USING MULTIWAVELENGTH EXTINCTION AND BACKSCATTER DATA AND TECHNIQUES . . . . .	115
7.1 Retrieval of Aerosol Properties from Aerosol Extinction Ratios at 0.45 um and 1.0 um . . . . .	115
7.2 Multiwavelength Aerosol Extinction Models . . . . .	116
7.3 High-Altitude Lidar Modeling . . . . .	118
SECTION 8. CONCLUSIONS . . . . .	123

SECTION 9. REFERENCES . . . . .	125
APPENDIX A - A COMPARATIVE STUDY OF AEROSOL EXTINCTION MEASUREMENTS MADE BY THE SAM II AND SAGE SATELLITE EXPERIMENTS . . . . .	A-1
APPENDIX B - POLAR STRATOSPHERIC CLOUD SIGHTINGS BY SAM II: 1978-1982 . . . . .	A-3
APPENDIX C - CHARACTERISTICS OF POLAR STRATOSPHERIC CLOUDS AS OBSERVED BY SAM II, SAGE, AND LIDAR . . . . .	A-5
APPENDIX D - SPATIAL CHANGES IN THE STRATOSPHERIC AEROSOL ASSOCIATED WITH THE NORTH POLAR VORTEX . . . . .	A-7
APPENDIX E - VARIATION IN THE STRATOSPHERIC AEROSOL ASSOCIATED WITH THE NORTH CYCLONIC POLAR VORTEX AS MEASURED BY THE SAM II SATELLITE SENSOR . . . . .	A-9
APPENDIX F - LATITUDINAL AND ALTITUDINAL VARIATION OF SIZE DISTRIBUTION OF STRATOSPHERIC AEROSOLS INFERRED FROM SAGE AEROSOL EXTINCTION COEFFICIENT MEASUREMENTS AT TWO WAVELENGTHS . . . . .	A-11
APPENDIX G - SAGE AND SAM II MEASUREMENTS OF GLOBAL STRATOSPHERIC AEROSOL OPTICAL DEPTH AND MASS LOADING . . . . .	A-13
APPENDIX H - BEHAVIOR OF ZONAL MEAN AEROSOL EXTINCTION RATIO AND ITS RELATIONSHIP WITH ZONAL MEAN TEMPERATURE DURING THE WINTER 1978-1979 STRATOSPHERIC WARMING . .	A-15
APPENDIX I - VARIATIONS IN STRATOSPHERIC AEROSOL OPTICAL DEPTH DURING NORTHERN WARMINGS . . . . .	A-17
APPENDIX J - RETRIEVAL OF STRATOSPHERIC AEROSOL SIZE DISTRIBUTION FROM ATMOSPHERIC EXTINCTION OF SOLAR RADIATION AT TWO WAVELENGTHS . . . . .	A-19

## LIST OF FIGURES

<b>Figure 2.1(a)</b>	SAGE map of the stratospheric optical depth, July 2 to August 10, 1981. . . . .	9
<b>Figure 2.1(b)</b>	SAGE measurements of zonal mean extinction July 2 to August 10, 1981. . . . .	9
<b>Figure 2.2</b>	Positions of SAGE observations between May 11, 1980 and June 23, 1980 . . . . .	12
<b>Figure 2.3</b>	Optical depth values (from 2 km above the tropopause) for the observation points shown in Figure 2.2. . . . .	13
<b>Figure 2.4</b>	Contour plot of interpolated optical depth values . . . . .	14
<b>Figure 2.5</b>	Seasonal meridional ozone mixing ratio (ppmv) distributions. . . . .	23
<b>Figure 2.6</b>	Seasonal meridional ozone mixing ratio-- percentage standard deviation from mean. . . . .	24
<b>Figure 2.7</b>	Comparison of seasonal latitudinal distributions of total ozone . . . . .	26
<b>Figure 2.8</b>	Seasonal variation of total ozone. . . . .	28
<b>Figure 2.9</b>	Contour plot of SAM II extinction data used in the generation of 16 mm film. . . . .	34
<b>Figure 2.10</b>	Histogram showing frequency of occurrence of different values of aerosol/molecular extinction ratio . . . . .	39
<b>Figure 2.11</b>	Shaded contour plots of SAM II aerosol/molecular extinction ratios for October 1979 - September 1981. . .	42
	(a) Southern hemisphere. . . . .	42
	(b) Northern hemisphere. . . . .	42
<b>Figure 3.1</b>	Linear correlation between SAM II aerosol optical depth (above 20 km) and associated 30 mb height for data from January to March 1979. . . . .	47
<b>Figure 3.2</b>	Projection plots of SAM II aerosol optical depth (a) and associated 30 mb height (b) as functions of longitude and time from January 24 to March 1979 . . . . .	51
<b>Figure 3.3</b>	Linear correlation between SAM II aerosol optical depth (above 20 km) and associated 30 mb height from January to March 1980. . . . .	52

LIST OF FIGURES (Cont'd)

<b>Figure 3.4</b>	Linear correlation between SAM II aerosol optical depth (above 20 km) and associated 30 mb height from January to March 1981. . . . .	53
<b>Figure 3.5</b>	Linear correlation between SAM II aerosol optical depth (above 20 km) and associated 30 mb height from January to March 1982. . . . .	54
<b>Figure 3.6</b>	Linear correlation between SAM II aerosol optical depth (above 20 km) and associated 30 mb height for 1980	
	(a) January. . . . .	57
	(b) February . . . . .	58
	(c) March. . . . .	59
<b>Figure 3.7</b>	Linear correlation between SAM II aerosol optical depth (above 20 km) and associated 30 mb height for 1980. Composite diagram. . . . .	61
<b>Figure 3.8</b>	SAM II aerosol extinction data at 30 mb for January to March 1980. . . . .	62
<b>Figure 5.1</b>	The latitudinal coverage of SAGE sunset measurements . . . . .	71
<b>Figure 5.2</b>	Constant pressure upper air maps at 30 mb for (a) January 14, 1981; (b) January 25, 1981; (c) February 15, 1981; and (d) February 22, 1981 . . . . .	75
<b>Figure 5.3</b>	Constant pressure upper air maps at 30 mb for (a) February 9, 1979; (b) February 18, 1979; (c) February 25, 1979; and (d) March 2, 1979 . . . . .	78
<b>Figure 5.4</b>	Evolution of the amplitudes ( $^{\circ}\text{C}$ ) of the first two temperature waves [(a) and (b), respectively, contour interval $1^{\circ}\text{C}$ ]; and (c) the zonal mean temperature K (contour interval $4^{\circ}\text{C}$ ) during the middle February 1981 warming ( $\sim 52^{\circ}\text{N}$ ) . . . . .	80
<b>Figure 5.5</b>	Evolution of the amplitudes ( $\text{ms}^{-1}$ ) of meridional velocity waves during the middle February 1981 warming ( $\sim 52^{\circ}\text{N}$ ). . . . .	82
<b>Figure 5.6</b>	Evolution of the amplitudes (ppmv) of the first two ozone waves, and the zonal mean ozone during the middle February 1981 warming ( $\sim 52^{\circ}\text{N}$ ) . . . . .	83
<b>Figure 5.7</b>	Evolution of (a) zonal mean ozone number density, contour interval 0.8, scale by $10^{-12}$ in unit $\text{cm}^{-3}$ ; and (b) ozone columnar density at altitude 10 km during the middle February 1981 warming ( $\sim 52^{\circ}\text{N}$ ). . . . .	85

LIST OF FIGURES (Cont'd)

<b>Figure 5.8</b>	Time variations of eddy ozone flux (ppm ms <sup>-1</sup> ) . . . . .	87
<b>Figure 5.9</b>	Time variations of eddy ozone mass transport (molecule cm <sup>-3</sup> ms <sup>-1</sup> ) . . . . .	89
<b>Figure 5.10</b>	Time variation of eddy heat flux (k ms <sup>-1</sup> ) . . . . .	91
<b>Figure 5.11</b>	Phase relationship between ozone mixing ratio, temperature and eddy meridional velocity waves during the middle February 1981 warming ( $\sim 52^\circ$ N) . . . . .	93
<b>Figure 5.12</b>	Time variation of the phase relationship between ozone mixing ratio, temperature, and eddy meridional velocity waves during the middle February 1981 warming ( $\sim 52^\circ$ N) . . . . .	96
<b>Figure 6.1</b>	Modeled variations in stratospheric aerosol layer optical depth (at 0.55 $\mu$ m) following volcanic eruptions with different amounts of injected material (Turco et al., 1982) . . . . .	105
<b>Figure 6.2</b>	SAGE/SAM II measurements of mean global stratospheric aerosol layer optical depth (at 1.0 $\mu$ m) . . . . .	108

LIST OF TABLES

TABLE 2.1	Stratospheric Aerosol Optical Depth Maps (February 21, 1979 - December 13, 1980 . . . . .	16
TABLE 2.2	Zonally Averaged, Meridional Ozone Mixing Ratio (PPMV) for Northern Spring-Southern Fall . . . . .	19
TABLE 2.3	Zonally Averaged, Meridional Ozone Mixing Ratio (PPMV) for Northern Summer-Southern Winter . . . . .	20
TABLE 2.4	Zonally Averaged, Meridional Ozone Mixing Ratio (PPMV) for Northern Fall-Southern Spring . . . . .	21
TABLE 2.5	Zonally Averaged, Meridional Ozone Mixing Ratio (PPMV) for Northern Winter-Southern Summer . . . . .	22
TABLE 2.6	Calibration Orbits Occurring in SAM II Data November 1978 - February 1983. . . . .	30
TABLE 2.7	Orbits Showing High Extinction Above 26 km For Which No Microfiche Is Available . . . . .	32
TABLE 3.1	Linear Correlation between SAM II Aerosol Optical Depth and Associated 30 mb Height From January to March. . . . .	56
TABLE 3.2	Linear Correlation between SAM II Aerosol Optical Depth and Associated 30 mb Height (1980) . . . . .	60
TABLE 5.1	The Number of Profiles and the Averaged Latitude of SAGE Observations From February 12 to 21, 1981. . . . .	73
TABLE 6.1(a)	Constants Derived from Empirical Fitting to Theoretical Models in Figure 1 . . . . .	106
TABLE 6.1(b)	Comparison of Constants Shown in Table 1(a) with Those Determined Directly from the Theoretical Models . . . . .	106
TABLE 6.2	Key Background and Volcanic Parameters Determined from Empirical Fitting. . . . .	109
TABLE 6.3	Estimates of Stratospheric Time Constants for Volcanic Injection Made by Other Workers . . . . .	113
TABLE 7.1	Modeled Stratospheric Aerosol Extinction . . . . .	117
TABLE 7.2	Theoretical Performance Figures for 48" Lidar System--Night. . . . .	119

LIST OF TABLES (Cont'd)

TABLE 7.3	Theoretical Performance Figures for 48" Lidar System--Daytime, Interference Filter . . . . .	120
TABLE 7.4	Theoretical Performance Figures for 48" Lidar System--Daytime, Interference Filter Plus Fabry-Perot Etalon. . . . . . . . . . .	121

## 1. INTRODUCTION

### 1.1 Background

The Stratospheric Aerosol Measurements II (SAM II) and Stratospheric Aerosol and Gas Experiment I (SAGE I) satellite experiments are respectively the second and third in a series of satellite-borne solar radiometers designed to monitor the concentration of aerosols and trace gases in the stratosphere. Various other in situ and remote sensing methods have also been developed to measure the concentration and variation of stratospheric constituents. Except for airborne systems, these other systems provide data at specific latitudes and longitudes only, and satellite measurements have made available, for the first time, information on a global scale.

The objective of the SAM II experiment was to obtain vertical profiles of the stratospheric aerosol with a vertical resolution of 1 km over the latitudinal range obtainable for solar occultation observations from the Nimbus-7 solar orbit, approximately  $64^{\circ}$ - $80^{\circ}$ N and  $64^{\circ}$ - $80^{\circ}$ S. These profiles were to be used to study the longitudinal and temporal variations in aerosol concentrations. The SAGE I experiment, in addition to measuring stratospheric aerosols, also measured the concentration of ozone and nitrogen dioxide. In contrast to SAM II, the latitudinal coverage of SAGE I extended from about  $72^{\circ}$ N to  $72^{\circ}$ S (some seasonal variation occurred within these latitude limits). Taken together, the satellites provide almost global coverage for the stratospheric aerosol, enabling phenomena such as volcanic injection and seasonal variations to be studied in detail.

The ultimate objective of the SAM II and SAGE I experiments lies in the use of the data to further our knowledge of the processes taking place in the stratosphere. Before this can be done, these data must be validated. In this process, the data are compared with preexisting models of stratospheric aerosols and gaseous constituents, as well as compared with correlative data sets, many of which are obtained from specifically designed correlative measurement series. The statistical nature of the data has to be examined for internal consistency and where SAM II and SAGE I independently make measurements at approximately the same time and location these should be intercompared. In this report, we describe the results of part of this validation process in which the data have been used to study a variety of physical, dynamical and chemical processes in the stratosphere. In the course of this study, which has yielded a quantity of new scientific information, the data have been carefully screened and compared with relevant models and data sets.

## 1.2 SAM II and SAGE I Satellite Measurements

The SAM II and SAGE I satellite sensors both consist of sun photometers designed to measure atmospheric extinction in certain wavelength pass bands during satellite sunrise and sunset (McCormick et al., 1979). SAM II has a single pass band centered at  $1.0 \mu\text{m}$  where gaseous absorption is negligible, designed to measure extinction due to atmospheric molecular and aerosol scattering and absorption. The molecular component of the extinction is removed during data processing providing just that due to aerosols. SAGE I has four channels, including two centered at  $1.0$  and  $0.45 \mu\text{m}$ , designated for aerosol measurement. The other two channels are at wavelengths of  $0.60 \mu\text{m}$  for the measurement of ozone and  $0.385 \mu\text{m}$  for the measurement of nitrogen dioxide, respectively.

The SAM II instrument is mounted, along with other sensors, on board the Nimbus 7 satellite. The orbit of this satellite is such that approximately 14 sunrise and 14 sunset events are observed in one day. The orbit is a high noon, sun-synchronous one with all sunrises occurring in the Antarctic region and all sunsets in the Arctic region. The exact latitude of the observations varies slowly with season between about  $64^{\circ}$  and  $80^{\circ}$ , successive events on the same day being separated by about  $26^{\circ}$  in longitude. Nimbus 7 was launched October 24, 1978, and continuous SAM II measurements have been made since then and the present date. This report includes analyses carried out on the data for the period October 1978 to February 1983. SAGE I was launched February 18, 1979, on a dedicated AEM-B (Application Explorer Mission B) spacecraft into a non-sun synchronous orbit with an inclination of  $55^{\circ}$ . Successive events on the same day are separated by about  $24^{\circ}$  in longitude, and the point of measurement changes slowly in latitude between about  $60^{\circ}\text{N}$  and  $60^{\circ}\text{S}$  (the value of latitude extreme depends upon time of year and can be as much as  $72^{\circ}\text{N}$  and  $72^{\circ}\text{S}$ ) taking 4-6 weeks to complete a cycle. As with SAM II, SAGE I initially made observations at both sunrise and sunset, a total of 30 events per day. Partial failure of the spacecraft power subsystem reduced this to sunset events only, about 5 months after launch. Sunset events continued to be recorded until final failure of the satellite power subsystem, about 34 months after launch.

As one of these satellites approach the shadow side of the earth (spacecraft sunset), the solar radiation reaching it passes through successively lower levels in the atmosphere. During this period, the radiometer locks onto the sun in azimuth and scans vertically across the solar disk. In the course of a sunrise or sunset event, measurements covering the whole stratosphere will be made within a period of 20-30 second

during which time the sun will be scanned approximately 10 times. The atmospheric attenuation is measured along an optical path approximately 300 km in length through the atmosphere with an instantaneous 0.5 km field of view. The data are then inverted to obtain the equivalent vertical extinction at each of the radiometer wavelengths (Chu and McCormick, 1979). In this inversion procedure, the assumption of horizontal homogeneity of the atmospheric constituents is made. In the case of SAGE I, it is necessary to separate the contributions to the slant path extinction from each species, as well as that due to the molecular atmosphere at each of the four wavelength bands. Following this step, the individual vertical profiles for each species may be obtained. Separation of contributions from each species increases the uncertainties in the data product. An estimate of this uncertainty is made along with the inversion and forms part of the final data set.

A significant part of the total post-launch data validation process is the operation of field experiments in which correlative data are collected on the aerosols and gaseous constituents. These measurements have been made from both ground based and high altitude platforms. The former includes lidar measurements of the stratosphere aerosol; the latter includes balloon and aircraft, in situ particle counters and lidar, rocket and balloon-borne ozone measurements and balloon-borne nitrogen dioxide measurements. In the present study, the emphasis has been less on the study of individual correlative measurements than of the overall data set characteristics. A major portion of the entire SAGE I and SAM II data sets have been scanned and used to create user-oriented data products. These have included visual displays, reference publications and data listings. In addition, the data

has been used for global analyses, modeling and related theoretical studies, as well as comparison with other long-term data sets. All of these processes have provided information on the internal data quality, individual errors and relationship to other data sets, as well as unique new information on stratospheric behavior.

### **1.3 Tasks and Organization of Report**

The Statement of Work, for this contract (NASI-17032), specifies eight task areas. Work has been carried out under each of these areas and this work is reported in sequence in Sections 2 through 7 of this report. The title given to each main section is the same as the work statement for Task Areas 1 through 6. Task Areas 7 and 8 of the Statement of Work significantly overlap other task areas and the description of the work done under these two areas has been incorporated with other sections of this report, as appropriate. Specifically, the work carried out under Task Areas 7 and 8 is reported in the following sections.

Task Area 7. - Use SAM II and where possible, SAGE satellite data to investigate the dynamics of the polar winter stratosphere.

Work described in Sections 2.8 and 3.1.

Task Area 8. - Investigate methods of automatically processing and displaying SAGE satellite data, such as aerosol optical depth, or suitable map projections showing the global variations of the quantity under study.

Work described in Sections 2.2 and 4.1.

Specific mention is also made within the body of the report whenever work carried out under Task Areas 7 and 8 is described. It should also be

noted that although work has been carried out under each task area, the division is not necessarily uniform. This division represents the results of discussions between the contractors and the NASA Technical Monitor as to the work areas requiring major attention. Subsections under each section correspond to separate studies within the task area.

A significant part of the work carried out has been presented at scientific meetings and has appeared in scientific journals. Where material has been published, the corresponding abstract has been included in the Appendix to this report and only a brief summary, together with the appropriate references, included in the text. Unpublished material, where it is believed to be useful and relevant, has been reproduced in detail in the text of this report.

2. TASK I--INVESTIGATE THE GLOBAL CLIMATOLOGY OF TROPOSPHERIC AND STRATOSPHERIC AEROSOLS, AND STRATOSPHERIC O<sub>3</sub> AND NO<sub>2</sub> INCLUDING SPATIAL AND TEMPORAL VARIABILITY

2.1 Production of Zonal Mean Plots and Tables for SAGE I Data (SAGE I, Reference Publication)

As indicated in Section 1.2, there are 34 months of aerosol, ozone and nitrogen dioxide data produced from observations made by the SAGE I satellite instrument. This entire data set has been stored, by month, on 34 magnetic tapes and archived at the National Space Sciences Data Center, NASA Goddard Space Flight Center, Greenbelt, Maryland 20771, where it is available to the scientific community. In addition, in order to provide the same community with the data in a more easily accessed form, reference publications have been developed containing tables and plots of the most significant characteristics of the data set. To achieve this goal, a ready-to-use format was developed by a small team under the leadership of Dr. M. P. McCormick of NASA/LaRC, with assistance from IFAORS and SASC Technologies Inc. Two volumes of the product for the SAGE I aerosol data have been produced as NASA reference publications (McCormick, 1985, 1986). The publication of the third year of aerosol results is expected to follow soon.

2.2 Production of SAGE I Aerosol Optical Depth Maps and Zonal Mean Extinction Plots (includes work carried out under Task Area 8)

One of the more useful quantitative measures of the stratospheric aerosol concentration that may be derived from the SAM II and SAGE I data sets is the optical depth at a wavelength of 1  $\mu\text{m}$ . In order to study this

quantity on a global scale, maps of stratospheric optical depth have been prepared for the complete SAGE I data set. The original production of these maps was manual and both color and black and white versions were prepared for some periods of data. Some of these maps have been used in publications and an example (taken from Kent and McCormick, 1984), is reproduced in Figure 2.1(a). A comparison data product, showing the zonal mean extinction as a function of altitude and latitude, has also been prepared and is shown in Figure 2.1(b).

Manual production of these types of display is not only lengthy and tedious, but can introduce subjective error into the interpolation of the data points. For these reasons, software has been written to produce the optical depth maps automatically by computer. This problem is not simple, as the SAGE data points are not distributed uniformly across the globe, but over a five or six-week period will scan the earth's surface in latitude from one extreme to another. An example of this work is shown in Fig. 2.2. In addition, data points may be missing, necessitating an interpolation procedure. The software to plot the required map has been divided into three parts as described below.

#### (a) Data Selection and Interpolation

Independent maps are prepared for sunrise and sunset events (only sunset after June 1979). The maps show the optical depth for a sunrise or sunset latitude "sweep," such as that in Figure 2.2. Sunrise or sunset data is selected that lies between two chosen dates that define the ends of the sweep. Individual events are sequenced from one end of the sweep to the other, the latitudes being examined to ensure that the event sequence moves steadily in one latitudinal direction. Following this, interpolation of data

ORIGINAL PAGE IS  
OF POOR QUALITY

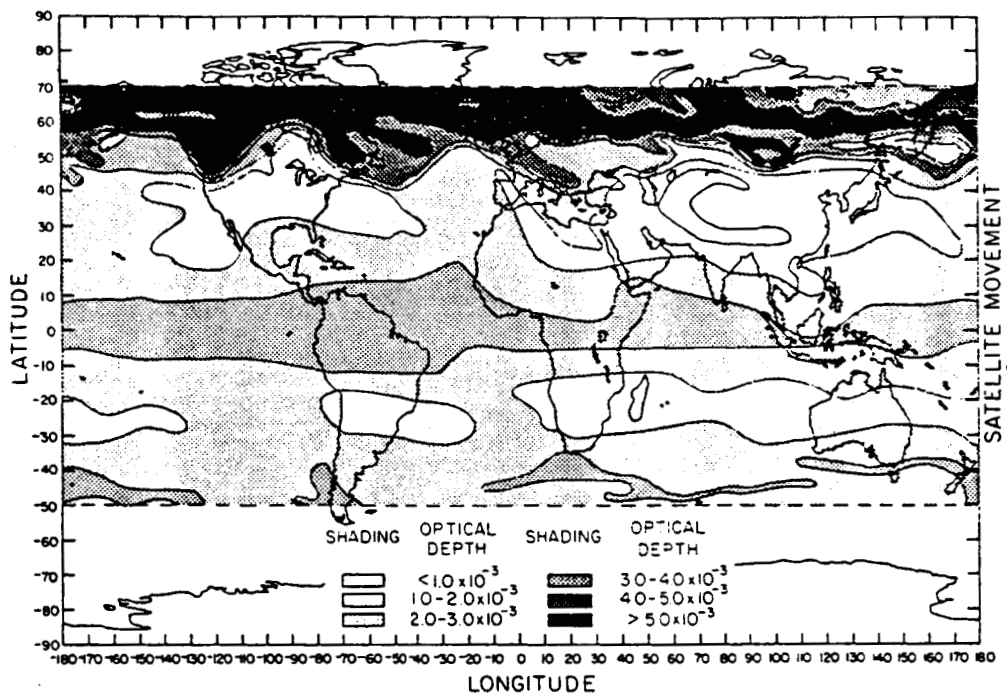


Figure 2.1(a). SAGE map of the stratospheric optical depth, July 2 to August 10, 1981. Note the concentration of volcanic material to the north, due to the eruption of Alaid and along the equator, due to the eruptions of Pagan and Ulawun.

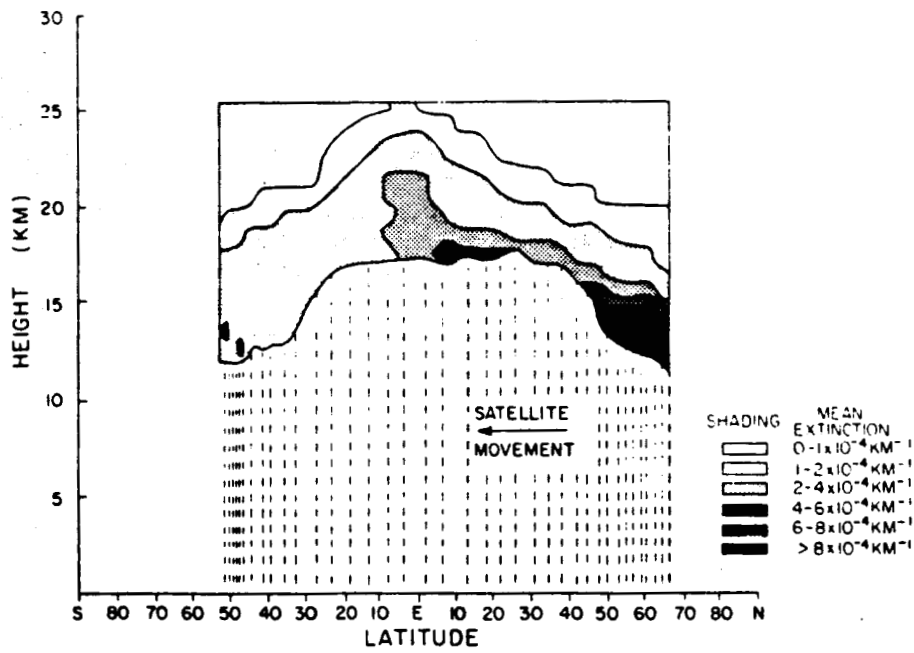


Figure 2.1(b). SAGE measurements of zonal mean extinction July 2 to August 10, 1981. The baseline below the shading is at an altitude 2 km above the tropopause. Dashed vertical lines show the mean latitude for each day's measurements. Note the concentrations of volcanic material due to the eruptions of Ulawun ( $5^{\circ}\text{S}$ ), Pagan ( $18^{\circ}\text{N}$ ), and Alaid ( $51^{\circ}\text{N}$ ).

gaps is carried out. Two classes of data loss may be identified. The first consists of those unavoidable occasions in which the satellite is in full sunlight and no data is obtainable. No interpolation is attempted on these occasions. The second class consists of those occasions on which system malfunctions (transmission drop-out, noise, etc.) have resulted in the loss of one or more data events. A computer routine identifies these events and, provided the loss does not involve too many geographically adjacent measurement locations, it carries out an interpolation between the neighboring points in a suitable manner so as to fill in the missing data. In this way, a typical latitude sweep (e.g., August 28-September 25, 1980) consisting of about four hundred observations (between latitudes of 66°S and 60°N) with about thirty missing observations is converted into a complete data sequence with no gaps.

(b) Interpolation to a Rectangular Grid

Even given a complete data sequence, problems still exist in its mapping. As noted above, the data points are non-rectangularly distributed, the latitude and longitudinal separations are different and the latitude separation is highly dependent on location on the earth's surface. Thus, at the equator, points at approximately the same longitude on successive days will be separated by about 5° in latitude. At high latitudes, this separation may be less than 1°. A decision was made to interpolate all data to a 1° latitude, longitude grid, this being a suitable base for plotting onto a mercator projection of the earth's surface. A computer routine divides the data sequence into skew quadrilateral areas on the earth's surface. The optical depth values on a rectangular 1° latitude-longitude grid within each quadrilateral are interpolated by a three-dimensional projection of the quadrilateral onto a rectangle, followed by a standard

bivariate interpolation routine. The resultant data matrix, consisting of values of optical depth at  $1^{\circ}$  latitude-longitude intervals is output and passed to the plotting routine.

(c) Production of global map

The plotting routine produces three maps.

(1) The first shows the measurement locations, an example has already been given in Figure 2.2.

(2) The second map is similar to the first with the optical depth values superimposed onto the measurement locations. An example is given in Figure 2.3.

The third is a shaded contour map prepared from the one degree interpolated optical depth grid described previously. Six shading levels are used. Considerable effort has been employed in creating a suitable shading scale with the required resolution. All maps are drawn 9" x 18" making  $1^{\circ}$  of latitude or longitude equal to 0.05". This represents the limits of resolution of the figure; when the figure is reduced to page size or smaller, the associated discontinuities become extremely small. The boundaries of the shaded regions are enhanced by the addition of contour lines. An example of this plot, showing the same data as in Figures 2.2. and 2.3, is reproduced in Figure 2.4.

Plotting time, particularly for Figure 2.3, is lengthy and can be expensive if much of the map is covered by high density shading. Plots of a quality suitable for scientific use may be made on the Varian plotter at the NASA-Langley Computing Center for which the charges are minimal. Plots of publication quality must be produced on the Calcomp plotter at considerably

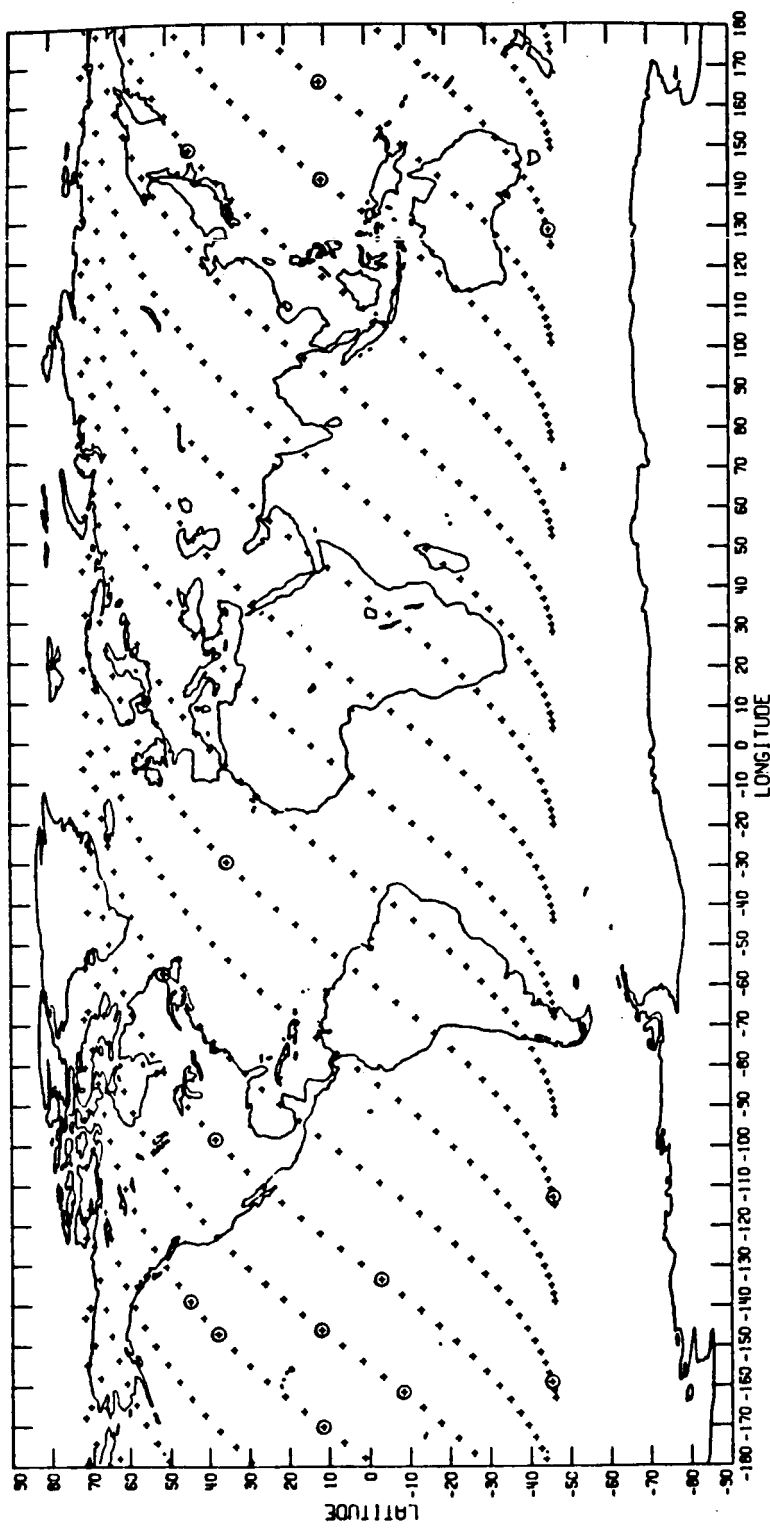


Figure 2.2. Positions of SAGE observations between May 11, 1980 and June 23, 1980. Positions are shown by plus signs. Missing data points, for which interpolation has been carried out, are shown by circled plus signs.

ORIGINAL PAGE IS  
OF POOR QUALITY

ORIGINAL PAGE IS  
OF POOR QUALITY

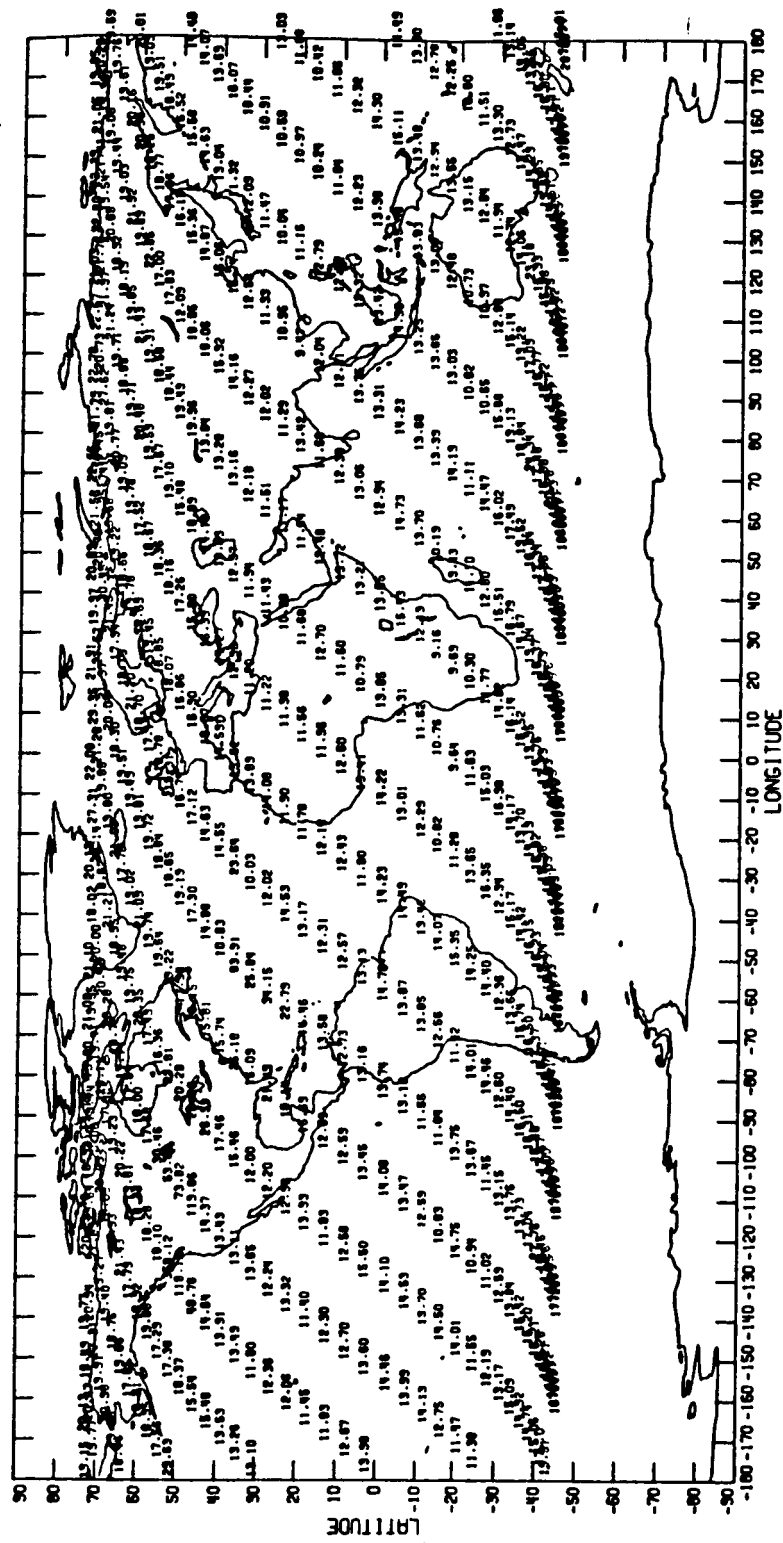


Figure 2.3. Optical depth values (from 2 km above the tropopause) for the observation points shown in Figure 2.2.

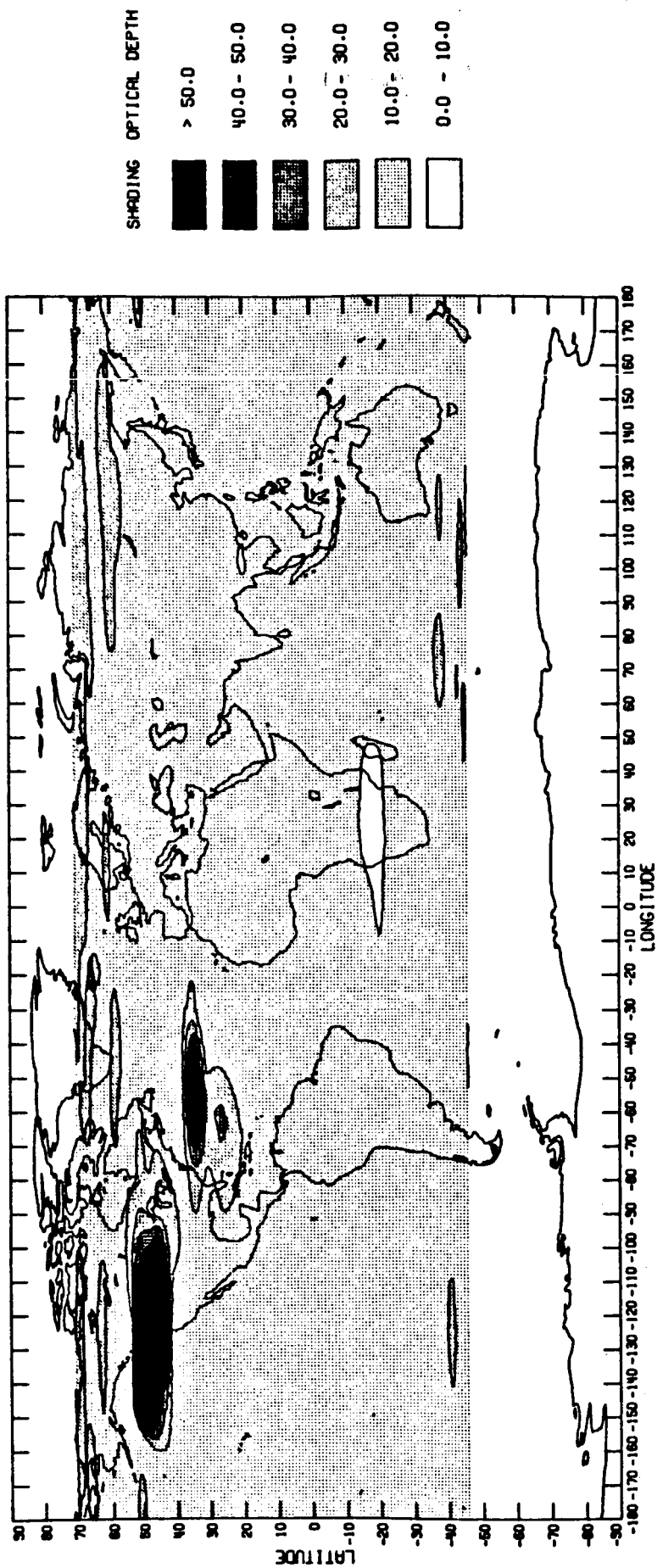


Figure 2.4. Contour plot of interpolated optical depth values. Obtained from data in Figure 2.3.

ORIGINAL PAGE IS  
OF POOR QUALITY

more cost. It may be noted that the output matrix file from stage (2) above may be used as input to other plotting devices to produce alternative color plots, vugraphs or black and white plots at less cost.

Routine production of the SAGE I optical depth maps has been carried out for all useful data between launch in February 1979 and December 1980. During this routine production, the computer codes were refined, particularly in terms of handling data gaps. These occurred in the SAGE I data sequence because of (a) sunlit periods, (b) telemetry problems, and (c) spacecraft power problems. Gaps due to sunlit periods are large and present no major plotting problems. Gaps due to telemetry and spacecraft power supply problems are erratic and of variable size. As noted earlier, the code contains an interpolation routine which will interpolate across data gaps that are below a certain size. This routine is capable of handling most of the data except during the period May-October 1979, when the data is very irregular due to partial failure in the spacecraft power supply. For this and other similar periods, the code was modified to plot only complete data segments after normal interpolation has been attempted. Up to ten separate data segments per sweep may be plotted although this has never been necessary in practice.

In addition to data gaps, problems have been encountered due to poor satellite ephemeris coordinates. Occasionally, the latitude (or longitude) of an observation is out of sequence. The code will detect and correct single errors of this type. If, however, as occasionally occurs, such an error is adjacent to a data gap or two such errors occur in sequence, then it is necessary to correct the latitude and longitude on the original data file. A list of optical depth maps prepared is shown in Table 2.1 which

TABLE 2.1. Stratospheric Aerosol Optical Depth Maps  
 (February 21, 1979 - April 8, 1980).

Sweep Code	Dates	Sunrise or Sunset	Sweep Direction	Latitude Coverage	Plotter Used
SSX 902A	Feb 21 - Mar 21, 1979	Sunset	N	58S-64N	Varian and Calcomp
SSX 902B	Feb 21 - Mar 3, 1979	Sunrise	N	52N-57N	Varian
SSX 903A	Mar 22 - Apr 29, 1979	Sunset	S	52S-64N	Varian
SSX 903B	Mar 3 - Apr 5, 1979	Sunrise	N	58S-57N	Varian
SSX 904A	Apr 28 - May 30, 1979	Sunset	N	52S-10S, 64N-68N	Varian
SSX 904B	Apr 4 - May 14, 1979	Sunrise	N	58S-71N	Varian
SSX 905A	May 30 - Jul 11, 1979	Sunset	S	46S-40S, 47N-68N	Varian
SSX 905B	May 14 - Jun 10, 1979	Sunrise	S	46S-5S, 68N-71N	Varian
SSX 905B	Jun 10 - Jul 10, 1979	Sunrise	N	63N-69N	Varian
SSX 907A	Jul 11 - Aug 5, 1979	Sunset	N	Data gaps occur throughout this sweep	
SSX 907B	Jul 21 - Jul 25, 1979	Sunrise	S	64N-69N	Varian
SSX 908A	Aug 7 - Sep 14, 1979	Sunset	S	60S-73N	Varian
SSX 909A	Sep 18 - Oct 20, 1979	Sunset	N	47S-19N 52N-54N	Varian
SSX 910A	Oct 20 - Nov 20, 1979	Sunset	S	43N-46N	Varian
SSX 911A	Nov 20 - Dec 31, 1979	Sunset	N	70S-46N	Varian
SSX 001A	Jan 1 - Jan 27, 1980	Sunset	S	15N-41N	Varian
SSX 002A	Jan 27 - Mar 3, 1980	Sunset	N	71S-55N	Varian
SSX 003A	Mar 7 - Apr 8, 1980	Sunset	S	21N-58N	Varian

TABLE 2.1. Stratospheric Aerosol Optical Depth Maps (cont'd)

Sweep Code	Dates	Sunrise or Sunset	Sweep Direction	Latitude Coverage	Plotter Used
SSX 004A	Apr 8 - May 11, 1980	Sunset	N	57S-71N	Varian
SSX 005A	May 11 - Jun 23, 1980	Sunset	S	46S-71N	Varian and Calcomp
SSX 006A	Jun 23 - Jul 20, 1980	Sunset	N	46S-24S	Varian
SSX 007A	Jul 20 - Aug 28, 1980	Sunset	S	55S-69N	Varian and Calcomp*
SSX 008A	Aug 28 - Sep 27, 1980	Sunset	N	55S-60N	Varian
SSX 009A	Sep 27 - Oct 31, 1980	Sunset	S	10S-61N	Varian
SSX 011A	Nov 1 - Dec 13, 1980	Sunset	N	73S-46N	Varian

\* Not filtered for quality factor.

indicates the dates of each sweep, the event type, sweep direction and the plotting device used (these maps have been delivered to NASA).

### 2.3 Ozone Climatology

The entire three years' (34 months) SAGE ozone measurements have been used to derive the seasonal meridional ozone mixing ratio distributions. The results are tabulated in Tables 2.2 to 2.5 and graphically displayed in Figures 2.5a to 2.5d. In general, the ozone mixing ratio shows a maximum above the equator at  $\approx 32$  km. The center of this maximum appears to follow the seasonal shift of the sun. We may also note that, in the winter high latitude lower stratosphere (between 25 and 35 km), the ozone shows a lower value than that in the corresponding region in the summer hemisphere. This occurrence could be the result of large-scale wave disturbances (planetary waves) in high latitudes during the winter. Planetary waves are believed to be able to transport trace species and heat to the polar region from lower latitudes.

The corresponding standard deviations (expressed in percentage of the mean) of the three-year seasonal means are given in Figures 2.6a to 2.6d. Generally, large values ( $>20\%$ ) of the standard deviation exist in regions above 45 km and below 20 km, especially in the low latitudes ( $<30^\circ$ ) in the lower stratosphere. Perhaps, these large values are partly due to large signal/noise ratios for the instrument in these altitude ranges. In the regions between 20 km and 45 km, the values are generally less than 20%. In fact, values less than 10% are found in the stratosphere between 23 and 38 km, except in the high latitudes. Since in this region the uncertainty of the retrieved  $O_3$  profiles is less than 10%, the larger values ( $>10\%$ ) in the high latitudes are indicative of the ozone variability in this region. Of

TABLE 2.2. Zonally Averaged, Meridional Ozone Mixing Ratio (PPMV) for Northern Spring-Southern Fall. Derived from the Three-Year SAGE Ozone Measurements.

Altitude (km)	Latitude										70
	-60	-50	-40	-30	-20	-10	0	10	20	30	
10	2.234	1.180	1.120	1.06	1.03	0.983	0.935	0.875	0.820	0.764	0.699
11	2.280	1.220	1.151	1.114	1.069	0.935	0.892	0.824	0.759	0.696	0.609
12	3.364	2.276	1.84	1.226	1.158	0.992	0.896	0.824	0.759	0.696	0.707
13	4.475	3.363	2.31	1.47	1.293	0.945	0.866	0.797	0.735	0.693	0.621
14	6.636	4.489	3.00	1.79	1.155	0.914	0.814	0.723	0.663	0.692	0.621
15	8.858	6.669	4.07	2.35	1.70	1.09	0.869	0.793	0.733	0.693	0.622
16	1.132	9.04	5.75	3.23	2.07	1.82	1.200	0.89	0.804	0.770	0.924
17	1.452	1.209	8.23	4.69	2.73	2.12	2.38	0.824	0.864	0.849	2.370
18	1.791	1.574	1.158	7.14	4.08	3.01	3.01	0.867	0.883	0.864	2.779
19	2.134	1.969	1.972	1.086	0.670	0.499	0.666	0.515	0.784	0.724	3.135
20	2.475	2.377	2.042	1.972	1.099	0.642	0.820	0.695	1.294	1.193	3.445
21	2.808	2.821	2.593	2.133	1.663	1.368	1.407	1.456	1.953	2.618	3.233
22	3.165	3.300	3.128	2.779	2.351	2.067	2.096	2.142	2.667	3.377	3.692
23	3.558	3.808	3.765	3.942	3.158	2.902	2.902	2.960	3.473	4.117	4.145
24	3.956	4.289	4.396	4.379	4.087	3.866	3.742	3.880	4.354	4.918	4.606
25	4.309	4.732	5.041	5.283	5.191	4.976	4.79	4.922	5.337	5.539	5.052
26	4.579	5.086	5.609	6.111	6.314	6.177	6.026	6.056	6.347	6.62	5.456
27	4.796	5.332	6.073	6.798	7.351	7.458	7.356	7.267	7.67	8.37	8.897
28	4.966	5.910	6.376	7.348	8.219	8.734	8.696	8.492	8.97	9.397	9.923
29	5.169	5.700	6.592	7.766	8.917	9.680	10.040	9.636	9.018	9.192	9.203
30	5.345	5.889	6.792	8.032	9.364	10.724	11.116	10.530	9.983	10.631	10.975
31	5.577	6.091	6.990	8.244	9.569	11.251	11.756	11.131	9.927	10.354	10.870
32	5.827	6.316	7.208	8.416	9.748	11.397	11.849	11.344	10.060	10.154	10.424
33	6.080	6.513	7.413	8.236	9.766	11.231	11.563	11.210	10.023	10.306	10.669
34	6.282	6.783	7.603	8.638	9.698	10.829	11.169	10.893	9.922	10.317	10.646
35	6.529	7.609	7.762	8.707	9.587	10.317	10.335	10.464	10.746	11.283	11.025
36	6.720	7.892	8.716	9.405	9.773	9.702	10.014	9.546	9.124	9.424	9.894
37	6.921	7.341	7.972	8.704	9.171	9.310	9.304	9.569	9.246	9.680	9.738
38	7.010	7.445	8.005	8.622	9.898	9.917	9.954	9.211	8.913	9.626	9.113
39	7.332	7.471	7.944	8.449	9.369	9.467	9.499	9.742	9.537	9.299	9.025
40	7.398	7.750	8.196	8.196	8.105	8.029	7.977	8.231	8.069	8.061	8.097
41	7.703	7.119	7.433	7.722	7.609	7.483	7.447	7.653	7.512	7.322	7.057
42	6.369	6.782	7.040	7.221	7.007	6.916	6.945	7.101	6.860	6.773	6.477
43	6.914	6.326	6.515	6.630	6.437	6.496	6.446	6.933	6.318	6.193	6.941
44	5.474	5.949	6.435	6.902	7.05	7.594	7.594	7.037	6.837	6.722	6.420
45	4.974	5.348	5.423	5.938	5.436	5.051	5.157	5.219	5.139	4.932	4.771
46	4.665	4.800	4.963	4.874	4.963	4.874	4.963	4.462	4.264	4.085	3.774
47	3.703	4.015	4.091	4.236	4.169	4.446	4.994	4.462	4.264	3.959	3.359
48	3.289	3.528	3.599	3.706	3.674	3.813	3.813	3.986	3.677	3.338	3.023
49	2.956	3.156	3.233	3.334	3.313	3.493	3.493	3.606	3.449	3.220	3.046
50	2.713	2.865	2.958	3.052	3.051	3.164	3.267	3.194	3.079	2.965	2.816
51	2.497	2.629	2.735	2.828	2.735	2.910	2.910	2.956	2.973	2.829	2.694
52	2.312	2.431	2.548	2.642	2.667	2.768	2.871	2.709	2.692	2.617	2.403
53	2.148	2.260	2.386	2.488	2.520	2.627	2.712	2.624	2.547	2.398	2.107
54	2.005	2.109	2.241	2.393	2.434	2.501	2.571	2.632	2.762	2.920	2.043
55	1.970	2.107	2.107	2.375	2.375	2.440	2.440	2.462	2.473	2.367	1.999

ORIGINAL PAGE IS  
OF POOR QUALITY

TABLE 2.3. Zonally Averaged, Meridional Ozone Mixing Ratio (PPMV) for Northern Summer-Southern Winter. Derived from the Three-Year SAGE Ozone Measurements.

Altitude (km)	Latitude										70
	-60	-50	-40	-30	-20	-10	0	10	20	30	
10	0.69	0.67	0.69	0.71	0.73	0.75	0.77	0.79	0.81	0.83	0.84
11	0.66	0.65	0.66	0.67	0.68	0.69	0.70	0.71	0.72	0.73	0.74
12	0.63	0.62	0.63	0.64	0.65	0.66	0.67	0.68	0.69	0.70	0.71
13	0.60	0.59	0.60	0.61	0.62	0.63	0.64	0.65	0.66	0.67	0.68
14	0.57	0.56	0.57	0.58	0.59	0.60	0.61	0.62	0.63	0.64	0.65
15	0.54	0.53	0.54	0.55	0.56	0.57	0.58	0.59	0.60	0.61	0.62
16	0.51	0.50	0.51	0.52	0.53	0.54	0.55	0.56	0.57	0.58	0.59
17	0.48	0.47	0.48	0.49	0.50	0.51	0.52	0.53	0.54	0.55	0.56
18	0.46	0.45	0.46	0.47	0.48	0.49	0.50	0.51	0.52	0.53	0.54
19	0.43	0.42	0.43	0.44	0.45	0.46	0.47	0.48	0.49	0.50	0.51
20	0.40	0.39	0.40	0.41	0.42	0.43	0.44	0.45	0.46	0.47	0.48
21	0.37	0.36	0.37	0.38	0.39	0.40	0.41	0.42	0.43	0.44	0.45
22	0.34	0.33	0.34	0.35	0.36	0.37	0.38	0.39	0.40	0.41	0.42
23	0.31	0.30	0.31	0.32	0.33	0.34	0.35	0.36	0.37	0.38	0.39
24	0.28	0.27	0.28	0.29	0.30	0.31	0.32	0.33	0.34	0.35	0.36
25	0.25	0.24	0.25	0.26	0.27	0.28	0.29	0.30	0.31	0.32	0.33
26	0.23	0.22	0.23	0.24	0.25	0.26	0.27	0.28	0.29	0.30	0.31
27	0.20	0.19	0.20	0.21	0.22	0.23	0.24	0.25	0.26	0.27	0.28
28	0.18	0.17	0.18	0.19	0.20	0.21	0.22	0.23	0.24	0.25	0.26
29	0.16	0.15	0.16	0.17	0.18	0.19	0.20	0.21	0.22	0.23	0.24
30	0.14	0.13	0.14	0.15	0.16	0.17	0.18	0.19	0.20	0.21	0.22
31	0.12	0.11	0.12	0.13	0.14	0.15	0.16	0.17	0.18	0.19	0.20
32	0.10	0.09	0.10	0.11	0.12	0.13	0.14	0.15	0.16	0.17	0.18
33	0.08	0.07	0.08	0.09	0.10	0.11	0.12	0.13	0.14	0.15	0.16
34	0.07	0.06	0.07	0.08	0.09	0.10	0.11	0.12	0.13	0.14	0.15
35	0.06	0.05	0.06	0.07	0.08	0.09	0.10	0.11	0.12	0.13	0.14
36	0.05	0.04	0.05	0.06	0.07	0.08	0.09	0.10	0.11	0.12	0.13
37	0.04	0.03	0.04	0.05	0.06	0.07	0.08	0.09	0.10	0.11	0.12
38	0.03	0.02	0.03	0.04	0.05	0.06	0.07	0.08	0.09	0.10	0.11
39	0.03	0.02	0.03	0.04	0.05	0.06	0.07	0.08	0.09	0.10	0.11
40	0.02	0.01	0.02	0.03	0.04	0.05	0.06	0.07	0.08	0.09	0.10
41	0.02	0.01	0.02	0.03	0.04	0.05	0.06	0.07	0.08	0.09	0.10
42	0.01	0.01	0.02	0.02	0.03	0.04	0.05	0.06	0.07	0.08	0.09
43	0.01	0.01	0.02	0.02	0.03	0.04	0.05	0.06	0.07	0.08	0.09
44	0.00	0.00	0.01	0.01	0.02	0.03	0.04	0.05	0.06	0.07	0.08
45	0.00	0.00	0.01	0.01	0.02	0.03	0.04	0.05	0.06	0.07	0.08
46	0.00	0.00	0.01	0.01	0.02	0.03	0.04	0.05	0.06	0.07	0.08
47	0.00	0.00	0.01	0.01	0.02	0.03	0.04	0.05	0.06	0.07	0.08
48	0.00	0.00	0.01	0.01	0.02	0.03	0.04	0.05	0.06	0.07	0.08
49	0.00	0.00	0.01	0.01	0.02	0.03	0.04	0.05	0.06	0.07	0.08
50	0.00	0.00	0.01	0.01	0.02	0.03	0.04	0.05	0.06	0.07	0.08
51	0.00	0.00	0.01	0.01	0.02	0.03	0.04	0.05	0.06	0.07	0.08
52	0.00	0.00	0.01	0.01	0.02	0.03	0.04	0.05	0.06	0.07	0.08
53	0.00	0.00	0.01	0.01	0.02	0.03	0.04	0.05	0.06	0.07	0.08
54	0.00	0.00	0.01	0.01	0.02	0.03	0.04	0.05	0.06	0.07	0.08
55	0.00	0.00	0.01	0.01	0.02	0.03	0.04	0.05	0.06	0.07	0.08

**ORIGINAL PAGE IS  
OF POOR QUALITY**

TABLE 2.4. Zonally Averaged, Meridional Ozone Mixing Ratio (PPMV) for Northern Fall-Southern Spring. Derived from the Three-Year SAGE Ozone Measurements.

Altitude (km)	Latitude										
	-70	-60	-50	-40	-30	-20	-10	0	10	20	
10	31.9	32.1	21.6	16.3	16.2	2.69	0.70	0.91	0.91	1.24	2.76
11	40.9	39.5	22.0	19.3	16.2	2.21	0.591	0.136	0.092	0.224	0.281
12	53.3	47.2	28.9	17.0	15.1	1.96	0.498	0.647	0.094	0.317	0.314
13	65.4	70.3	26.6	34.0	19.1	1.46	0.176	0.164	0.109	0.261	0.644
14	70.7	70.0	41.5	22.6	14.7	1.61	0.386	0.157	0.126	0.327	0.678
15	79.7	91.3	1.615	5.18	29.3	16.3	1.346	1.156	0.167	0.431	0.794
16	105.2	107.3	1.015	1.153	7.40	4.09	2.06	0.326	0.191	0.117	0.382
17	117.7	119.9	1.320	1.039	6.01	3.62	2.216	0.234	0.216	1.167	1.292
18	127.0	147.3	1.441	9.06	4.41	3.64	0.344	0.371	0.374	1.652	1.654
19	144.0	247.9	2.673	1.961	1.349	0.621	0.545	0.576	0.660	1.675	2.004
20	172.0	322.4	2.989	2.208	1.927	1.321	0.647	0.698	1.061	1.358	2.259
21	204.0	356.1	3.201	3.123	2.615	1.941	1.432	1.312	1.392	1.903	2.660
22	339.3	3.850	3.970	3.741	3.359	2.650	2.048	1.939	2.242	2.974	3.404
23	375.6	4.142	4.403	4.308	4.000	3.457	2.639	2.794	3.131	3.364	3.995
24	414.9	4.459	4.836	4.735	4.301	3.765	3.057	3.676	4.218	4.366	4.215
25	452.1	4.336	5.122	5.380	5.361	5.165	4.849	4.429	5.050	5.114	5.121
26	493.8	5.236	5.467	5.827	5.940	6.108	6.076	6.075	6.221	6.149	5.994
27	510.5	5.590	5.764	6.346	6.263	6.966	7.274	7.405	7.419	7.216	5.999
28	538.2	5.919	6.082	6.772	7.459	7.776	8.306	8.660	8.101	7.493	6.367
29	566.2	6.208	6.413	7.161	7.716	8.461	9.307	9.718	9.822	8.681	7.954
30	584.6	6.402	6.772	7.924	9.160	10.459	9.972	10.352	10.176	9.320	8.434
31	597.4	6.533	7.695	7.902	3.904	6.412	10.412	10.493	10.494	9.650	8.742
32	610.3	6.713	7.348	9.129	8.759	9.713	10.412	10.506	10.506	9.639	8.672
33	616.2	6.860	7.957	8.291	8.376	9.614	10.433	10.477	10.377	9.832	9.145
34	617.9	6.963	7.762	7.950	9.040	9.790	10.234	10.289	10.126	9.642	9.125
35	617.0	6.990	7.902	8.449	9.024	9.652	9.679	9.996	9.767	9.423	9.032
36	618.6	6.936	7.762	8.472	8.781	9.438	9.713	9.940	9.385	9.121	8.043
37	599.6	6.806	7.717	8.436	8.889	9.181	9.209	9.145	8.970	8.798	8.743
38	576.3	6.690	7.540	8.200	8.627	8.803	8.807	8.752	8.522	8.406	8.103
39	552.6	6.367	7.301	7.986	9.201	8.325	8.260	8.277	8.053	8.166	7.372
40	522.1	6.049	6.945	7.424	7.713	7.012	7.758	7.758	7.679	7.758	7.329
41	495.7	5.662	6.457	6.934	7.123	7.177	7.139	7.118	7.160	7.185	6.867
42	442.4	5.267	5.639	6.161	6.573	6.448	6.474	6.500	6.562	6.565	6.571
43	428.7	4.839	5.474	6.075	6.964	6.917	5.917	5.962	5.973	6.111	6.001
44	389.4	4.952	3.803	5.579	5.474	5.497	5.522	5.614	5.458	5.459	5.182
45	396.4	4.436	4.883	5.033	5.032	5.078	5.124	5.184	5.054	4.987	4.622
46	341.7	3.626	4.411	4.280	4.361	4.561	4.526	4.404	4.342	3.995	3.662
47	269.7	2.992	3.320	3.727	3.831	3.829	3.864	3.870	3.772	3.732	3.444
48	245.0	2.017	2.127	2.302	2.428	2.454	2.477	2.499	2.401	2.352	2.079
49	226.3	2.461	2.683	2.969	3.059	3.059	3.064	3.115	3.124	3.026	2.730
50	211.6	2.286	2.468	2.732	2.809	2.807	2.816	2.870	2.882	2.721	2.361
51	200.5	2.144	2.287	2.546	2.602	2.613	2.633	2.659	2.680	2.510	2.078
52	190.5	2.017	2.127	2.302	2.428	2.454	2.477	2.499	2.401	2.352	2.079
53	180.9	1.976	2.235	2.287	2.325	2.312	2.337	2.349	2.337	2.219	2.073
54	171.9	1.839	2.101	2.162	2.216	2.208	2.216	2.216	2.191	2.063	1.798
55	169.5	1.695	1.714	2.034	2.034	2.034	2.034	2.034	2.034	2.034	1.773

TABLE 2.5. Zonally Averaged, Meridional Ozone Mixing Ratio (PPMV) for Northern Winter-Southern Summer. Derived from the Three-Year SAGE Ozone Measurements.

Altitude (km)	Latitude									
	-70	-60	-50	-40	-30	-20	-10	0	10	20
10	• 35°F	• 216	• 135	• 120	• 261	• 359	• 404	• 130	• 069	• 100
11	• 40°N	• 252	• 156	• 117	• 261	• 306	• 354	• 116	• 071	• 229
12	• 45°N	• 301	• 198	• 115	• 236	• 265	• 306	• 107	• 079	• 115
13	• 50°N	• 609	• 174	• 126	• 210	• 211	• 260	• 111	• 098	• 130
14	• 55°N	• 653	• 287	• 124	• 226	• 199	• 224	• 114	• 092	• 126
15	• 60°N	• 114	• 615	• 303	• 203	• 213	• 207	• 119	• 116	• 629
16	• 65°N	• 116	• 631	• 237	• 277	• 243	• 201	• 139	• 162	• 363
17	• 70°N	• 620	• 113	• 762	• 611	• 311	• 260	• 231	• 188	• 543
18	• 75°N	• 774	• 113	• 767	• 663	• 447	• 362	• 336	• 265	• 664
19	• 80°N	• 971	• 771	• 1467	• 1467	• 713	• 568	• 508	• 475	• 267
20	• 85°N	• 219	• 219	• 173	• 476	• 1001	• 911	• 829	• 154	• 101
21	• 90°N	• 693	• 494	• 300	• 341	• 423	• 443	• 257	• 302	• 102
22	• 94°N	• 940	• 752	• 713	• 452	• 058	• 744	• 204	• 226	• 080
23	• 95°N	• 953	• 612	• 620	• 920	• 475	• 205	• 162	• 192	• 923
24	• 96°N	• 100	• 182	• 100	• 298	• 295	• 887	• 605	• 766	• 205
25	• 97°N	• 402	• 119	• 6db	• 124	• 298	• 113	• 867	• 360	• 97
26	• 98°N	• 690	• 690	• 215	• 702	• 079	• 219	• 128	• 853	• 226
27	• 99°N	• 606	• 606	• 601	• 364	• 934	• 292	• 305	• 459	• 130
28	• 100°N	• 207	• 100	• 138	• 973	• 699	• 230	• 567	• 210	• 130
29	• 101°N	• 524	• 516	• 144	• 455	• 357	• 035	• 928	• 094	• 468
30	• 102°N	• 667	• 667	• 799	• 782	• 833	• 625	• 104	• 950	• 283
31	• 103°N	• 943	• 943	• 010	• 043	• 133	• 997	• 667	• 563	• 643
32	• 104°N	• 116	• 116	• 219	• 219	• 217	• 167	• 108	• 889	• 119
33	• 105°N	• 309	• 309	• 402	• 329	• 329	• 235	• 980	• 839	• 175
34	• 106°N	• 474	• 475	• 204	• 359	• 304	• 167	• 672	• 763	• 284
35	• 107°N	• 571	• 571	• 590	• 521	• 315	• 131	• 843	• 611	• 604
36	• 108°N	• 616	• 616	• 663	• 473	• 240	• 965	• 576	• 119	• 635
37	• 109°N	• 593	• 593	• 491	• 376	• 054	• 677	• 163	• 666	• 424
38	• 110°N	• 519	• 521	• 135	• 775	• 269	• 751	• 140	• 965	• 327
39	• 111°N	• 364	• 045	• 729	• 340	• 756	• 245	• 556	• 261	• 128
40	• 112°N	• 092	• 94	• 571	• 590	• 131	• 637	• 023	• 967	• 336
41	• 113°N	• 092	• 741	• 571	• 521	• 315	• 131	• 843	• 611	• 604
42	• 114°N	• 936	• 936	• 663	• 473	• 240	• 965	• 576	• 119	• 635
43	• 115°N	• 917	• 917	• 447	• 447	• 054	• 677	• 163	• 966	• 424
44	• 116°N	• 646	• 646	• 135	• 135	• 135	• 135	• 135	• 135	• 135
45	• 117°N	• 157	• 157	• 993	• 993	• 993	• 993	• 993	• 993	• 993
46	• 118°N	• 636	• 636	• 636	• 636	• 636	• 636	• 636	• 636	• 636
47	• 119°N	• 092	• 94	• 571	• 590	• 131	• 637	• 023	• 967	• 336
48	• 120°N	• 205	• 205	• 478	• 478	• 084	• 561	• 561	• 956	• 456
49	• 121°N	• 542	• 542	• 983	• 379	• 610	• 666	• 909	• 010	• 957
50	• 122°N	• 997	• 997	• 936	• 936	• 335	• 399	• 037	• 739	• 327
51	• 123°N	• 229	• 229	• 447	• 447	• 027	• 611	• 611	• 956	• 456
52	• 124°N	• 694	• 694	• 057	• 057	• 199	• 327	• 375	• 311	• 147
53	• 125°N	• 205	• 205	• 478	• 478	• 084	• 561	• 561	• 956	• 456
54	• 126°N	• 626	• 626	• 265	• 265	• 012	• 116	• 302	• 474	• 456
55	• 127°N	• 994	• 994	• 994	• 994	• 994	• 994	• 994	• 994	• 994

ORIGINAL PAGE IS  
OF POOR QUALITY

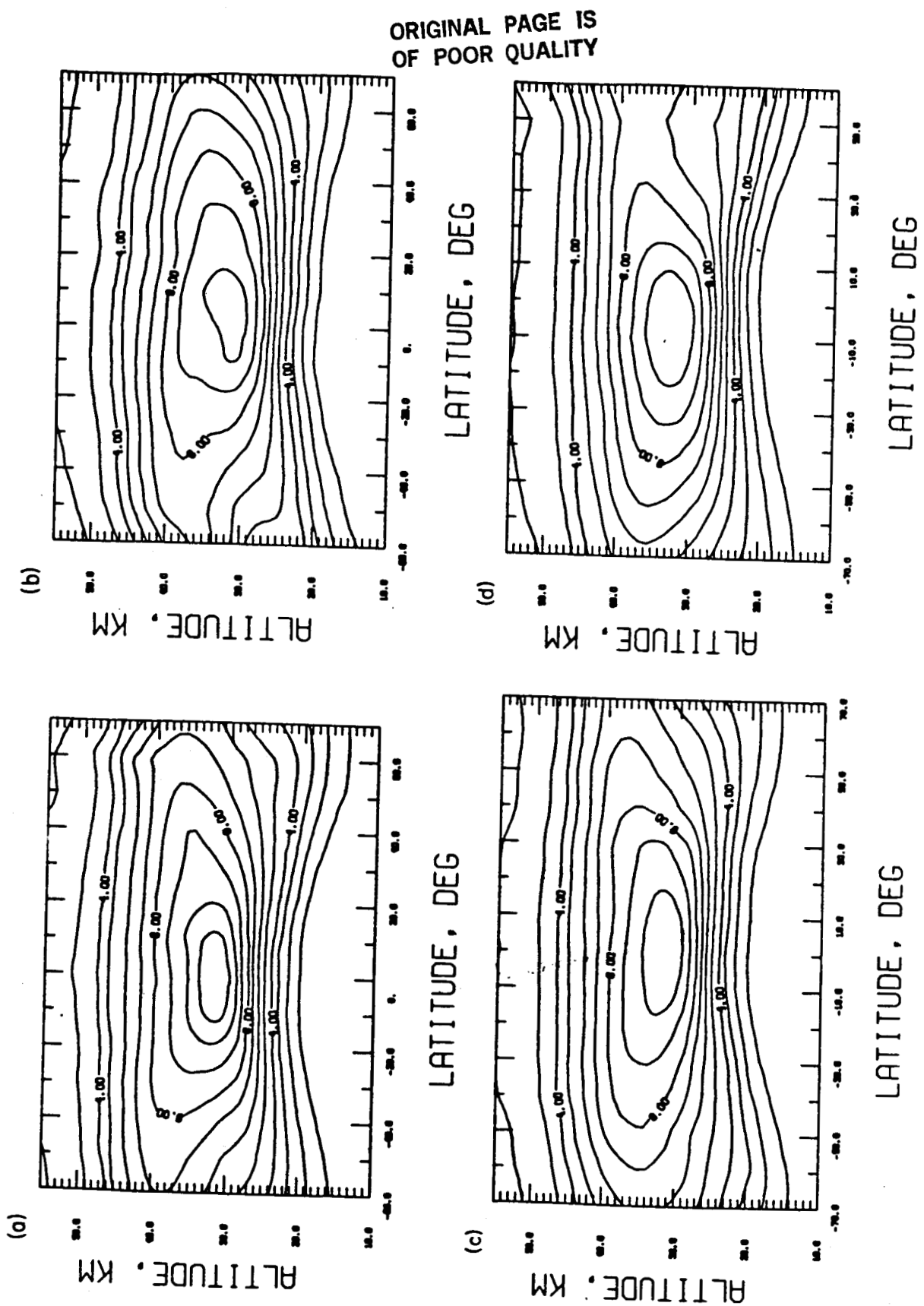


Figure 2.5. Seasonal meridional ozone mixing ratio (ppmv) distributions. Derived from 3-year SAGE ozone measurements (a) March to May, (b) June to August, (c) September to November, and (d) December to February.

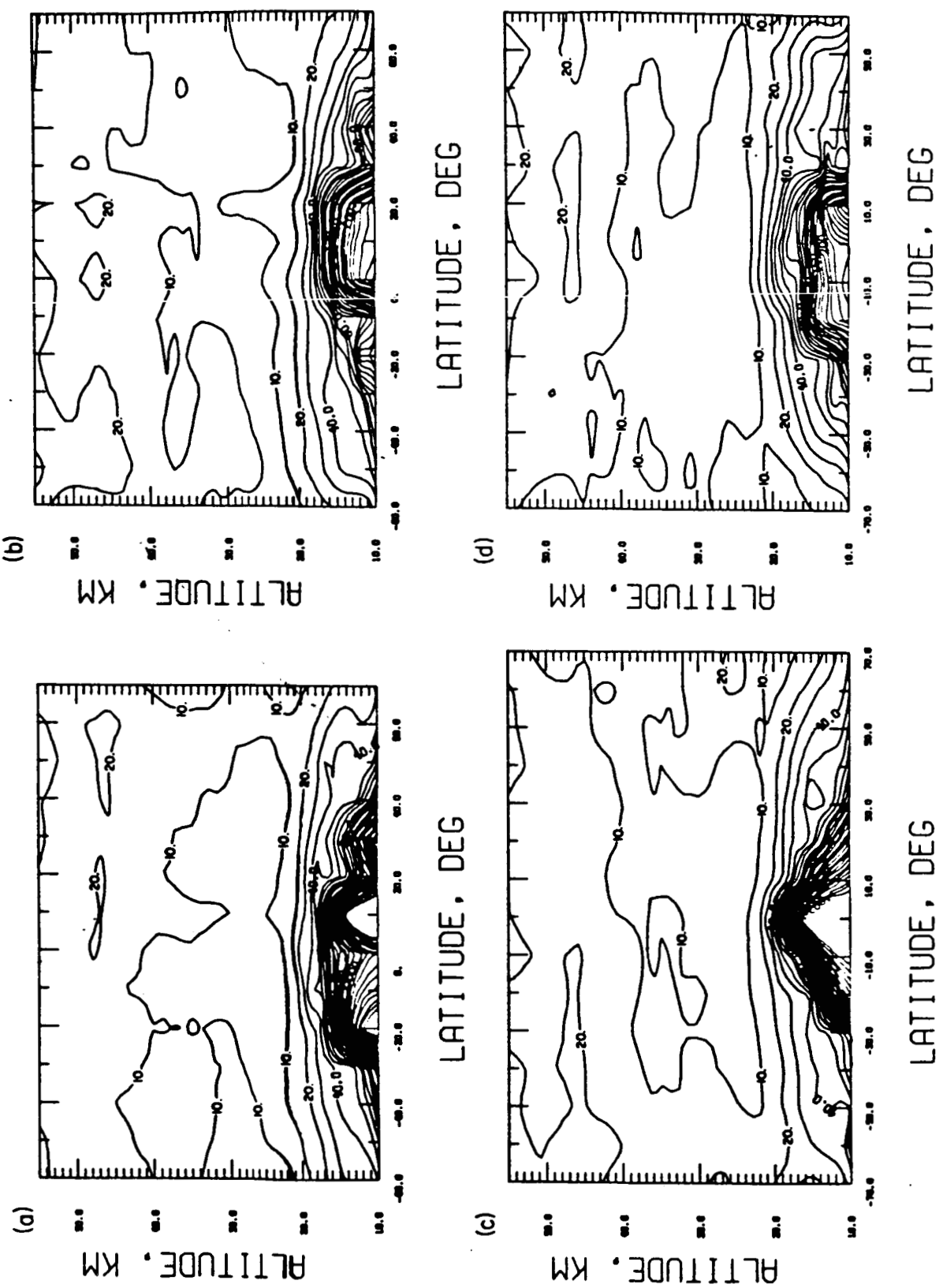


Figure 2.6. Seasonal meridional ozone mixing ratio--percentage standard deviation from mean. Derived from 3-year SAGE ozone measurements (a) March to May, (b) June to August, (c) September to November, and (d) December to February.

ORIGINAL PAGE IS  
OF POOR QUALITY

particular interest is the extinsion of the the 10% contour line from winter high latitudes to about  $+10^{\circ}$  centered at altitude 32 km (Figures 2.6b and 2.6d). There are reasons to believe that this feature is primarily a result of planetary wave activity during the winter. Since these wave activities are prevalent through about the end of March (Labitzke, 1982, J. Meteo. Soc., Japan, 124-139) relatively high values of standard deviation are also expected to be shown in high latitudes during the period of spring equinox. This feature is indeed noticeable in Figures 2.6a and 2.6c.

For the reason that the ozone column plays an important role in uv solar radiation attenuation, extensive investigations have been made of the variation of total ozone on a global scale. To examine the seasonal variation of the zonally averaged total ozone distribution, three-year ozone profiles derived from the SAGE instrument have been used for this particular purpose. In this analysis, the ozone column is integrated from 2 km above the tropopause up to 55 km. The 34-month SAGE ozone profiles are grouped seasonally. The ozone column is then determiend for each of the profiles. A zonal average is then calculated for the  $15^{\circ}$   $10^{\circ}$  latitude bins from  $75^{\circ}$ S to  $75^{\circ}$ N. The associated standard deviations of the means have also been derived. These deviations may indicate the variabilities of the ozone column at different latitudes during different seasons. The four seasonal means are shown in Figure 2.7. In general, large seasonal variations of ozone columns exist in regions outside the tropics. In both hemispheres, Figure 2.7 shows that the mean ozone column reaches its lowest value in the Fall. A rapid increase occurs from the Fall to Winter at high latitudes. This increase seems to extend to Spring in the Northern Hemisphere. In the Southern Hemisphere, the variations are similar to those in the Northern Hemisphere,

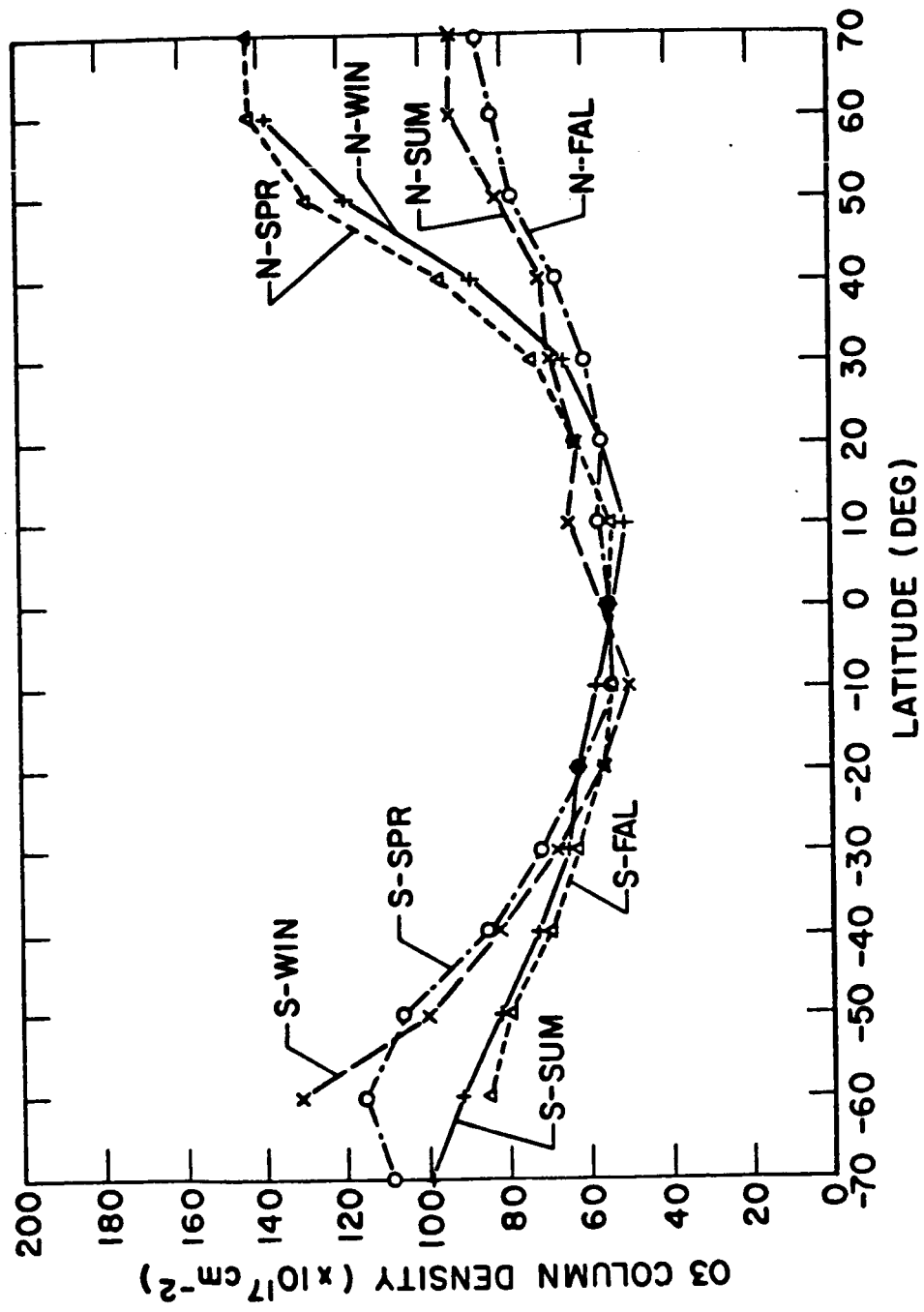


Figure 2.7. Comparison of seasonal latitudinal distributions of total ozone derived from SAGE 34-month data set.

except poleward of 50°S. At the latter latitudes, the ozone column decreases, rather than increases from Winter to Spring.

The standard deviations of the seasonally averaged zonal mean ozone column are given in Figures 2.8a to 2.8d. The remarkable features are the larger values of the deviation during the Winter and Spring, and the relatively low values during the Fall in high latitudes. In general, the values for the deviation in the Northern Hemisphere are generally greater than those in the Southern Hemisphere during the same seasons. These large deviations at the high latitudes during Winter and Spring, especially in the Northern Hemisphere, are believed to be linked with the high latitude dynamic activity during these particular seasons. It is well known that the stratosphere is characterized by large-scale disturbances (planetary waves) as the circulation pattern changes from Winter to Summer. At low latitudes, the standard deviation is much smaller compared to those at high latitudes. Nevertheless, Figure 2.8 shows a mild local maximum of the deviation at the tropics and two local minima near +20 degrees latitude.

#### 2.4 Identification of Calibration Orbits

The SAM II satellite system is mounted, along with other sensors, aboard the Nimbus-7 spacecraft. Periodic earth radiation budget instrument calibrations, carried out on board Nimbus-7, result in perturbations to the spacecraft attitude control/pointing which interfere with the data being measured by SAM II. These calibrations are carried out at approximately 24-day intervals and perturb only a small fraction of the SAM II measurement orbits. Despite this, the interference, which simulates a high extinction at altitudes above the aerosol layer maximum, is sufficiently large to seriously affect average values that include the perturbed data.

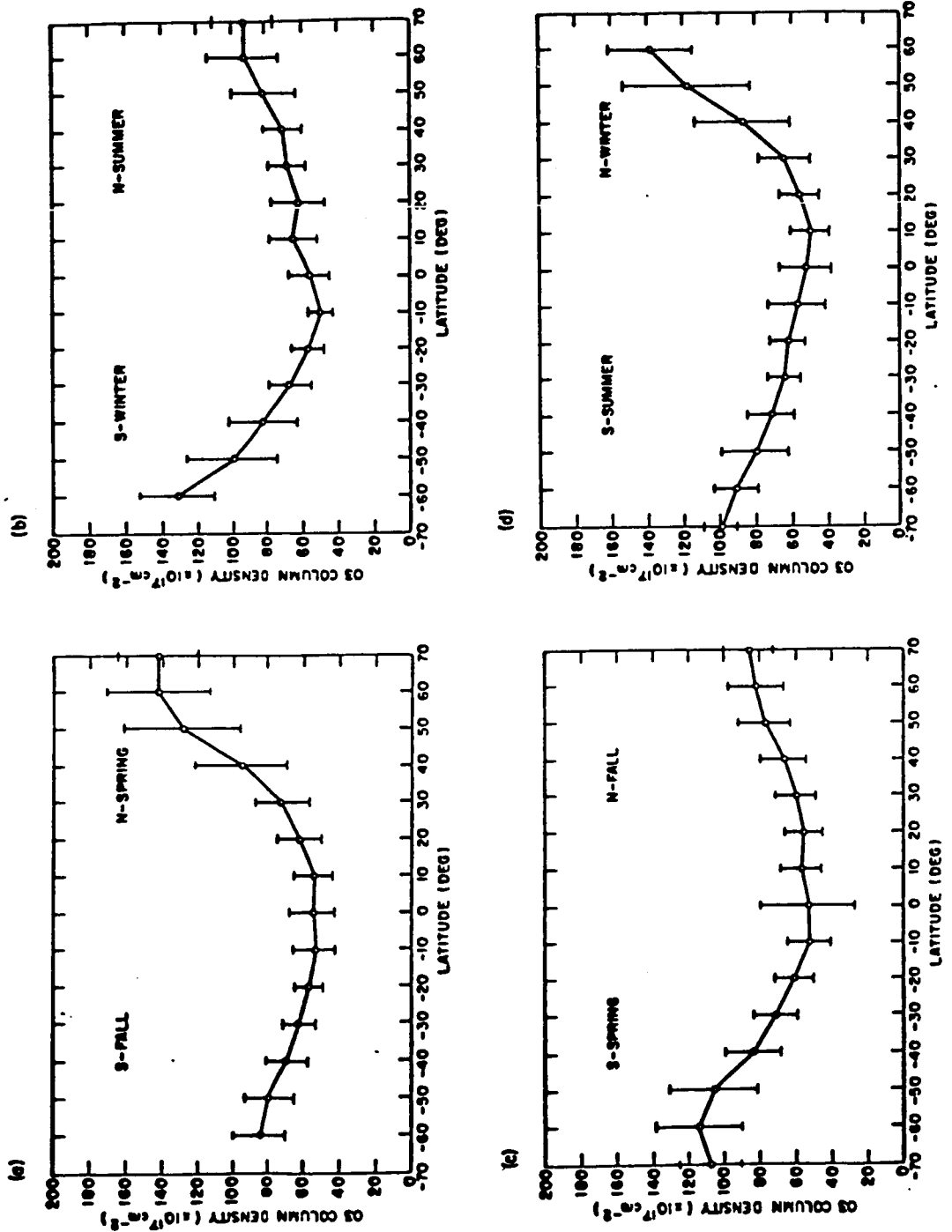


Figure 2.8. Seasonal variation of total ozone. Vertical bars are the standard deviations at corresponding latitude bins.

In order to identify SAM II events that are affected by calibration, a computer search was made for the apparent high extinction that appears on the SAM II extinction profile. The computer program integrates the SAM II extinction profiles over the altitude range 26-30 km and has been applied to all data obtained between 1978 and 1981. For later years, which contained high altitude extinction enhancements as a result of the eruption of El Chichon, the integration range was shifted to 31-35 km. A list of orbit numbers for those orbits then judged to be affected by calibration are listed in Table 2.6. In this table, asterisks mark those orbits for which no clear conclusion was possible. Data that were not available on the microfiche, but which showed an obviously high extinction, are shown in Table 2.7.

## 2.5 Production of a 16 mm Movie Film of SAM II Data

In order to observe the temporal variation of the aerosol extinction coefficient, especially the generation, movement and disappearance of polar stratospheric clouds, a computer program was written to generate a 16 mm movie film from the SAM II data set. In this movie, the aerosol extinction contours are shown within a height versus longitude frame. The height range is fixed from 5 km to 30 km, while the longitude range is fixed from  $-180^{\circ}$  to  $180^{\circ}$ . SAM II sunrise observations occur only in the Southern Hemisphere while sunset observations occur in the Northern Hemisphere. In order to show the aerosol behavior in each hemisphere independently, the sunrise and sunset events are separated into two different sequences. Each frame of the movie for either hemisphere is generated using a single day's sunrise or sunset data. The date and the latitude of the first observation on each day are shown at the top of each frame. In addition, the position of the tropopause is shown by a solid line with dots on it.

TABLE 2.6. Calibration Orbits Occurring in SAM II Data.  
November 1978 - February 1983.

Year	Orbit Number	Month/Day	SAM II Week	ISUN
1978	490	Nov 28	006	0
	797	Dec 20	009	1
1979	1552	Feb 13	017	0
	1773	Mar 01	019	0
	2105	Mar 25	023	0
	2105	Mar 25	023	1
	2568	Apr 28	027	0
	2568	Apr 28	027	1
	2928	May 24	031	0
	3259	Jun 16	034	0
	3259	Jun 16	034	1
	3591	Jul 11	038	0
	3591	Jul 11	038	1
	3923	Aug 04	041	0
	4254	Aug 28	045	0
	4586	Sep 12	048	0
	4586	Sep 12	048	1
	5097	Oct 28	054	1
	5249	Nov 08	055	1
	5560*	Nov 30	058	1
	5581	Dec 01	059	0
	5915	Dec 26	062	0
1980	6244	Jan 19	065	0
	6576	Feb 12	069	0
	7239	Mar 31	076	0
	7571	Apr 24	079	0
	7903	May 18	083	0
	8567	Jul 05	089	0

TABLE 2.6 (Cont'd)

Year	Orbit Number	Month/Day	SAM II Week	ISUN
1980 (cont'd)	8567	Jul 05	089	1
	8897	Jul 29	093	1
	9561	Sep 15	100	0
	9892	Oct 09	103	0
	10225	Nov 02	107	1
	10887	Dec 02	113	1
1981	11219	Jan 13	117	0
	11549	Feb 05	120	0
	11549	Feb 05	120	1
	11882	Mar 02	124	0
	11882	Mar 02	124	1
	12214	Mar 26	127	0
	12878	May 13	134	0
	13210	Jun 06	137	1
	13873	Jul 24	144	1
	14205	Aug 17	148	0
	14536	Sep 01	151	0
	14868	Oct 04	155	0
	15533	Nov 21	161	0
1982	15863	Dec 15	165	0
	16195	Jan 08	168	0
	16195	Jan 08	168	1
	16858	Feb 25	175	0
	16858	Feb 25	175	1
	17190	Mar 21	179	0
	17190	Mar 21	179	1
	17521*	Apr 14	182	1
	17853	May 08	185	1
	18185	Jun 10	189	0
	18185	Jun 10	189	1
	18517	Jun 25	192	0
	18517	Jun 25	192	1

TABLE 2.6 (Cont'd)

Year	Orbit Number	Month/Day	SAM II Week	ISUN
1982 (cont'd)	18848	Jul 19	196	0
	18848	Jul 19	196	1
	19512	Sep 05	203	0
	19512	Sep 05	203	1
	19844	Sep 29	206	0
	19844	Sep 29	206	1
1983	21834	Feb 20	227	1

TABLE 2.7. Orbits Showing High Extinction Above 26 km for which  
No Microfiche is Available

Year	Orbit Number	Month/Day	SAM II Week	ISUN
1979	5130	Oct 30	054	1
	5133	Oct 30	054	1
1980	6033	Jan 03	063	1
	6034	Jan 03	063	1
1982	21148	Dec 31	219	1

Two movies were generated from the developed software. One movie shows polar stratospheric clouds in the northern winter of 1978 (sunset observations only). The other movie shows polar stratospheric clouds in the Southern Hemisphere winter of 1979 (sunrise observations only). The development of polar stratospheric clouds and their apparent vertical movement associated with the vertical variation of the tropopause height are clearly shown in these films (these films have been delivered to NASA).

A contour plot of SAM II extinction data used in the generation of a 16mm film is shown in Figure 2.9.

## 2.6 Comparison of SAM II and SAGE I Data

The SAM II and SAGE I satellite experiments are each designed to measure stratospheric aerosol extinction coefficients using the technique of solar occultation or limb extinction. Both SAM II and SAGE I have an aerosol measurement channel centered at  $1.0 \mu\text{m}$  wavelength, and have a similar optical bandpass and instrument field of view. There are occasions when the measurement locations of the two satellites are nearly coincident, providing opportunities for a measurement comparison.

In this study, the aerosol extinction profile and daily contour plots for the coincident events in 1979 have been compared. The first approach was to compare individual SAM II and SAGE measurement profiles obtained on the same day and within  $1^\circ$  in both longitude and latitude. It was found that there are thirteen profiles in 1979 that satisfy this criterion. The second approach was to compare the daily aerosol extinction contour plots for the two satellites. Again, comparisons were made when the difference between the latitude coverages of SAM II and SAGE I was  $1^\circ$  or less. It was found that there were eighteen daily contour plots in 1979 that satisfy this criterion.

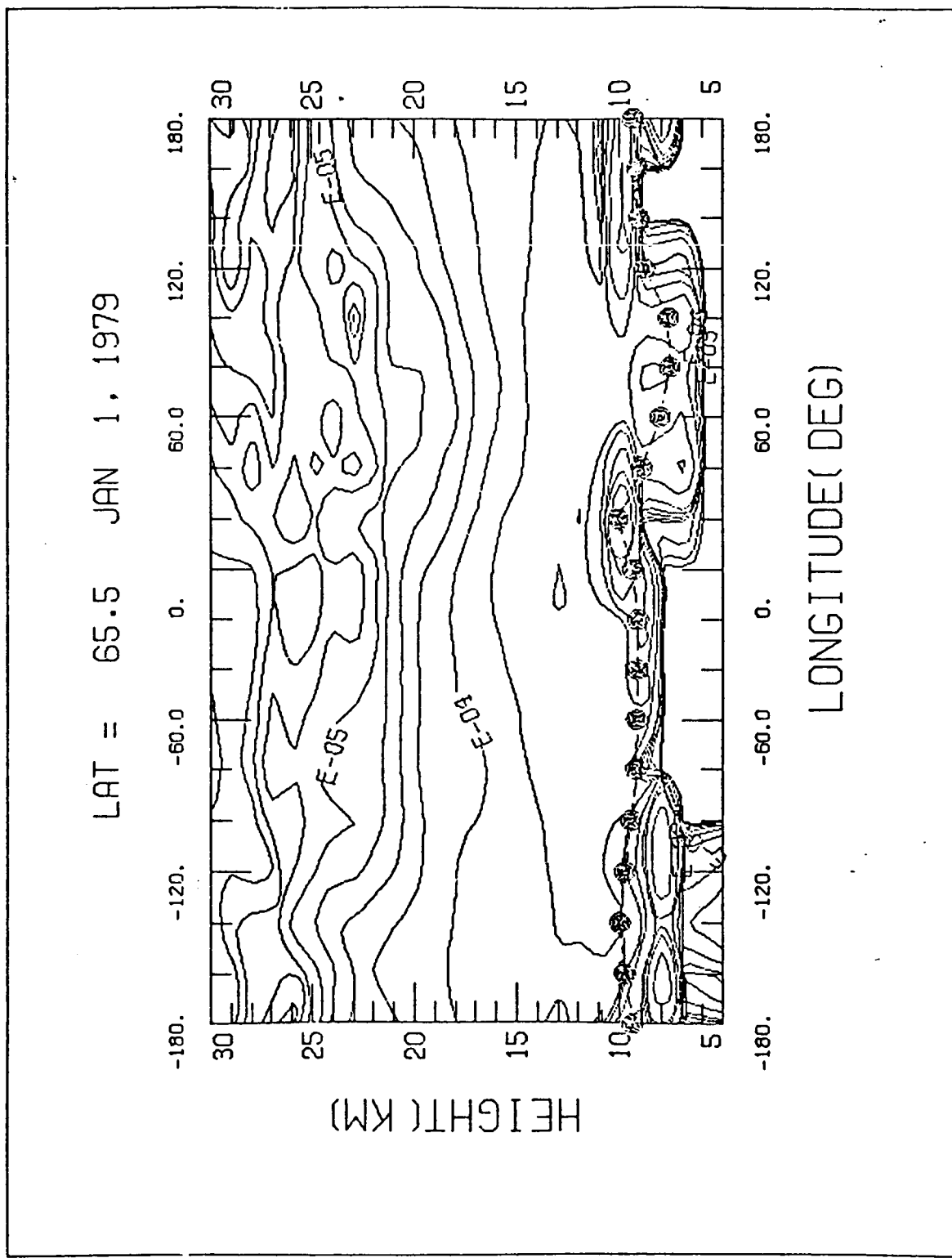


Figure 2.9. Contour plot of SAM II extinction data used in the generation of 16mm film.

After carefully comparing the individual profiles of aerosol extinction and daily contour plots obtained by SAM II and SAGE I for occasions when the measurements were nearly coincident in time and space, we concluded that both profiles and daily contour plots agreed within the uncertainties associated with each experiment. Thus, because SAM II profiles are in good agreement with results obtained using more conventional remote and in situ sensors, the results of this study validate the data obtained with the SAGE I, 1.0  $\mu\text{m}$  sensor channel.

This work has been published in the Journal of Geophysical Research (Yue et al., 1984) and the Abstract to this publication is reproduced as Appendix A.

## 2.7 Polar Stratospheric Cloud Studies

Polar stratospheric clouds (PSC's) appear on the SAM II data as enhancements in the 1  $\mu\text{m}$  aerosol extinction at altitudes between zero and ten kilometers above the tropopause; a few sightings of these clouds have also been found in the SAGE I data set. PSC's occur only at high latitude, in winter, when the ambient stratospheric temperature falls below about 195K. Their characteristics, as seen on the satellite data, and theories of their formation have formed the basis of several publications by members of the Aerosol Research Branch, LaRC (McCormick et al., 1981, 1982, 1985; Steele et al., 1983, Hamill and McMaster, 1984). As part of the work carried out under this contract, a study was made of the occurrence statistics for PSC's and this work has formed the subject of a NASA Contractor Report (Farrukh 1985). Data for both hemispheres were studied for the period 1978-1982. The following features were examined in particular:

1. The increase in extinction (for a PSC) relative to the extinction of the background (non PSC) aerosol.
2. The altitude variation of minimum stratospheric temperatures.
3. The longitudinal distribution of PSCs.
4. The longitudinal distribution of minimum stratospheric temperatures.
5. The probability of occurrence of PSCs as a function of minimum stratospheric temperature.

Principal findings from this analysis are summarized in the abstract to the report cited above (Farrukh 1985) which is reproduced as Appendix B. Part of the material has also been included in a further publication (McCormick et al., 1985). The abstract for the publication is included as Appendix C.

#### **2.8 Study of Aerosol Concentrations Near the North Polar Vortex (includes work carried out under Task Area 7)**

Airborne lidar measurements made in the arctic region in January 1983 showed strong gradients in aerosol concentration to exist across the region of the polar night jet stream. Similar differences were observed in the SAM II data taken at the same time as the lidar flights, indicating that for altitudes between 18 and 26 km, the aerosol concentrations within the polar vortex were about one order of magnitude lower than that outside. This analysis has been published (McCormick et al., 1983) and the abstract is reproduced as Appendix D. The observations just outlined were made shortly after the eruption of El Chichon had injected a very large quantity of fresh aerosol into the stratosphere. It was not clear whether the aerosol concentration variations observed were entirely due to the action of the

north polar vortex or if there may have been some effect of inhomogeneities in concentration remaining from the volcanic eruption. Partly because of this uncertainty and also because of a need to investigate the underlying mechanisms, an indepth study was made of the aerosol extinction in high latitudes in the northern winter of 1978-1979, as measured by SAM II. These studies confirmed that the concentration changes were produced as the result of dynamical changes associated with the north polar vortex. Subsidence was observed to occur within the vortex, bringing air down from higher altitudes containing a lower aerosol concentration and mixing out air with a high aerosol concentration through the base of the vortex. Rates of subsidence were established and a base for the vortex was determined at an altitude of about 14 km. This work has been published in the Journal of the Atmospheric Sciences (Kent et al., 1985a) and the abstract is reproduced as Appendix E.

## 2.9 Tropospheric Aerosol Climatology

As part of a program of work carried out under NASA Contract NAS8-35594, a study was made of aerosol extinction values measured by SAM II and SAGE I for altitudes below the tropopause (Kent et al., 1985b). The SAM II and SAGE I satellites were designed for stratospheric use but it was found that, in the absence of high altitude cloud, tropospheric measurements are not only possible, but are available from a significant fraction of the total number of measurement opportunities. In the previous work, SAM II data for October 1978 - October 1979 and SAGE I, 1  $\mu\text{m}$  data for October 1979 - November 1981 were studied in terms of the probability distribution of extinction values at different altitudes and latitudes. The 50% probability level or median extinction was chosen as a measure of central tendency for the extinction values. The main results to emerge from this analysis were:

1. Median extinction values in the Northern Hemisphere for altitudes between 5 and 10 km were one-half to one order of magnitude greater than in the Southern Hemisphere.
2. A seasonal variation by a factor of 1.5 - 2 was observed in both hemispheres with maximum extinction being observed in local Spring and Summer.
3. Following major volcanic eruptions, a long-lived enhancement of the aerosol extinction was observed for altitudes above 5 km.

Further analysis of the tropospheric data from SAGE II, as well as SAM II and SAGE I, has continued under Contract NASI-18252 and also under the present contract. The work under the current contract has concentrated upon the SAM II data, of which only one year (October 1978-October 1979) was previously studied. The emphasis of the newer work has been to use the aerosol/molecular extinction ratio as the parameter to be studied, rather than the extinction itself. The former is a quantity which, to a first order of approximation, is conserved under transport and thus more suitable for use in a region where both horizontal transport and vertical convection can occur. In addition, instead of using the median as a description of aerosol properties, the probability distribution has been examined for modes (most probable values) in the extinction ratio. The variation of these with altitude and season has then been studied. In both present and past analyses, we have tended to use a logarithmic scale to describe the aerosol extinction or extinction ratio. This choice has been necessitated by the large dynamic ranges for these variables found in the tropospheric data.

Figure 2.10. shows a typical extinction ratio probability distribution for SAM II data. This histogram shows the frequency of occurrence of various

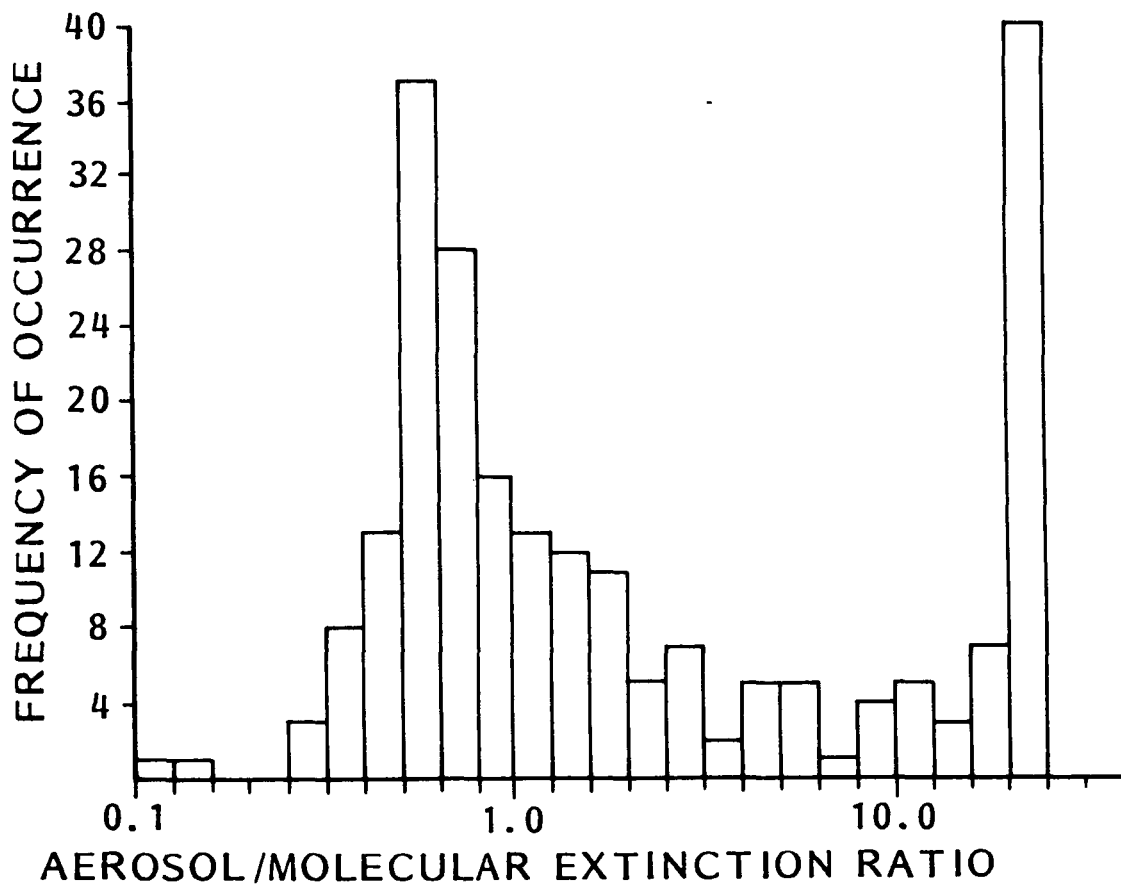


Figure 2.10. Histogram showing frequency of occurrence of different values of aerosol/molecular extinction ratio. SAM II data, November 19 - December 16, 1979, Northern hemisphere. Data are for an altitude of 7 km.

values of extinction ratio for one month of SAM II data taken in the Northern Hemisphere. The data is for an altitude of 7 km and was taken between November 19 and December 16, 1979. The extinction ratio is shown on a logarithmic scale, each interval in the histogram corresponding to a change of 0.1 in the logarithm of the extinction ratio. The histogram clearly shows two maximas, one at an extinction ratio of about 0.6 and the other at a value of about 22. The former is believed to be associated with the tropospheric aerosol but the latter, which lies at the threshold of measurement of the satellite instrument (at this altitude) is believed to be associated with subvisible clouds. Support for this interpretation is given by the multiwavelength SAGE I and SAGE II data which show similar modes. For data from these two satellites, it is possible to calculate the ratio of the extinction at a shorter wavelength (0.45  $\mu\text{m}$  for SAGE I or 0.525  $\mu\text{m}$  for SAGE II) to that at 1  $\mu\text{m}$ , for the same altitude and the same event. It is found that such ratios, for the mode just identified as aerosol, typically have values around 2 or 3. For the other mode, this ratio is normally around unity. The latter is to be expected for larger cloud particles, lending credence to the interpretation just given.

It is possible to study the manner in which the tropospheric aerosol modes, as just described, vary with both altitude and season in either hemisphere. The results of this study are shown in Figure 2.11 in the form of a shaded contour plot. The time period covered in the plot is October 1979 - September 1981, the data being divided into four-week time segments. The altitude range is from 5 to 15 km, with a vertical resolution of 1 km. The horizontal bars on the diagram show the mean altitude of the tropopause for each four-week period. The interval 5-15 km was chosen to show behavior in the lower stratosphere, as well as that in the upper troposphere. Some

tropospheric data below 5 km is available but the quantity is low and statistical fluctuations in the mode values are large; for this reason, it has not been plotted. It may also be noted that Figure 2.11 shows some data missing above 5 km; this occurrence is common after volcanic injection into the upper troposphere and lower stratosphere has raised the extinction to such a level that the signal received from the sun at the satellite falls below the threshold of detection of the instrument. The quantity plotted in the figure is the aerosol/molecular extinction ratio at the aerosol mode as shown in Figure 2.10. Six levels of extinction ratio are shown covering most of the values encountered in the non-volcanic situation.

Figure 2.11(a) shows data for the Antarctic Region. In the stratosphere, the seasonal cycle is clearly evident with extinction maxima occurring in June-August in each year (associated with the formation of polar stratospheric clouds). There is also a gradual increase in the extinction ratio between 1979 and 1981, most likely associated with the eruption of Sierra Negra in late 1979. In the troposphere, there is a high degree of vertical uniformity in extinction ratio. There is also a weak seasonal cycle with minimum values in the April-July time frame. Figure 2.11(b) shows the variation of the same quantity for the Northern Hemisphere. In general, values are higher than in the Southern Hemisphere even before the eruptions of St. Helens in 1980 and Alaid in 1981 produced very high extinction ratios. There is also a strong seasonal cycle with maxima in the summer period that is partially masked by the volcanic effects in 1980-1981. Summer 1979 and late Spring 1980, prior to the May eruption of St. Helens, show uniformly high values of extinction ratio up to the tropopause indicating a high degree of vertical mixing. The winters of 1978-1979, 1979-1980, and

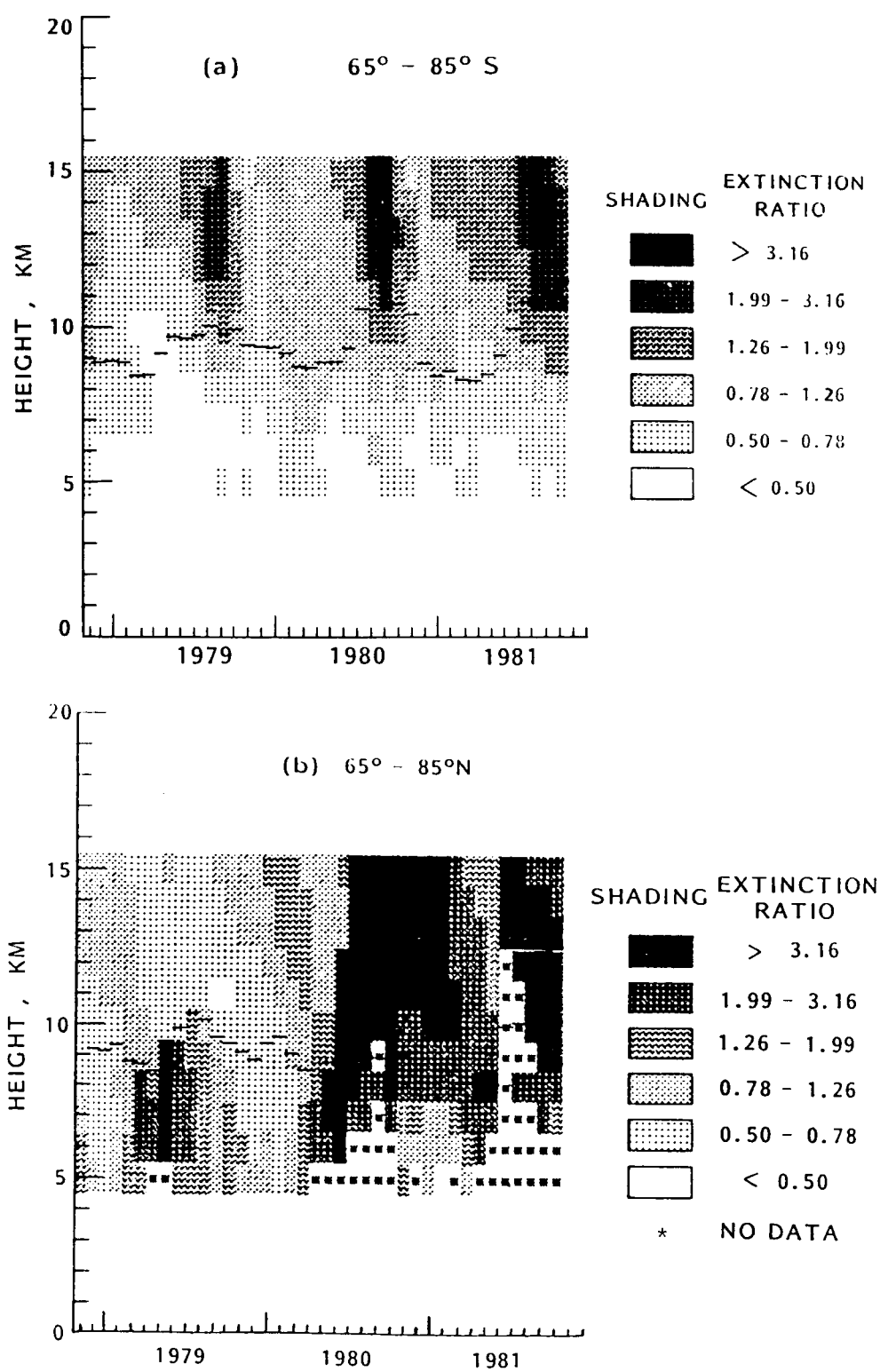


**Figure 2.11.** Shaded contour plots of SAM II aerosol/molecular extinction ratios for (a) Southern hemisphere, (b) Northern hemisphere, October 1979 – September 1981. Time interval is four weeks, height interval is one kilometer. The short horizontal bars on the plots show the tropopause altitudes.

1980-1981 show low extinction ratios (as in the Antarctic Region), even in 1980-1981 when the volcanic effects might be expected to be important.

#### In summary

1. Extinction ratio values are higher in the Northern Hemisphere.
2. There is a seasonal cycle in both hemispheres with maxima in local Spring-Summer and minima in local fall-winter.
3. There is a high degree of vertical uniformity in the extinction ratio for altitudes between 5 km and the tropopause.
4. Volcanic effects are strong in the upper troposphere, as well as the stratosphere but do not totally mask the seasonal cycle.

#### 2.10 The Aging Process of Aerosol Particles in the Stratosphere

In situ measurements of stratospheric aerosols at different latitudes have shown that large numbers of small particles exist in the tropical zone, and that the aerosol layer extended from higher altitudes near the equator to lower ones at higher latitudes. This behavior indicates that the upper troposphere in tropical regions may be a source of condensation nuclei in the stratosphere and that these particles mature as they move to higher altitudes and latitudes.

In this study, the aerosol extinctions measured at 0.45  $\mu\text{m}$  and 1.0  $\mu\text{m}$  from the SAGE I data set were utilized to deduce the aerosol size distribution (See Section 7.1. Retrieval of Aerosol Properties from Aerosol Extinction Ratios at 0.45  $\mu\text{m}$  and 1.0  $\mu\text{m}$ ). In order to find out the latitudinal and altitudinal variation of the aerosol size distribution, the atmosphere was divided into a grid consisting of 1 km intervals in altitude

and  $5^{\circ}$  intervals in latitude. The altitudes under consideration ranged from 10 km to 25 km and the latitudes from  $55^{\circ}$ S to  $50^{\circ}$ N. The 25 km upper limit for altitude was necessary since  $0.45 \mu\text{m}$  extinction values at altitudes above 25 km have much larger error bars. For each gridpoint, the average value of the ratio of extinctions at the two wavelengths for the same month of SAGE I data was calculated. This value was then converted to mode radius in the assumed lognormal size distribution of aerosol particles. The variation of mode radius with latitude and altitude was then studied. Although only March 1979 and April 1979 data were analyzed, our results support the view that aerosols grow as they rise through the stratosphere as predicted by the modeling results of Turco et al., (1979) and concluded by different experimentalists, including Bigg (1976), Farlow (1979), and Oberbeck et al., (1981). This work has been published in Geophysics Research Letters (Yue and Deepak, Geophys. Res. Lett., 11, 999-1002, 1984). The abstract is included as Appendix F.

3. TASK 2--TO INVESTIGATE THE CORRELATION OF STRATOSPHERIC AEROSOLS,  $O_3$  AND  $NO_2$ , WITH EACH OTHER AND VARIOUS METEOROLOGICAL PARAMETERS

3.1 Correlation Between Aerosol Optical Properties and 30 mb Pressure Height  
(includes work carried out under Task Area 7)

3.1.1 Introduction

Aerosol optical depths at 1  $\mu m$  wavelength above 18 km, derived from the Stratospheric Aerosol Measurement (SAM II) on February 1, 1983, were shown to be lower by approximately one order of magnitude within the polar vortex than those outside (McCormick et al., 1983). This result indicates the effect of winter circulation on the distribution of aerosols during the winter season. The downward motion<sup>1</sup> in the polar region during the development stage of the circumpolar vortex, can be the major reason for this feature since the aerosol extinction decreases with altitude. Furthermore, the relatively low aerosol optical depth is also evident during periods of stratospheric warmings when the circumpolar vortex is substantially disturbed by amplified planetary waves, (Wang and McCormick, 1985; see also Section 5.2). The reason for this is that the air mass within the low pressure system(s) is largely able to preserve its polar characteristics as the planetary waves intensify. Cross-contour mixing is rather inefficient due to the prevailing geostrophic balance, (Wang and McCormick, 1985; See Section 5.2). Aerosol extinction data from both SAM II and SAGE for four selected days in different years taken in the high latitude Northern Hemisphere, were used in that analysis. (The results obtained have been further substantiated using SAGE  $O_3$  and  $NO_2$  data.) The results of Wang and McCormick (1985), suggest that a significant

-----  
1. The development of the downward motion and the polar vortex has been discussed in the model analyses by Leovy (1964) and Holton and Wehrbein (1980), and also in the texts by Craig (1965) and Holton (1975).

correlation exists between the aerosol optical depth (above 20 km) and the height at 30 mb pressure level. The work presented here is devoted to the investigation of this correlation. In this study, we have used almost all the SAM II measurements during periods when the stratospheric planetary waves are most active.

### 3.1.2 Approach

The Arctic extinction profiles from January to March of the first four years of SAM II measurements (1979-1982) have been used to study the linear correlation between aerosol optical depth and 30 mb height. The extinction profiles for the same period in 1983 are found showing enhanced aerosol loading due to the effects of the El Chichon volcanic eruption. For this reason, the SAM II measurements made in 1983 have not been included in this study. In addition, large variations in extinction associated with polar stratospheric clouds have been reported (McCormick et al., 1982). For our purpose, it was necessary to filter out those special events by including only profiles above 14 km for which the SAM II extinction ratio is less than 4. We have also investigated the results obtained when using extinction ratios of 3.5 and 4.5 as the criterion. The change in the calculated results was found to be less than 2% using these three alternatives.

### 3.1.3 Results and discussion

The analysis of the linear correlation between aerosol optical depth (above 20 km) and the height of the 30 mb pressure level for January-March 1979 is displayed in Figure 3.1. In the derivation of the correlation coefficient, the 30 mb height has been taken as the dependent variable. There are 1036 data pairs in this 1979 case. The constant (a) and slope (b) for a linear least-square fit were found to be 22.1 and  $2.69 \times 10^3$ ,

ORIGINAL PAGE IS  
OF POOR QUALITY

1979  
JANUARY-MARCH

LINEAR CORRELATION,  $y = a + bx$

$$a = 22.1, b = 2.69 \times 10^3$$

LINEAR CORRELATION COEFF = .834

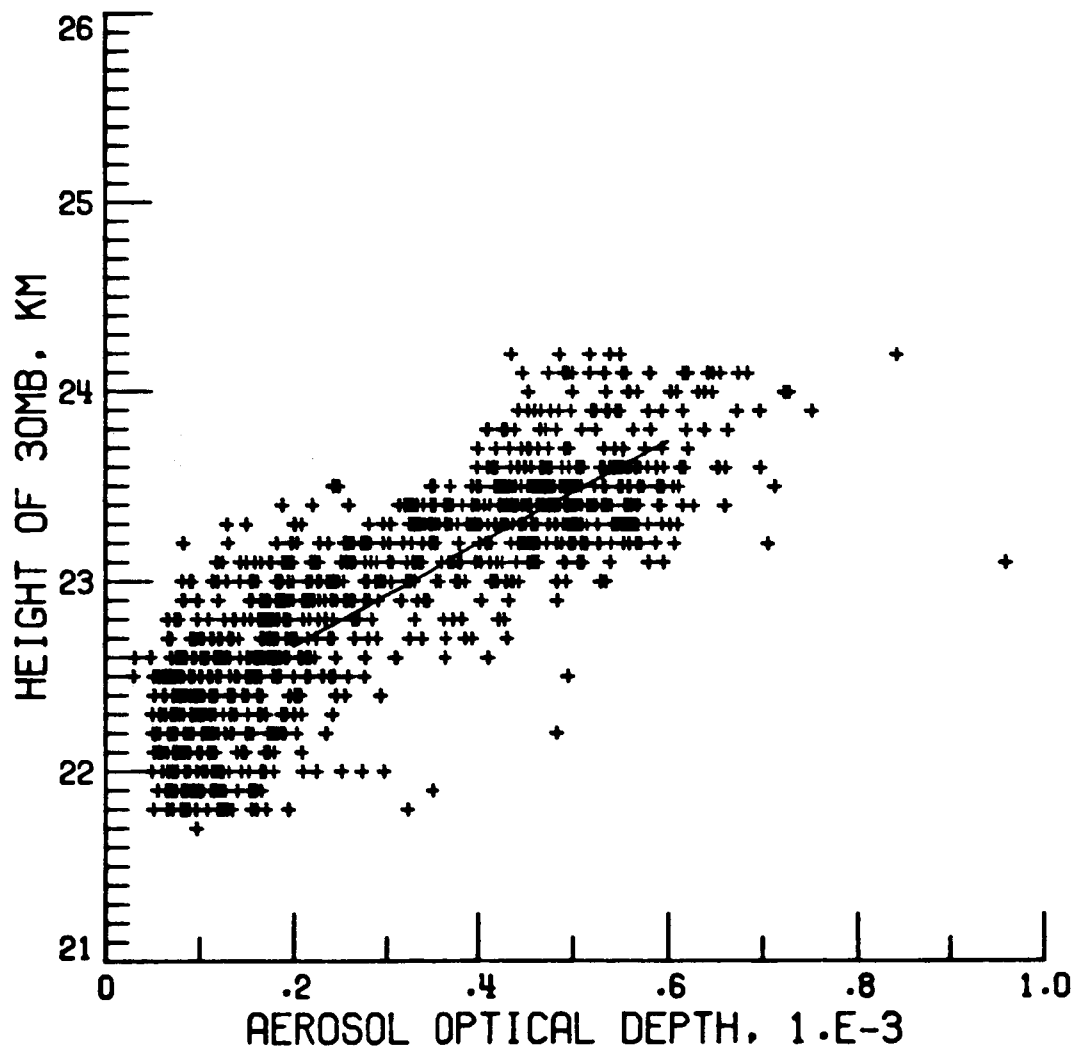


Figure 3.1. Linear correlation between SAM II aerosol optical depth (above 20 km) and associated 30 mb height for data from January to March 1979.

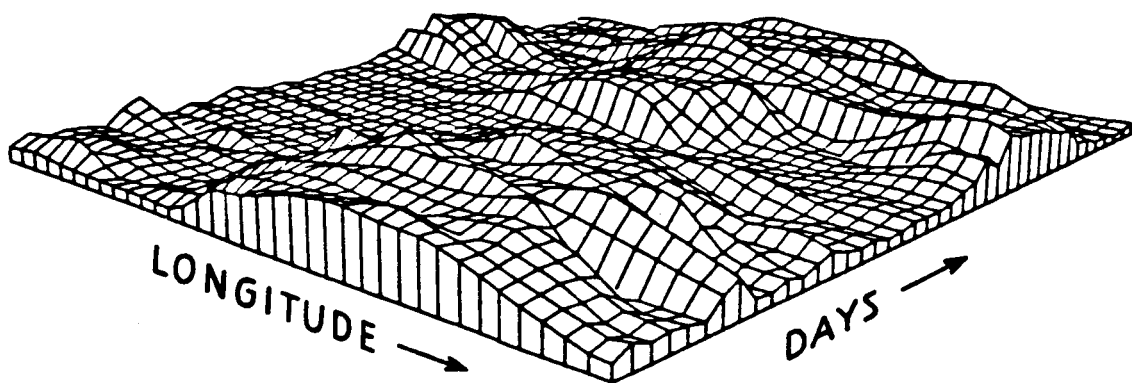
respectively. The computed linear correlation coefficient is 0.834. This result indicates a significant positive correlation between the aerosol optical depth and the 30 mb height. This relationship is also illustrated in Figure 3.2 which shows 3-D projective plots of the aerosol optical depth (Figure 3.2a) and the 30 mb height (Figure 3.2b) as functions of longitude and time (day). The period for these plots is from February 24 to March 2, 1979. Although the results for aerosol optical depth (Figure 3.2a) exhibit more fine structures than that of height field, their spatial and temporal variations are, as a whole, similar.

The results for the 1980 data are given in Figure 3.3. In this case, the coefficients  $a$  and  $b$  are found to be 22.3 and  $1.81 \times 10^3$ , respectively. The value of the linear correlation coefficient is 0.525, derived from 853 data pairs. In contrast to the 1979 case, the linear correlation in 1980 is relatively poor. We have investigated this particular case in some detail and will discuss the results later.

Figure 3.4 shows the results of the analysis for 1981. The number of data pairs used in this calculation is 647. The linear least-squares fitting yields a constant 22.4 and a slope  $2.47 \times 10^3$ . The calculated correlation coefficient is 0.753. Although this value is less than that of 1979 case, the linear correlation between aerosol optical depth and height is significant.

The result of the analysis for January-March 1982 is displayed in Figure 3.5. The number of data pairs employed in the calculation is 918. The values for  $a$  and  $b$  are found to be 22.1 and  $2.19 \times 10^3$ , respectively. The linear correlation coefficient is 0.812. Thus, there is a significant correlation between aerosol optical depth and 30 mb height. The degree of the linear

(a) AEROSOL OPTICAL DEPTH



(b) HEIGHT OF 30 MB

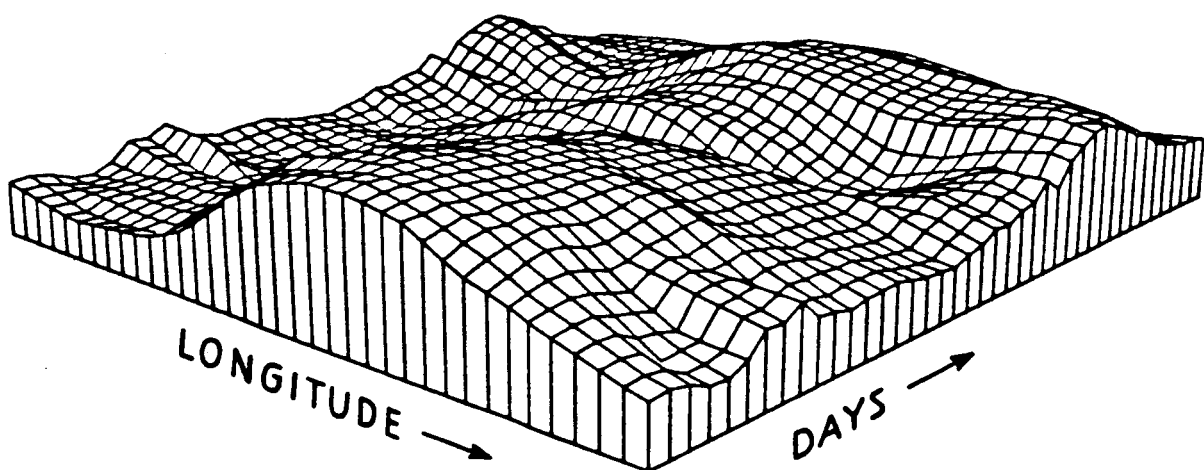


Figure 3.2. Projection plots of SAM II aerosol optical depth (a) and associated 30 mb height (b) as functions of longitude and time from January 24 - March 2, 1979.

PRECEDING PAGE BLANK NOT FILMED

1980  
JANUARY-MARCH  
LINEAR CORRELATION,  $y = a + bx$   
 $a = 22.3, b = 1.81 \times 10^3$   
LINEAR CORRELATION COEFF = .525

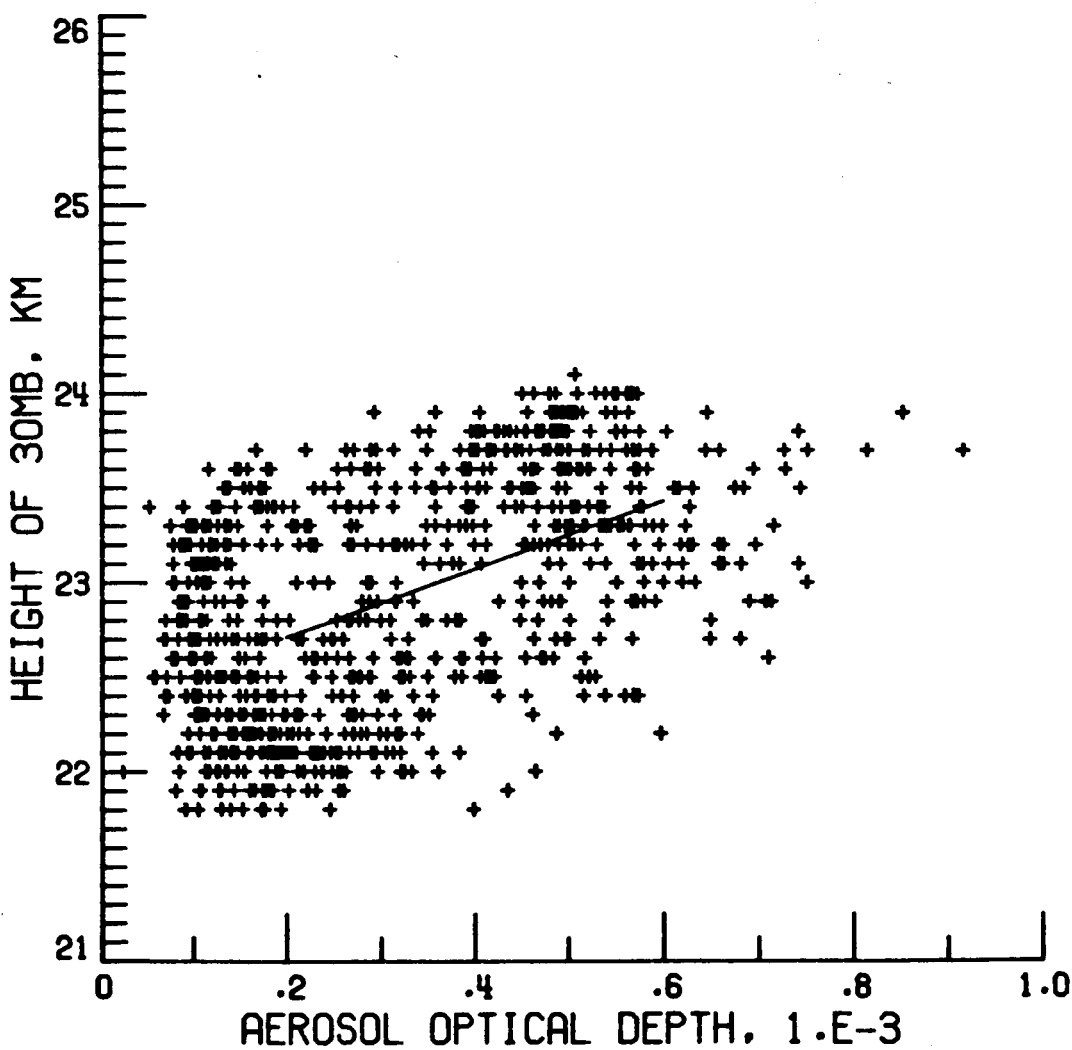


Figure 3.3. Linear correlation between SAM II aerosol optical depth (above 20 km) and associated 30 mb height from January to March 1980.

ORIGINAL PAGE IS  
OF POOR QUALITY

1981  
JANUARY-MARCH

LINEAR CORRELATION,  $y = a + bx$

$$a = 22.4, b = 2.47 \times 10^3$$

LINEAR CORRELATION COEFF = .753

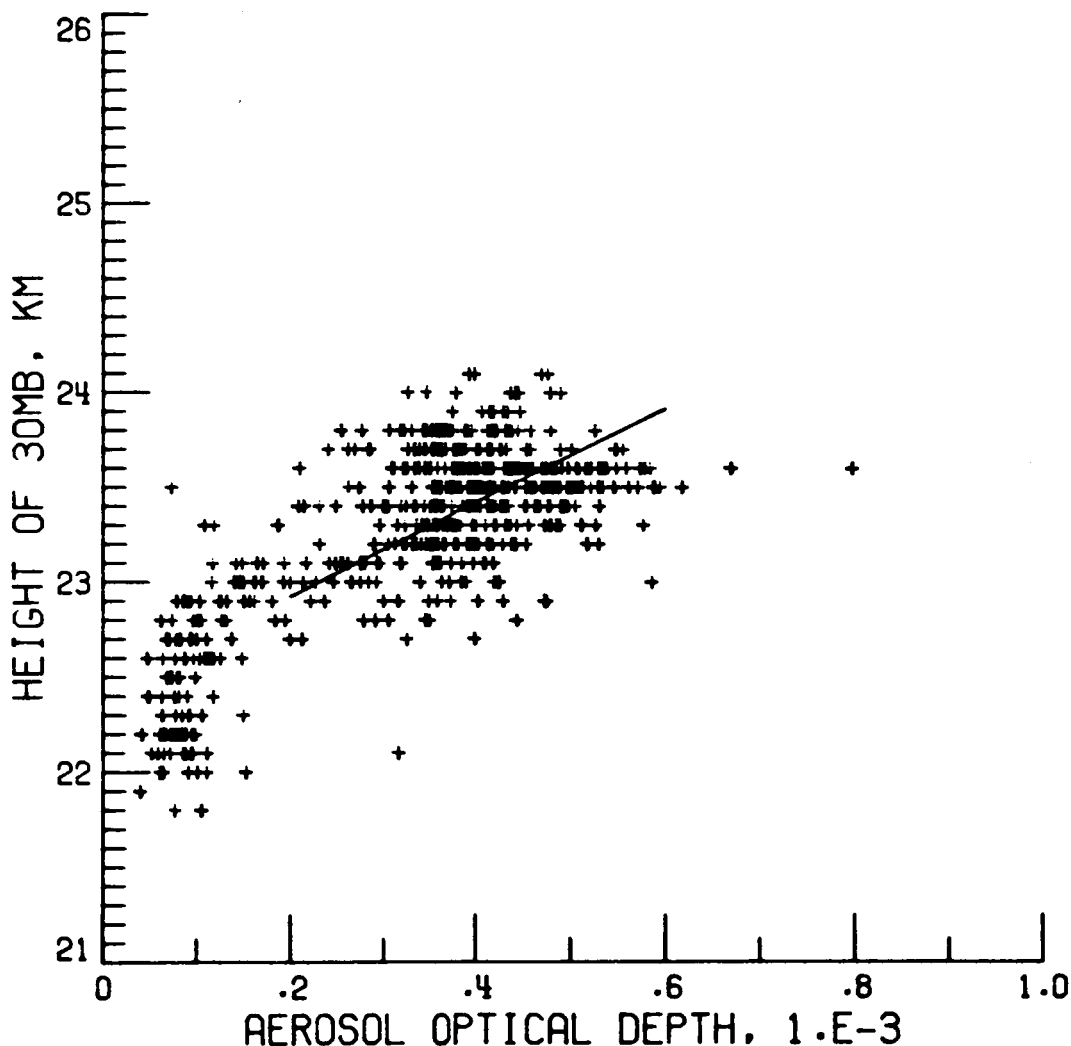


Figure 3.4. Linear correlation between SAM II aerosol optical depth (above 20 km) and associated 30 mb height from January to March 1981.

1982  
JANUARY-MARCH

LINEAR CORRELATION,  $y = a + bx$

$$a = 22.1, b = 2.19 \times 10^3$$

LINEAR CORRELATION COEFF = .812

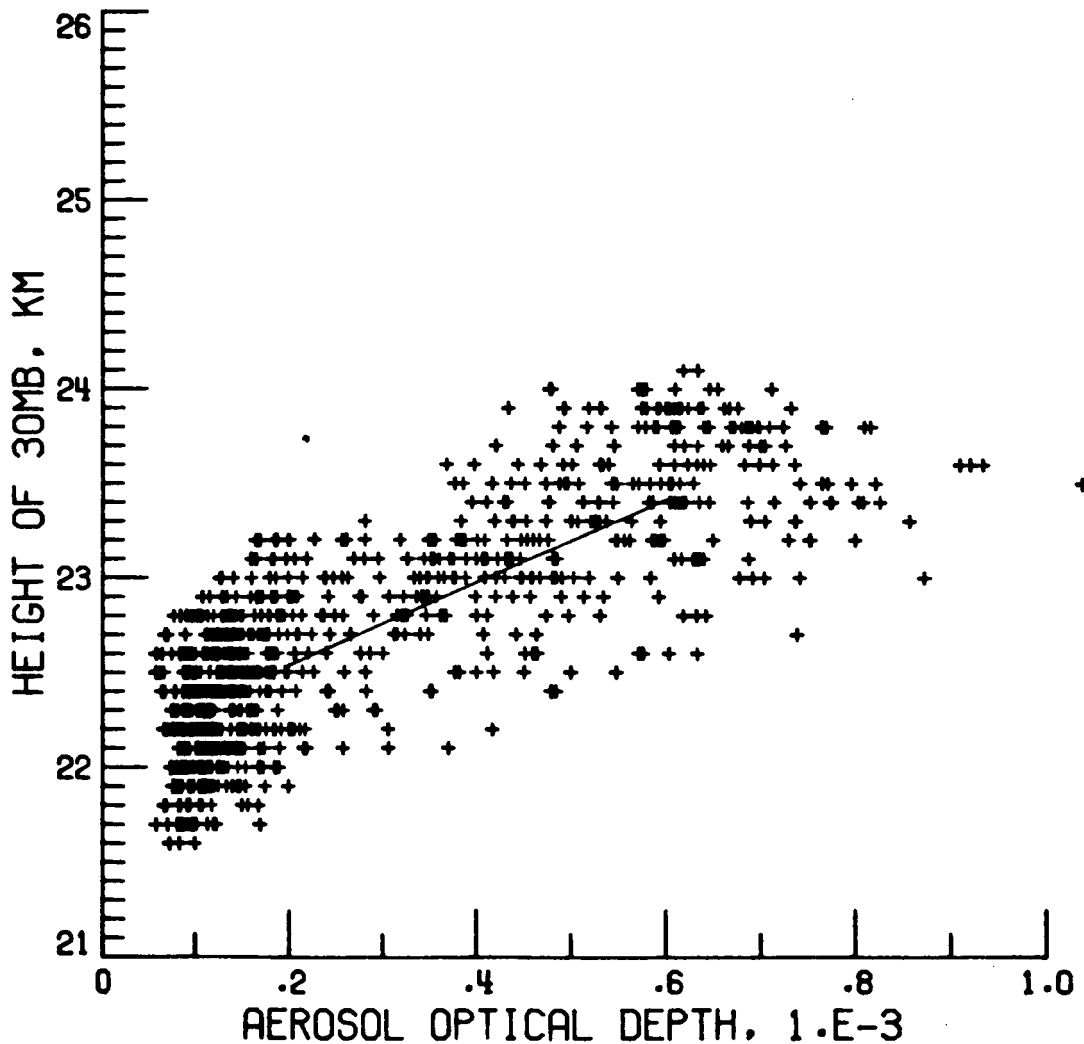


Figure 3.5. Linear correlation between SAM II aerosol optical depth (above 20 km) and associated 30 mb height from January to March 1982.

correlation shown in this case is comparable with that of 1979. Table 3.1 summarizes the results of the four described cases.

To examine the January-March 1980 case in detail, the correlation analysis has been applied separately to the three individual months of 1980. The results are shown in Figures 3.6a to 3.6c and are summarized in Table 3.2. As one may see, significant correlation values for the individual months are evident. A question is why the correlation is lower when it is evaluated with three months all together. It is found that the 30 mb heights for each of the three monthly data sets are substantially different from each other. This is apparent from Figure 3.7 where Figure 3.6 a-c are replotted on top of each other and are labelled differently for different months. The data pairs in January are shown by crosses (+), February by circles (o), and March by triangles( $\Delta$ ). The March data set as a whole is characterized by the highest 30 mb height, the January data set by the lowest, while the February data set is intermediate. Since the atmosphere is very close to hydrostatic equilibrium, the greater 30 mb height implies generally the higher temperature. This feature is evident in Figure 3.8 which also shows the SAM II extinction and the corresponding temperature at 30 mb. The data pairs for different months are labeled as in Figure 3.7. Figure 3.8 indicates that the temperature in March as a whole is indeed the highest, January has the lowest temperature, and that February is intermediate. In conclusion, the correlation for January-March 1980 (Figure 3.3) is strongly dependent upon the temporal variations of the stratospheric temperature in the polar region, which do not seem to be as significant in 1979, 1981, and 1982.

#### 3.1.4 Remarks

January to March aerosol extinction profiles from 1979 to 1982, derived from SAM II measurements and the associated meteorological information, have

TABLE 3.1. Linear Correlation between SAM II Aerosol Optical Depth and Associated 30 mb Height from January to March.

Year	No. of data points	a <sup>†</sup>	b <sup>†</sup> ( $\times 10^3$ )	$\sigma^*$
1979	1036	22.1	2.69	0.834
1980	853	22.3	1.81	0.525
1981	647	22.4	2.47	0.753
1982	918	22.1	2.19	0.812

<sup>†</sup>a and b are the coefficients of a linear least-squares fitting ( $y = a + bx$ )

\* $\sigma$  is the linear correlation coefficient.

1980  
JANUARY

LINEAR CORRELATION,  $y = a + bx$   
 $a = 21.9, b = 2.05 \times 10^3$   
 LINEAR CORRELATION COEFF = .748

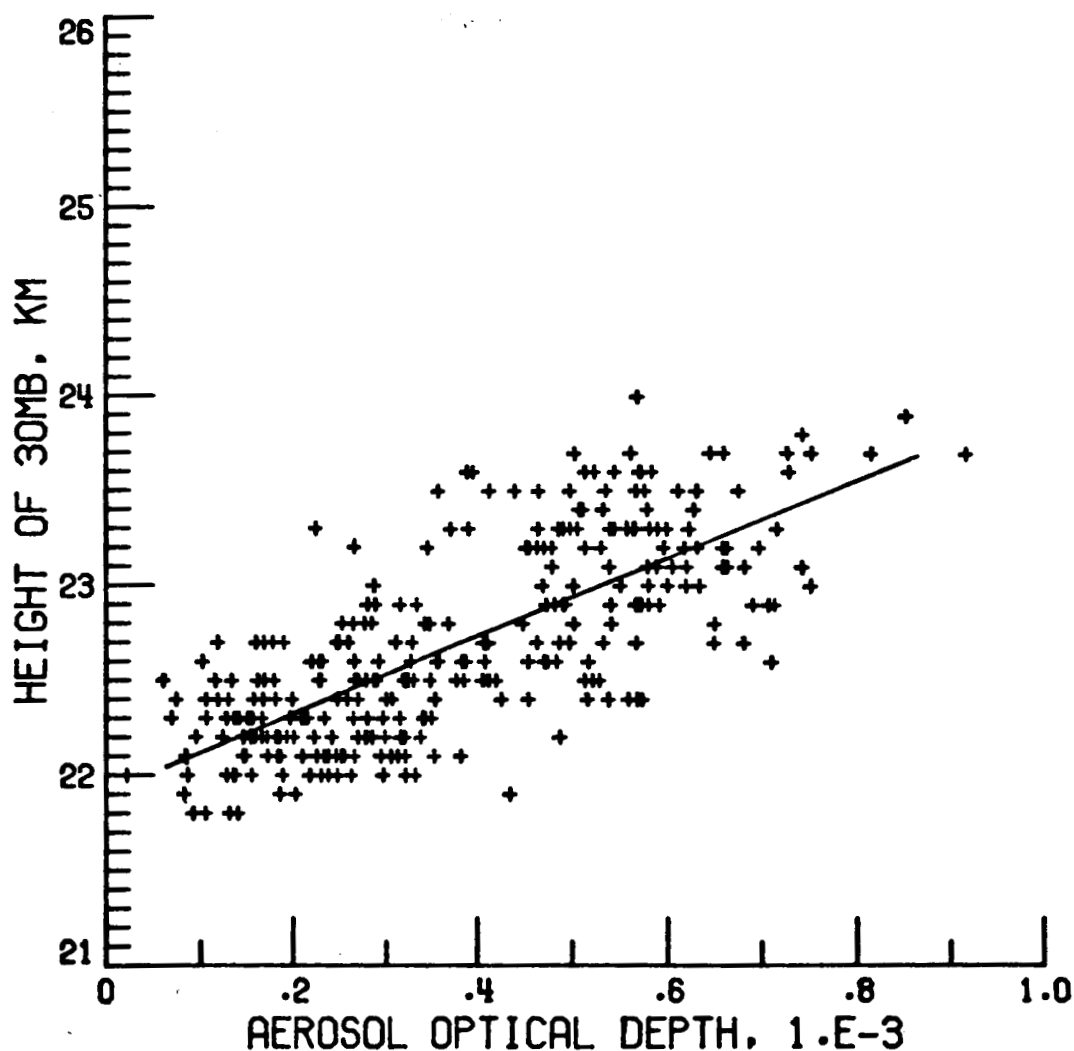


Figure 3.6. Linear correlation between SAM II aerosol optical depth (above 20 km) and associated 30 mb height for 1980. (a) January.

1980  
FEBRUARY  
LINEAR CORRELATION,  $y = a + bx$   
 $a = 21.8, b = 2.97 \times 10^3$   
LINEAR CORRELATION COEFF = .760

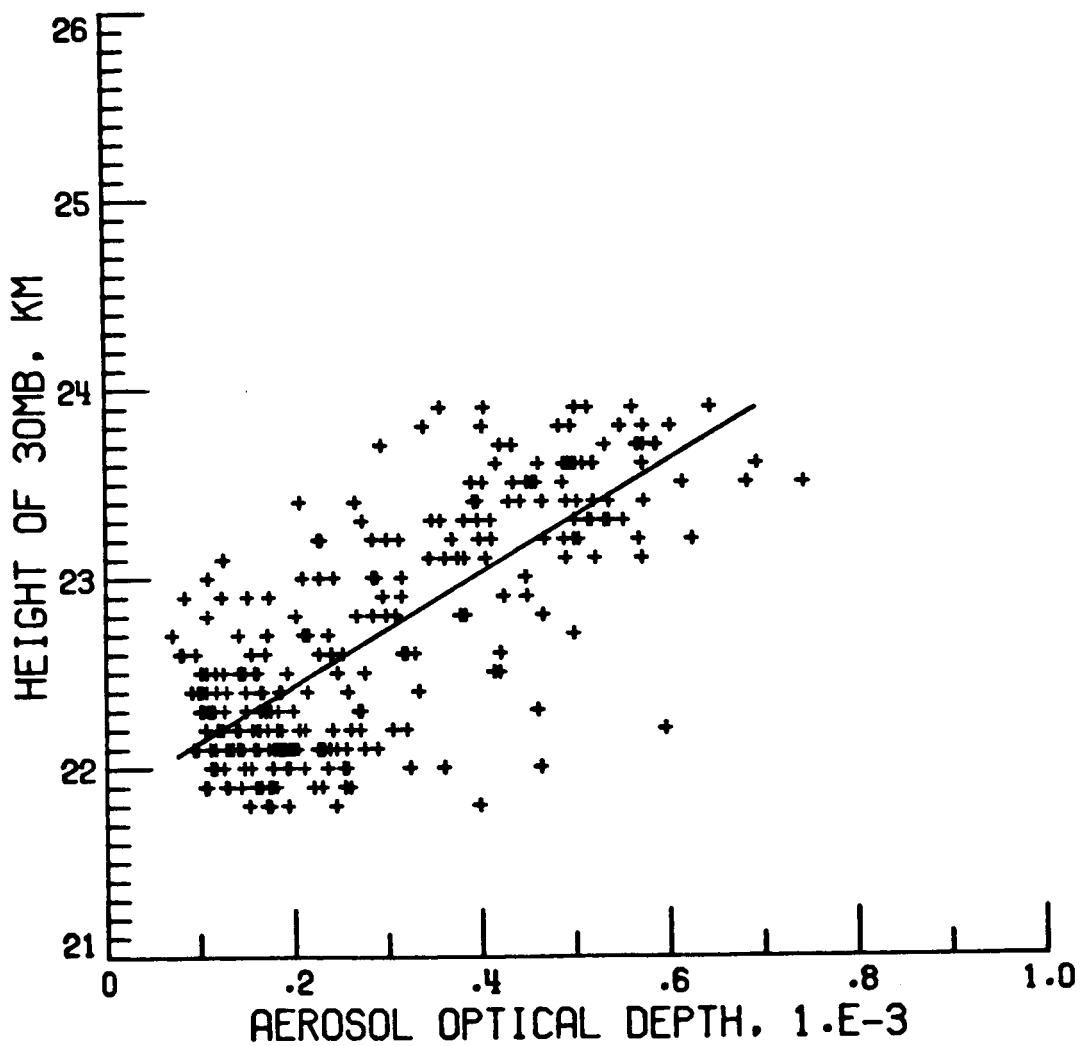


Figure 3.6 (continued). (b) February.

1980  
MARCH

LINEAR CORRELATION,  $y = a + bx$

$$a = 22.8, b = 2.10 \times 10^3$$

LINEAR CORRELATION COEFF = .813

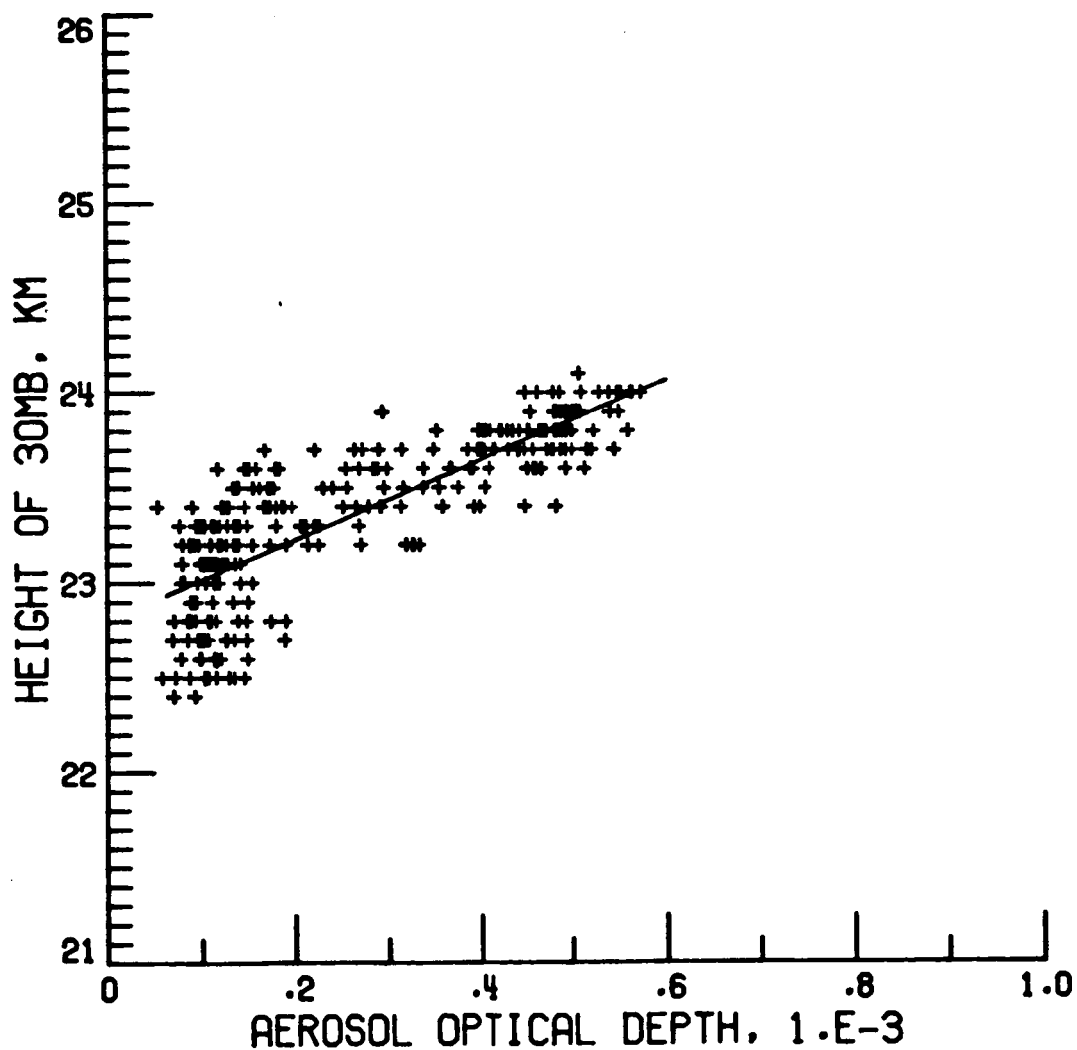


Figure 3.6 (continued). (c) March.

TABLE 3.2. Linear Correlation between SAM II Aerosol Optical Depth and Associated 30 mb Height (1980).

Month	No. of data points	a <sup>†</sup>	b <sup>†</sup>	$\sigma^*$
January	279	21.9	2.05	0.748
February	279	21.8	2.97	0.760
March	277	22.8	2.10	0.813

<sup>†</sup>a and b are the coefficients of a linear least-squares fitting ( $y = a + bx$ ).

1980  
JANUARY-MARCH

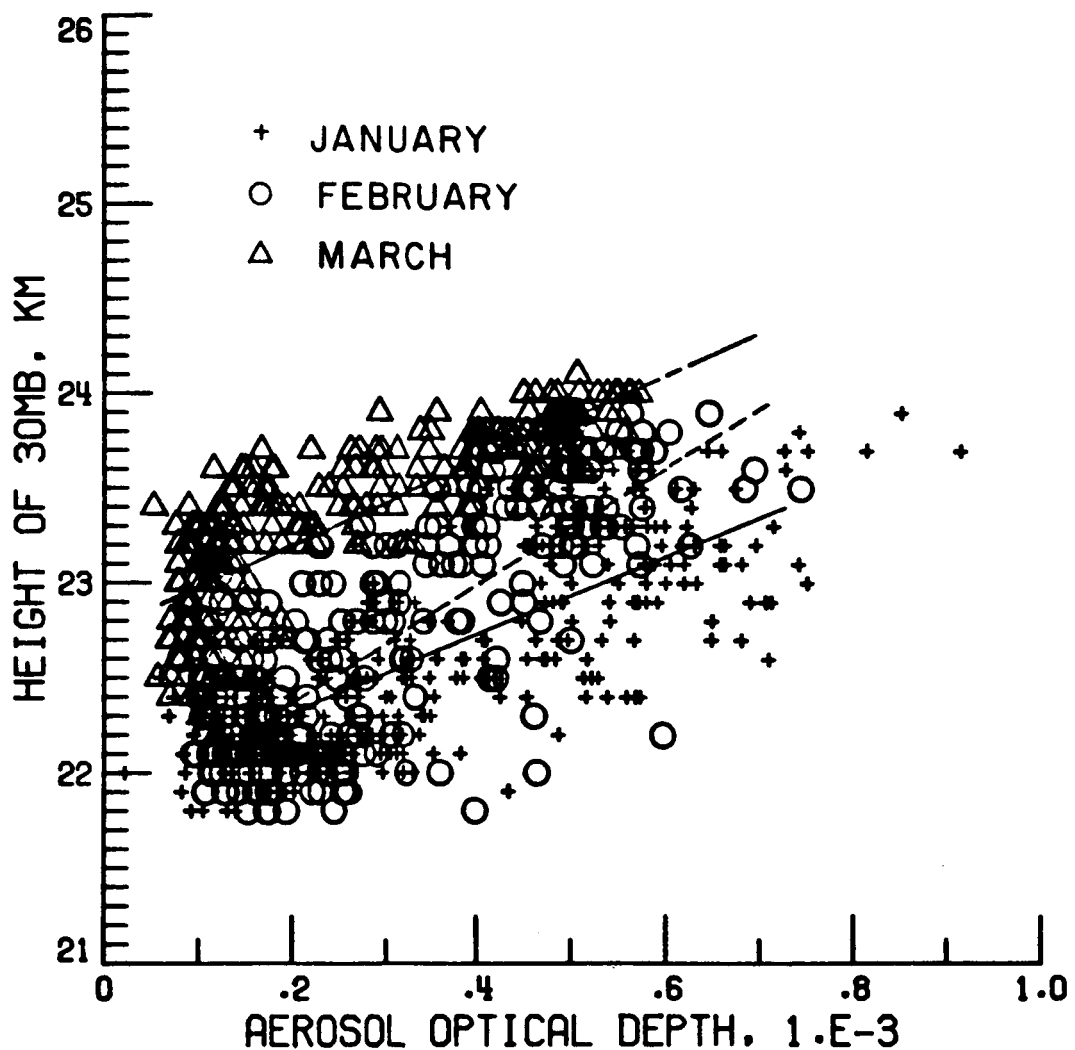


Figure 3.7. Linear correlation between SAM II aerosol optical depth (above 20 km) and associated 30 mb height for 1980. Composite diagram.

1980  
JANUARY-MARCH

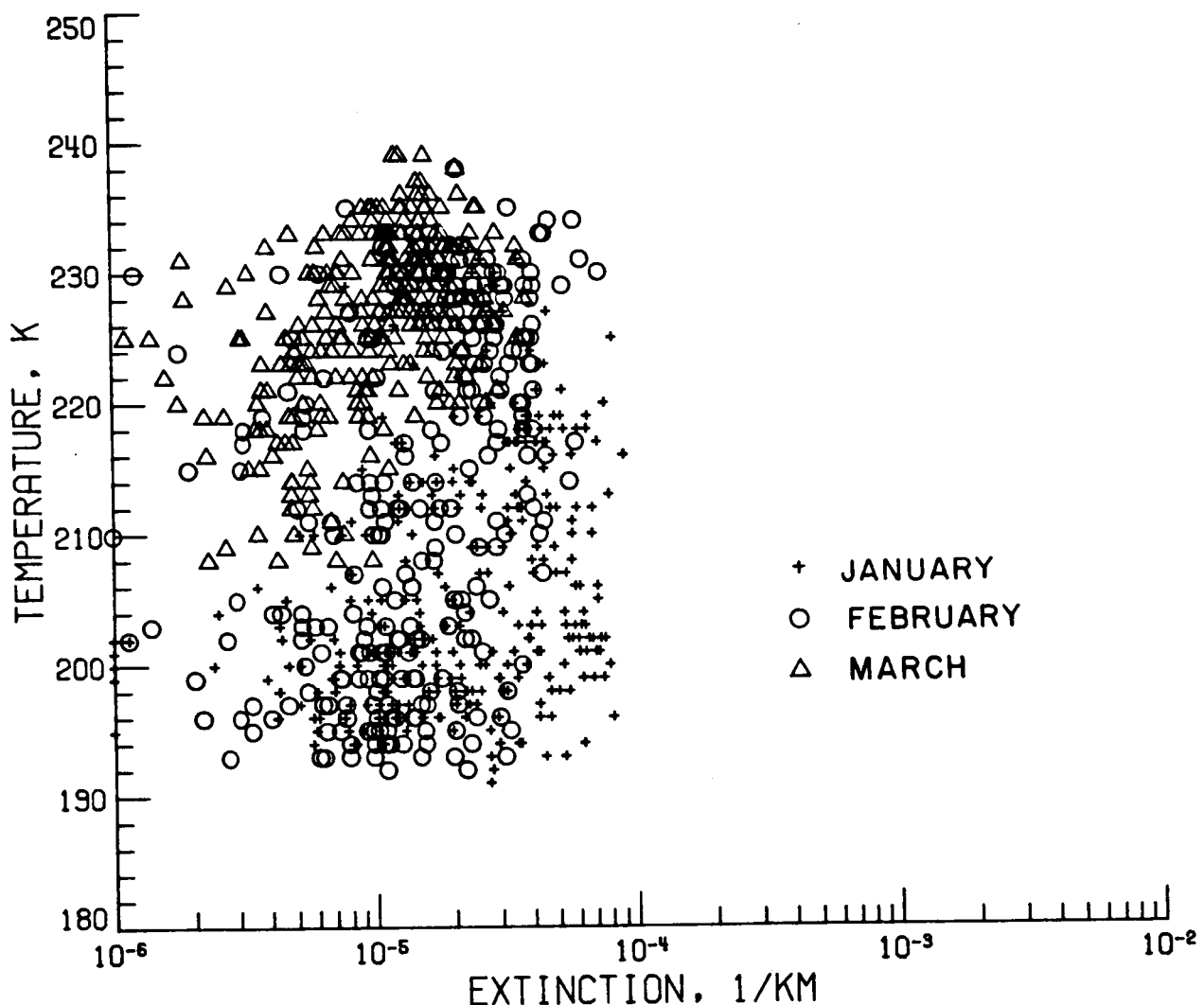


Figure 3.8. SAM II aerosol extinction data at 30 mb for January-March 1980.

been used to study the degree of linear correlation between aerosol optical depth (above 20 km) and the height of the 30 mb pressure level. Significant positive correlation is found for all the years except 1980. However, for 1980, significant correlation does exist if the data is analyzed on a monthly basis. The different correlation behavior for 1980 when the three months are considered together can be attributed to the substantial temperature rise in the Arctic Region between January to March 1980. It should be noted that this is a period of stratospheric warming associated with amplifying planetary waves in the polar region. There is considerable variability in the manifestation of the warming events and amplifying planetary waves from year to year (Schorbel, 1978, Labitzke, 1981, Labitzke and Goretzki, 1982). The results in this study may indicate also that the change in the circulation pattern from Winter to Summer for 1979-1980 took place much later in comparison with what happened in the other three cases. This seems to be supported by the study of Labitzke (1981) and Labitzke and Goretzki (1982).

4. TASK 3--TO INVESTIGATE THE INJECTION OF VOLCANIC MATERIALS INTO THE STRATOSPHERE, INCLUDING GLOBAL LOADING AND TRANSPORT (includes work carried out under Task Area 8)

4.1 Volcanic Loading and Transport

Several volcanic eruptions between 1979 and 1981 injected solid and gaseous material into the stratosphere, raising the mass of aerosol stored there. The resultant changes in 1  $\mu\text{m}$  aerosol extinction were monitored by SAM II and SAGE I giving an almost global picture of the development and movement of the aerosol. The aerosol extinction was used to calculate approximate values for the aerosol mass loading in the stratosphere. From these values the global background mass loading has been determined for the prevolcanic period of 1979, together with an estimate of the seasonal variation of this quantity in each hemisphere. The changes in aerosol extinction in 1980 and 1981, following each volcanic eruption, have been used to calculate the mass of aerosol injected into the stratosphere by each eruption. The manner in which the material injected by these eruptions has divided itself between the Northern and Southern Hemispheres has permitted some general conclusions to be drawn about stratospheric circulation features.

The analysis described above has been published in the Journal of Geophysical Research (Kent and McCormick, 1984), the abstract for this publication is given in Appendix G. Additional analysis of the same data set describing the rates of changes of aerosol mass loading following each eruption is given in Section 6.1 of this report.

~~PRECEDING PAGE BLANK NOT FILMED~~

5. TASK 4--TO INVESTIGATE STRATOSPHERIC PLANETARY WAVES AND THEIR EFFECT ON  
TRANSPORT OF AEROSOLS,  $O_3$  and  $NO_2$

5.1 Aerosol Extinction and Temperature Changes Associated with Planetary Waves

This section summarizes the analysis of behavior of the zonal mean aerosol extinction ratio and its relationship with the zonal mean temperature during the winter of 1978-1979 stratospheric warming. The detailed description of the investigation can be found in the report by Wang and McCormick (1985a, Appendix H). It is generally understood that the distribution of stratospheric aerosols is strongly influenced by aerosol microphysics and atmospheric dynamics. By examining the concurrent variations of aerosol extinction ratio and temperature, it is possible to recognize the key mechanism which controls the distribution of stratospheric aerosols. It is found that, based on SAM II aerosol extinction measurements, the zonal mean aerosol extinction ratio exhibits distinct variations during the January-February 1979 stratospheric sudden warming; and that the transport effect of planetary waves may have played a significant role in determining the distribution of values observed.

5.2 Variations of Aerosol,  $O_3$  and  $NO_2$  Concentrations during Stratospheric Warmings

In the previous section, we have examined the effect of planetary waves on the distributions of stratospheric aerosols. In this section, the variations of stratospheric aerosols, and  $O_3$  and  $NO_2$  concentrations during stratospheric warmings are investigated by utilizing both SAM II and SAGE I observations. Four specific data sets taken during the peak development of

planetary waves have been selected for this analysis. As mentioned earlier, both SAM II and SAGE I instruments provide about 15 measurements per day distributed along an approximately constant latitude at high latitudes. This measurement characteristic allows us to examine the variations of the SAM II and SAGE I measured species that are associated with amplified planetary waves. It is found that there is a strong correlation between the 30 mb pressure height and the aerosol optical depth (at 1 year). Strong longitudinal gradients are found with the low values occurring within and wherever the vortex exists. Similar characteristics are also found to exist for the simultaneously observed SAGE  $O_3$  and  $NO_2$  columnar density distributions. The detail of this analysis can be found in Wang and McCormick (1985b, Appendix I.)

### 5.3 Ozone and Temperature Changes and Associated Fluxes During the Mid-February 1981 Stratospheric Warming

#### 5.3.1. Introduction

In a sense, observation of the development of large-scale stratospheric ozone and temperature waves during the Winter at high latitudes would provide a unique opportunity for comparison with theoretical model prediction to assess current understanding of the behavior of the stratospheric ozone. The development of these large-scale waves as a response of the stratosphere to tropospheric disturbances and also the transport effects of these waves have been investigated using theoretical models (Hartmann and Garcia, 1979; Garcia and Hartman, 1980; Kawahira, 1982; Kurziga et al., 1984; Rood and Schoeberl, 1983a,b, etc.). Meanwhile, studies based on satellite observations are becoming available (Barnett et al., 1975; Gille et al., 1980; Nagatani and Miller, 1984; Wu et al., 1985). In addition, ozone data based on the

Stratospheric Aerosol and Gas Experiment (SAGE) have been used in conjunction with the associated meteorological information to study the behavior of planetary waves of ozone and temperature, and their wave transports during the late February 1979 stratospheric warming (Wang, McCormick and Chu, 1983). Even though the analysis did not derive the detailed ozone budgets due to insufficient data, the results in Wang, McCormick and Chu, (1983) show many interesting features. More specifically, the ozone and temperature waves are shown to be in-phase in the lower stratosphere (below  $\sim$ 25 km), out-of-phase in the upper stratosphere (above  $\sim$ 38 km), with a transition region in between. In the upper stratosphere, an intense equatorward eddy ozone transport was shown to be accompanied by a poleward eddy heat transport during this specific warming. The analysis in Wang, McCormick and Chu (1983) also shows a rapid increase in ozone column density above 10 km over the data period analyzed. This increase was found to be primarily a response to the change of zonal mean ozone number density in the lower stratosphere. It should be understood that Wang, McCormick and Chu (1983) is a single case study. Since there is considerable variability in the manifestation of warming events and amplifying planetary waves from year to year (Schoeberl, 1978; Labitzke, 1981; Labitzke and Goretzki, 1982), results from observations of different warmings are highly desirable.

The purpose of this study is two-fold. First, the behavior of planetary waves of ozone and temperature and their wave transports during the middle February 1981 stratospheric warming will be studied in detail by utilizing the SAGE ozone measurements and associated meteorological data. Second, the analyzed results of this middle February 1981 warming will be compared with those of the late February 1979 warming described in Wang, McCormick and Chu (1983).

As will be shown, these two warming events correspond to two quite different stratospheric circulations at high latitudes. A comparison of the behavior of ozone and temperature waves between those two events is thus significant, and leads to enhancement of our understanding of their behavior during warming events.

### 5.3.2 Data and approach

Similar to Wang, McCormick and Chu (1983), the results of SAGE ozone measurements and the associated meteorological information provided by NOAA's National Meteorological Center are used in this analysis of the mid-February 1981 warming event. In Wang, McCormick and Chu (1983), we have described the general characteristics of the SAGE ozone and the meteorological data sets relevant to the planetary wave studies. In this study, we will mention only specific aspects of these observations which are important to this particular analysis. As noted in Sec. 1.2, the AEM 2 satellite power system developed problems about 5 months after the SAGE instrument was launched. As a result, there were no sunrise measurements available after July 1979. The entire SAGE sunset observation period covers 34 months from February 1979 to November 1981 (Figure 5.1). For the purpose of examining the behavior of winter planetary waves, it is desirable to use data obtained at high latitudes where the waves are most active. As shown in Figure 5.1, the SAGE measurement locations reach the highest latitudes on two occasions centered around January 1 and March 6, during the winter 1979-1980. Unfortunately, the highest latitude of the SAGE measurements [around January 1, 1980 is about  $46^{\circ}\text{N}$ . As for the measurements near March 6, 1980], the highest latitude reached was  $58^{\circ}\text{N}$ , but data gaps are found in the retrieved profiles during this period. For these reasons, it was decided to examine the case of Winter 1980-1981 instead. During this winter, there are 10 consecutive daily SAGE

ORIGINAL PAGE IS  
OF POOR QUALITY

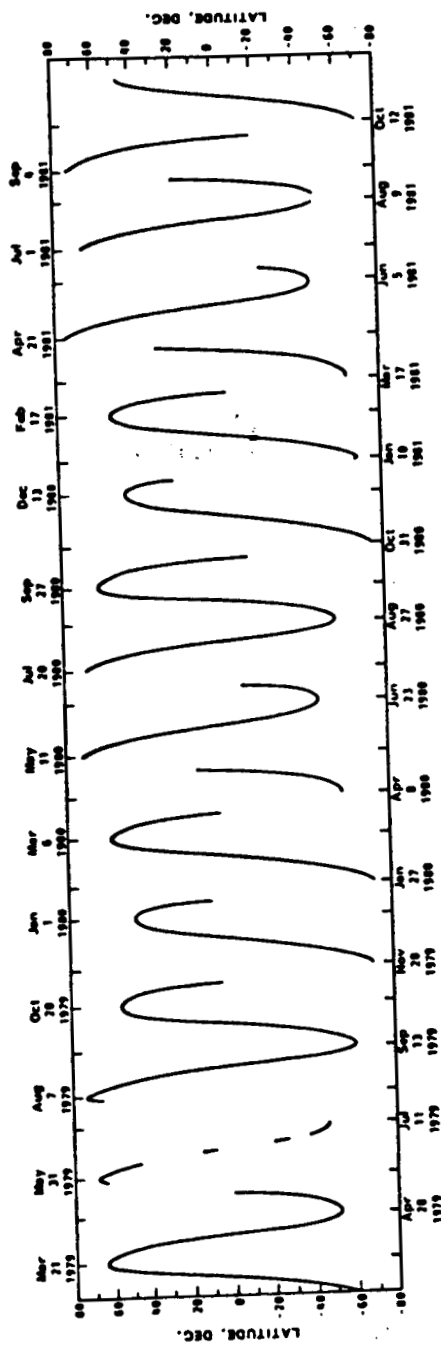


Figure 5.1. The latitudinal coverage of SAGE sunset measurements.

ozone profiles from February 12 to 21, 1981 available for the analysis. The peak latitude near  $55^{\circ}\text{N}$  occurred on February 17, 1981. Table 5.1 indicates the average latitude and the number of profiles of the SAGE daily measurements for these 10 days. The overall averaged latitude for this 10-day period is about  $52^{\circ}\text{N}$  which is only slightly lower than the February 1979 case discussed in Wang, McCormick and Chu (1983). It is important to note that this 10-day period covers approximately the second half of the major midwinter warming which occurred in February 1981 and reported by Labitzke (1982).

In this analysis, the method for deriving the planetary waves of ozone and temperature and their fluxes using SAGE ozone and meteorological data sets is essentially the same as that described in Wang, McCormick and Chu (1983). For this reason, we will not repeat the discussion here. Since one of the purposes of this study is to compare the ozone and temperature waves and their eddy transports between the late February 1979 and the middle February 1981 warmings, a general description of the synoptical meteorological aspects of the northern high latitude stratosphere during these warming periods is included in the analysis. This will help to bring out some features of the atmospheric circulation and the thermal structure which are not obvious from an examination entirely in terms of their harmonic components. As will be seen in the next section, there are considerable differences in the stratospheric circulation pattern between these two warming events.

### 5.3.3 Results and discussion

In this section, we first show the development of the arctic circulation pattern for the middle February 1981 warming. For comparison, a description

TABLE 5.1. The Number of Profiles and the Averaged Latitude  
of SAGE Observations from February 12 to 21, 1981.

Date (February)	Number of Profiles	Averaged Latitude (°N)
12	15	49.47
13	14	50.94
14	15	52.05
15	15	52.84
16	15	53.34
17	15	53.55
18	15	53.50
19	15	53.18
20	15	52.59
21	14	51.69

of the late February 1979 warming is included. The results of harmonic analyses of ozone mixing ratio, temperature and eddy meridional velocity, are given in the second part of this section, followed by a description of the horizontal meridional ozone and temperature transports by the planetary waves. In the last part of this section, the phase relationship between the waves of ozone mixing ratio, temperature and eddy meridional velocity is examined.

#### 5.3.3.1 Synoptical meteorology of the high latitude stratosphere for the middle February 1981 warming

Some aspects of the warming event of 1980-1981 have been discussed by Labitzke and Goretzki (1982). It began with the development of an Aleutian anticyclone which indicated the amplification of the wavenumber 1 disturbance in November 1980--the so-called Canadian Warming. In December 1980, the wave activities were generally mild and the monthly mean 30 mb North Pole temperature was  $-82^{\circ}\text{C}$ --the coldest temperature since the winter 1958-1959. This situation extended to the middle of January 1981. During this period, the high latitude Northern Hemisphere was characterized by the development of a vast quasi-circular polar vortex as shown in the 30 mb upper air map on January 14 1981 (Figure 5.2a). Thereafter, this polar vortex was disturbed by amplifying planetary waves, mainly wavenumber 1 (Figure 5.2b). By middle February, the high latitude zonal mean thermal structure had shown a reversal of the latitudinal temperature gradient, indicating the occurrence of a major midwinter warming. According to Labitzke and Goretzki (1982), the monthly mean 30 mb North Pole temperature had increased from  $-82^{\circ}\text{C}$  in December 1980 to  $-56^{\circ}\text{C}$  in February 1981. Figure 5.2c shows the 30 mb upper air map on February 15, 1981, in which the remainder of the wavenumber 1 disturbance is still clearly evident on this particular day. It is interesting to note that

ORIGINAL PAGE IS  
OF POOR QUALITY

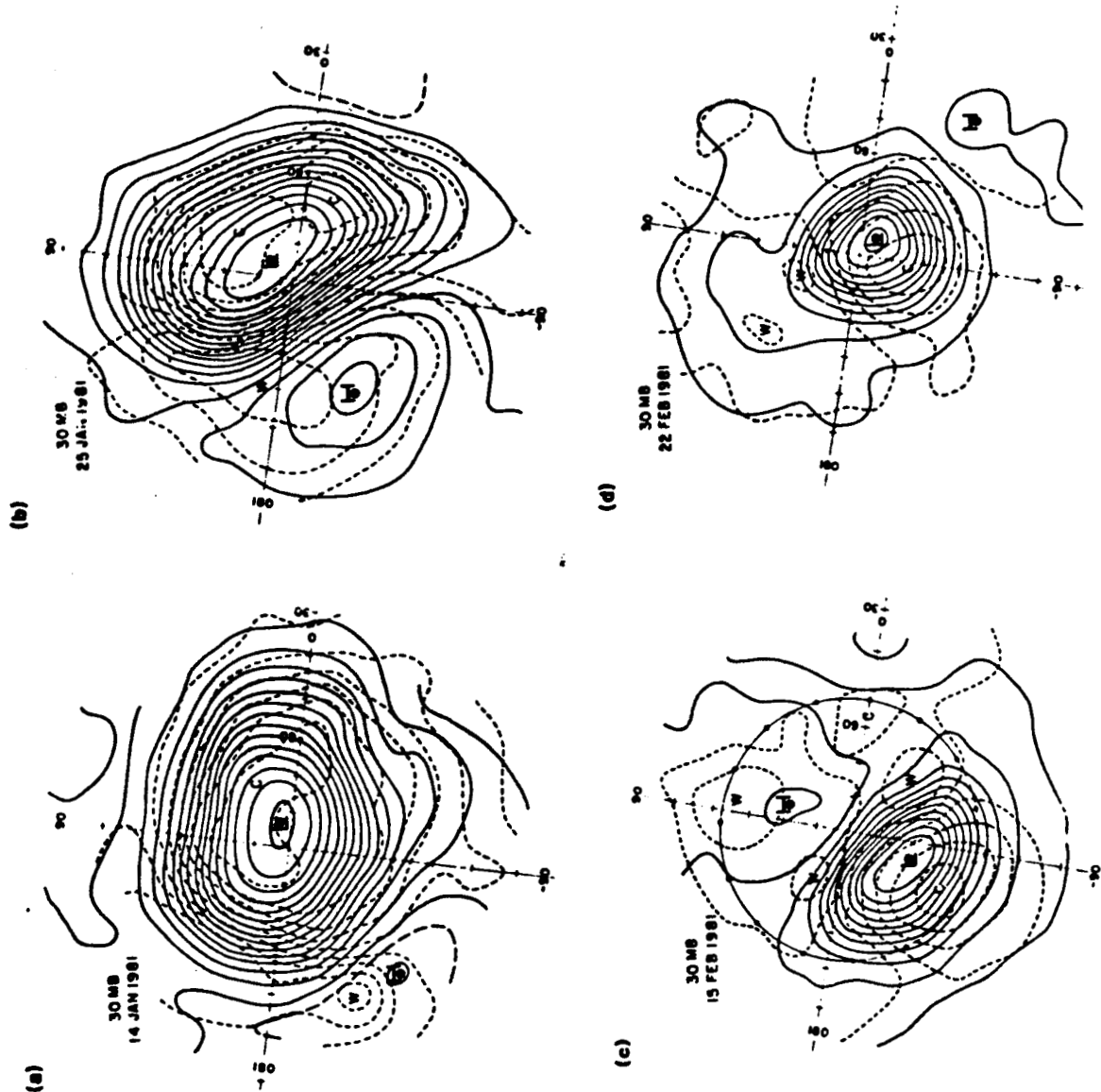


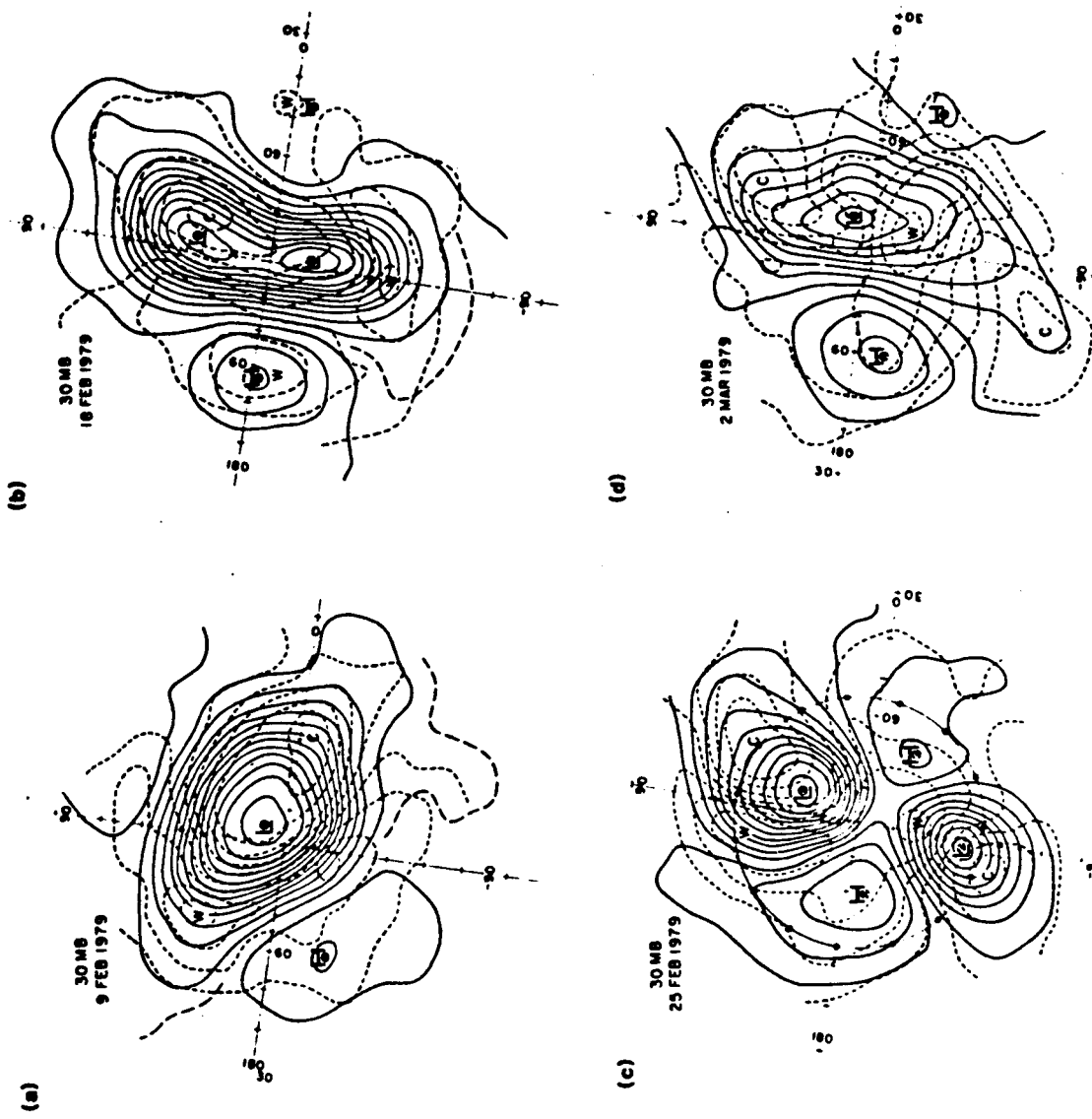
Figure 5.2. Constant pressure upper air maps at 30 mb for (a) January 14, 1981; (b) January 25, 1981; (c) February 15, 1981; and (d) February 22, 1981. —— isobaric altitude lines, --- isotherms. Solid circles on (c) denote the SAGE measurement locations.

the wavenumber 1 height disturbance had shifted its phase by an amount close to  $180^{\circ}$  from January 25 to February 15. Note also that the cold center, which was located near the North Pole just before the development of planetary wave disturbances on January 14, 1981 (Figure 5.2a), had moved to  $\sim 60^{\circ}\text{N}$  latitude west of Canada by February 15, 1981. At the same time, warmer air masses had appeared in the polar region (Figure 5.2c). In the second half of February, the activity of planetary wave disturbances became much weaker and the polar vortex began to regain some of its strength (Figure 5.2d). This is a stage corresponding to a period of the so-called "late winter cooling" (Labitzke and Goretzki, 1982). Later, there was a further development of wavenumber 1 disturbance which reached its peak intensity on about March 3, 1981. Thereafter, the arctic stratosphere was gradually replaced by the summer circulation system. It is interesting to note that Labitzke (1982) had shown that this wavenumber 1 dominated winter disturbance took place during the westerly phase of the equatorial quasi-biennial oscillation (at 50 mb) and not on the easterly phase as for most wavenumber 1 development. She further indicated that only wavenumber 1 winter events which occurred near sunspot maxima exhibit this unusual feature. For comparison purposes, it is essential to this investigation to also describe the circulation which occurred in the polar region during the late February 1979 warming.

The synoptic aspects of the circulation of Winter 1978-1979 have been discussed by Noxon et al. (1979), and Syed and Harrison (1981) in their studies on the behavior of  $\text{NO}_2$  abundance during the warming of January-February 1979. The behavior of planetary wave disturbances of the temperature and height fields of this winter also have been investigated by Quiroz (1979) and Labitzke (1981) in detail. Before January 15, 1979, the polar stratospheric circulation system showed only mild fluctuations in these

fields except for a few days around December 8, 1978. During these days, an Aleutian anticyclone developed indicating an amplification of height wavenumber 1. In the period January 15 to early March 1979, the northern polar stratospheric circulation system went through several interesting changes. First, there was the formation of an unusually strong Aleutian anticyclone which led to the amplification of height wavenumber 1 disturbance at 30 mb with the peak intensity occurring on about January 26. Around the same day, the stratosphere showed the first reversal of the meridional gradient of mean stratospheric temperature. Thereafter, this anticyclonic system weakened and the disturbed polar vortex tended to regain its strength with its center moving back toward the pole. Figure 5.3a shows the 30 mb arctic upper air map for February 9, 1979. This polar vortex became well established again by about 12 February. Beginning that day, the vortex exhibited an elongation of its circulation pattern approximately along the east-west axis, with the appearance of two low pressure systems (Figure 5.3b). Meanwhile, two high pressure systems developed on each side of the elongated polar vortex (Figure 5.3b), indicating an amplification of height wavenumber 2. This development in the arctic stratosphere culminated in the splitting of the polar vortex (Figure 5.3c) and the reversals of the zonal mean arctic flow, as well as the meridional gradient of mean stratospheric temperature--a major final warming (Quiroz, 1979). By the end of February, these wavenumber 2 dominated disturbances began to decay. In the following month, there were only mild fluctuations of the height field in the form of wavenumber 1. During the month of April 1979, the flow in the arctic winter stratosphere was gradually replaced by the summer circulation system.

From the above discussion, it is clear that the development of the arctic winter disturbances in the two Winters 1978-1979 and 1980-1981 are



ORIGINAL PAGE IS  
OF POOR QUALITY

Figure 5.3. Constant pressure upper air maps at 30 mb for (a) February 9, 1979; (b) February 18, 1979; (c) February 25, 1979; and (d) March 2, 1979. — isobaric altitude lines, - - - isotherms. Solid circles on (c) denote the SAGE measurement locations.

rather different. In 1980-1981, the arctic disturbances involved primarily wavenumber 1 fluctuations during the entire winter season. In 1978-1979, however, the polar stratosphere showed disturbances involving both wavenumbers 1 and 2 with each dominating during different periods. It should also be mentioned that in Wang, McCormick and Chu (1983), the period of the data set analyzed only covered the peak of the height wavenumber 2 development. On the other hand, the data set used in this analysis covers essentially the second half of the major midwinter warming which was during the decaying stage of a strong height wavenumber 1 disturbance.

#### 5.3.3.2 Evolution of the planetary waves

Figures 5.4a - 5.4c show the evolution of the temperature wavenumber 1 and 2 disturbances and also the zonally averaged temperature during the mid-February 1981 stratospheric warming from February 12 to 21, 1981, respectively. In the case of the wavenumber 1 evolution (Figure 5.4a), the stratosphere exhibits three distinct layers. They are centered approximately at 22 km, 32 km, and 44 km, respectively. In the middle layer, a mild decrease in the wave amplitude is shown. The behavior of the waves in the lower and upper layers, is very similar, showing an intensification in the first 4 days, and a rather steady decay afterwards. The maxima of the wave amplitudes, approximately  $12^{\circ}\text{C}$  and  $10^{\circ}\text{C}$  in the upper and lower layers, respectively, appeared on February 15. The calculated amplitudes for temperature wavenumber 2 show generally a mild decay of the wave in the altitude region from 10 km to 50 km throughout the entire data period of this analysis (Figure 5.4b). From Figure 5.4a and 5.4b, it is clear that the temperature disturbances in this mid-February warming are dominated by wavenumber 1 activities. In the case of the zonal mean component (Figure 5.4c), no significant variation is shown during this 10-day data period.

ORIGINAL PAGE IS  
DE POOR QUALITY

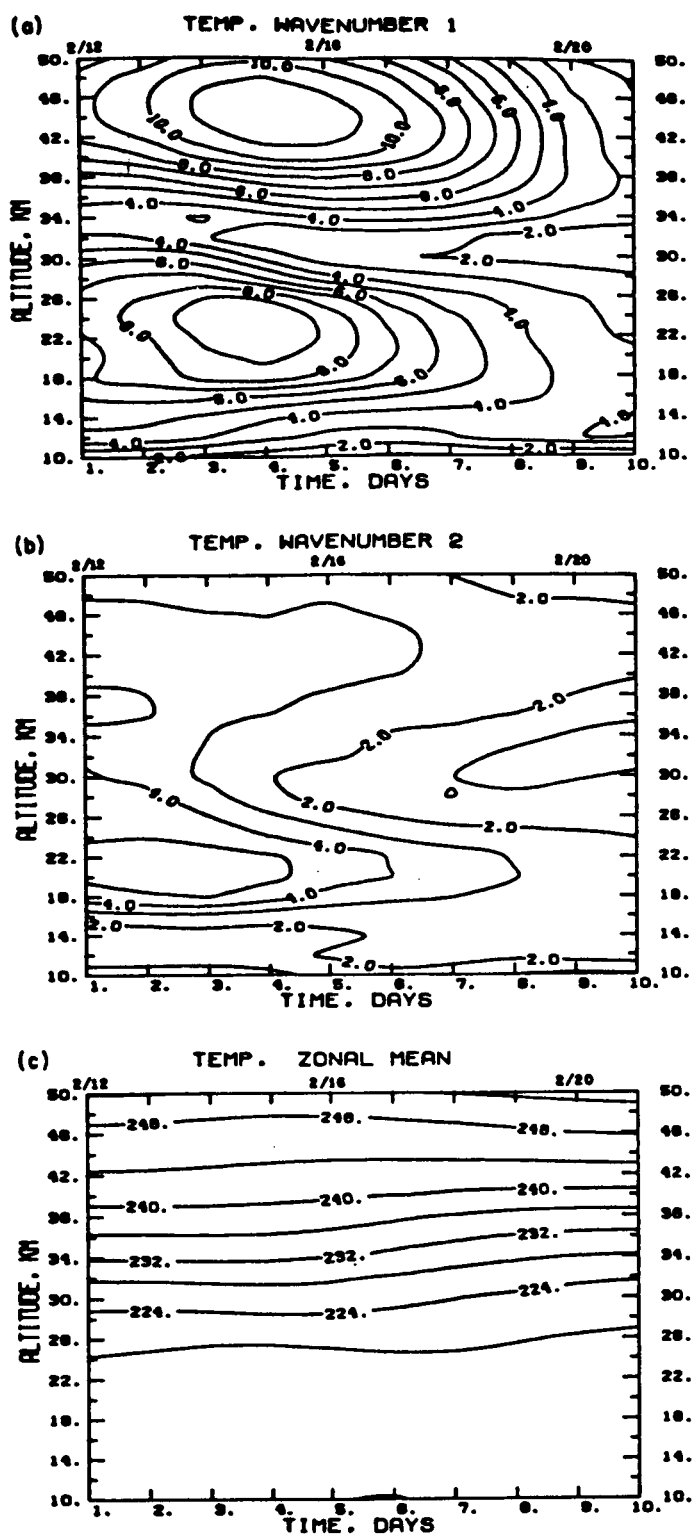


Figure 5.4. Evolution of the amplitudes ( $^{\circ}\text{C}$ ) of the first two temperature waves [(a) and (b), respectively, contour interval  $1^{\circ}\text{C}$ ]; and (c) the zonal mean temperature K (contour interval  $4^{\circ}\text{C}$ ) during the middle February 1981 warming ( $\sim 52^{\circ}\text{N}$ ).

However, a  $2^{\circ}\text{C}$  increase in the mean temperature is noticeable between 28 km and 38 km in the period from the 5th day to the 10th day.

In comparison with the case in Wang, McCormick and Chu (1983), the wavenumber 2 and mean temperature disturbances for this mid-February warming are smaller in magnitude. The wavenumber 1, however, is more intense overall, except in regions above  $\approx 38$  km where the two wavenumbers are comparable in magnitude.

The derived amplitude of the first two harmonic components of the eddy meridional velocity are shown in Figures 5.5a and 5.5b, respectively. The wavenumber 1 shows an intensification from day 1 to day 3 above approximately 20 km (Figure 5.5a). A peak value of 16.5 m/sec appeared on day 3 at about 37 km. Thereafter, the wave decayed. Below about 20 km, the wave amplitudes are relatively small (Figure 5.5a). In Figure 5.5b, the result of wavenumber 2 shows a decay of the wave throughout the data period of this study between 10 km and 50 km. The strength of the wavenumber 1 disturbance (Figure 5.5a) is about 1.5 times that observed in Wang, McCormick and Chu (1983), while the wavenumber 2 strength of the disturbance is only about half.

The first two harmonic components of ozone mixing ratio are given in Figures 5.6a and 5.6b. The noticeable features of the first component (Figure 5.6a) are the appearance of a maximum at 44 km about February 15, 1981. The variation of ozone mixing ratio in a layer between 40 and 50 km seems to be associated with that of the temperature wavenumber 1 (Figure 5.4a). Below about 40 km, (Figure 5.6a), a relatively steady-state condition is observed. In the case of ozone wavenumber 2, the amplitude is only about half that of the wavenumber 1 (Figure 5.6b). Figure 5.6b also shows that most of the wavenumber 2 activities were in the upper stratosphere above about 30 km.

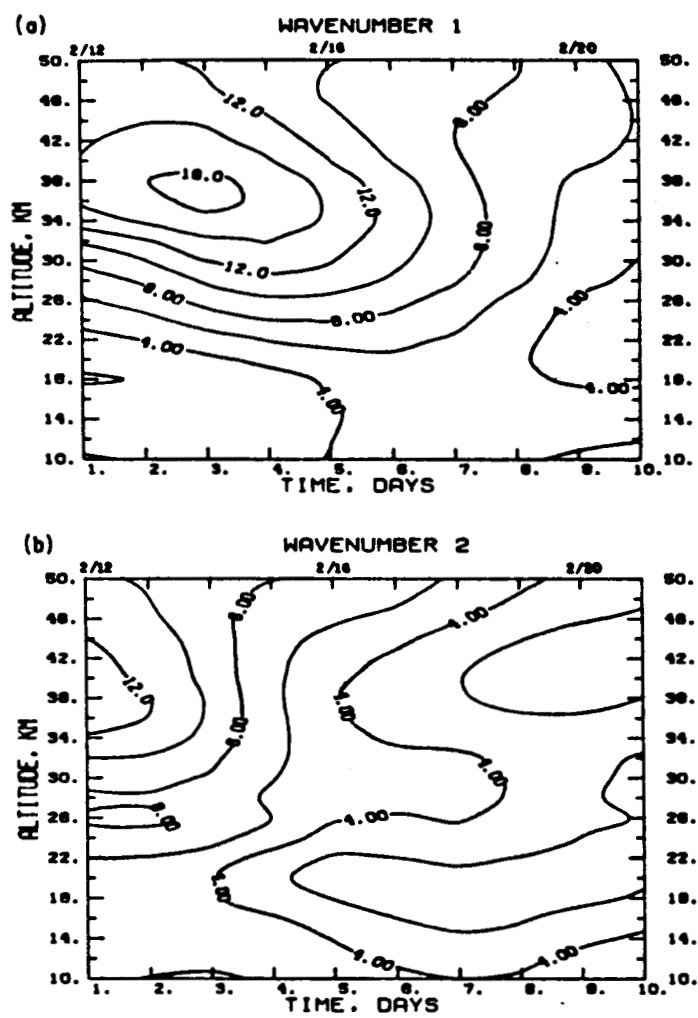


**Figure 5.5.** Evolution of the amplitudes ( $\text{ms}^{-1}$ ) of meridional velocity waves during the middle February 1981 warming ( $\sim 52^\circ\text{N}$ ); (a) wavenumber 1, (b) wavenumber 2; contour interval  $4 \text{ ms}^{-1}$ .

ORIGINAL PAGE IS  
OF POOR QUALITY

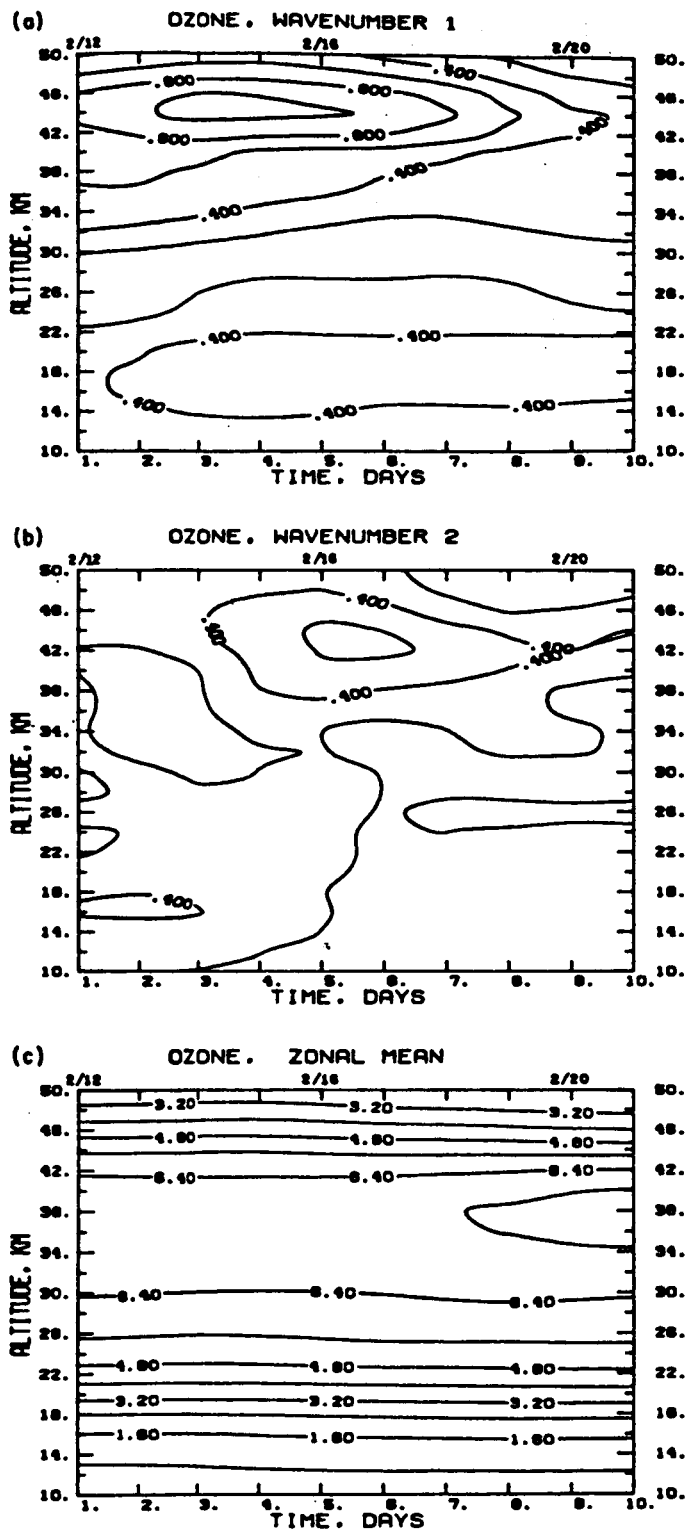


Figure 5.6. Evolution of the amplitudes (ppmv) of the first two ozone waves, and the zonal mean ozone during the middle February 1981 warming ( $\sim 52^\circ\text{N}$ ); (a) wavenumber 1; (b) wavenumber 2, contour interval 0.2 ppmv, and (c) zonal mean ozone, contour 0.8 ppmv.

Below 30 km, the wavenumber 2 is relatively weak. The evolution of zonal mean ozone mixing ratio is given in Figure 5.6. Below about 30 km (Figure 5.6c) little change is observed in the mean ozone mixing ratio during the data period of this study. In the layer between 30 km and 42 km, there is a slow increase in the ratio in the late half period. Above 42 km, there is a noticeable decrease in the ozone mixing ratio in the entire data period of this study. In comparison, the data shown in Figures. 5.6a and 5.6c are, in many respects, similar to those shown in Wang, McCormick and Chu (1983, Figure 5.6.) In both cases, the ozone wavenumber 1 disturbances are observed to be more intense in the upper stratosphere component. Slight increases are also observed in the zonal mean ozone mixing ratio lower stratosphere below 30 km. Particular noteworthy is the fact that ozone wavenumber 1 disturbances in the upper stratosphere are clearly correlated to that of temperature wavenumber 1 in these two different warmings. This correlation between temperature and ozone wavenumber 2 amplitudes, however, is less clear in the analysis of these two warmings.

In order to examine the changes in the columnar ozone above 10 km during this mid-February 1981 stratospheric warming, the evolution of zonal mean ozone number density in this event is also derived based on the SAGE ozone data set. Figure 5.7a shows the computed results. From Figure 5.7a, it is evident that there is an increase in ozone concentration in the lower stratosphere centered at altitude 20 km. Above 24 km (Figure 5.7a) no apparent changes in the mean number density are observed. It is interesting to note that the behavior of zonal mean ozone density in this mid-February 1981 warming is very similar to the late February 1979 event (Wang, McCormick and Chu, 1983). The associated time variation in the ozone columnar density is given in Figure 5.7b. It shows a monotonical increase in value except for

ORIGINAL PAGE IS  
OF POOR QUALITY

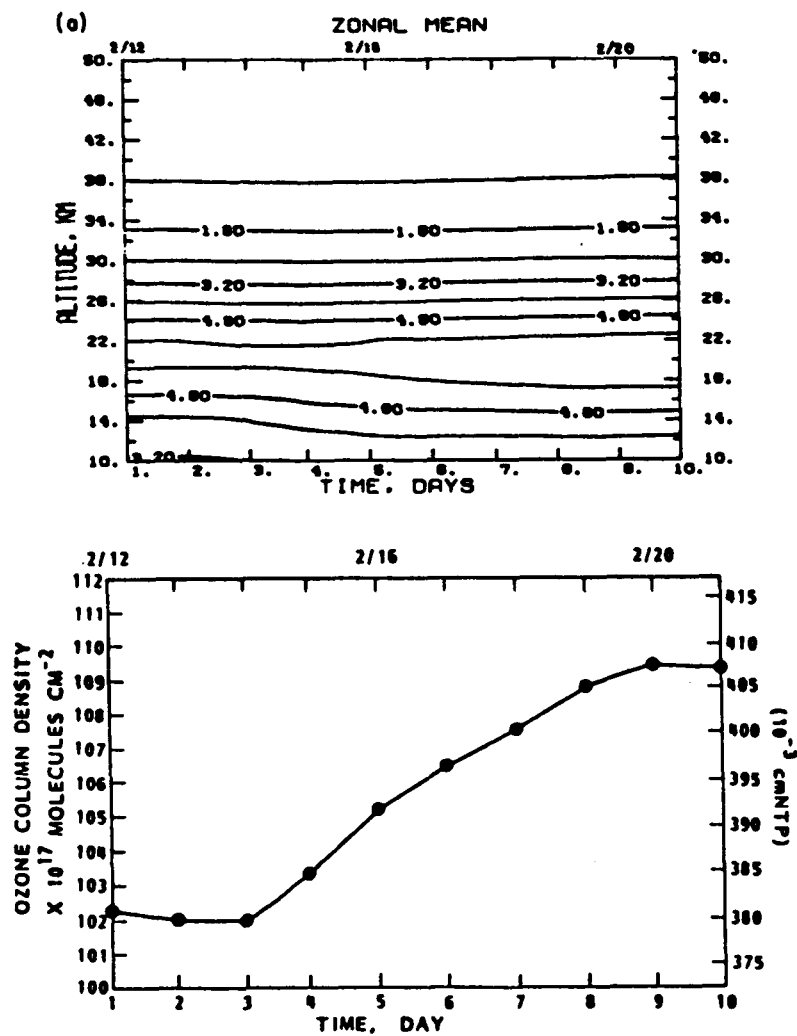


Figure 5.7. Evolution of (a) zonal mean ozone number density, contour interval 0.8, scale by  $10^{-12}$  in unit  $\text{cm}^{-3}$ ; and (b) ozone columnar density at altitude 10 km during the middle February 1981 warming ( $\sim 52^\circ\text{N}$ ).

the first two days. This increase in ozone columnar abundance is primarily a response to the increase in the ozone concentration in the lower stratosphere as illustrated in Figure 5.7a. A similar situation was also found in the late February 1979 stratospheric warming event (Wang, McCormick and Chu, 1983). In comparing the ozone columnar density of this analysis with that described in Wang, McCormick and Chu (1983), it is found that the overall values in the late February 1979 event are generally greater than those occurring in this mid-February 1981 warming.

#### 5.3.3.3 Horizontal ozone and temperature transports by planetary waves

The computed eddy ozone transports associated with the first two wave components in the mid-February 1981 warming are displayed in Figures 5.8a and 5.8b. The remarkable features of the wavenumber 1 transport (Figure 5.8a) are the clearly defined altitude regions for the poleward and the equatorward ozone transports throughout the entire data period of this analysis. Above 40 km, a distinct layer of equatorward eddy ozone transport is observed (Figure 5.8a), with a maximum value of  $4.5 \text{ ppmv ms}^{-1}$  occurring on February 14, 1981 at 44 km. Below about 28 km, an equatorward transport is also observed (Figure 5.8a), but it is much weaker in comparison with the one above 40 km. In the layer between 28 and 40 km, the eddy ozone transport is mainly toward the North Pole. A slight increase in the transport is observed in this region during the first 4 days which decayed thereafter. A maximum poleward transport of  $\sim 3 \text{ ppmv ms}^{-1}$  appeared at 36 km on the same day (February 15, 1981) that the equatorward transport reached its peak value in the upper stratosphere.

An analysis of the ozone transport associated with wavenumber 2, indicates a poleward transport below 40 km and equatorward transport above 40

ORIGINAL PAGE IS  
OF POOR QUALITY

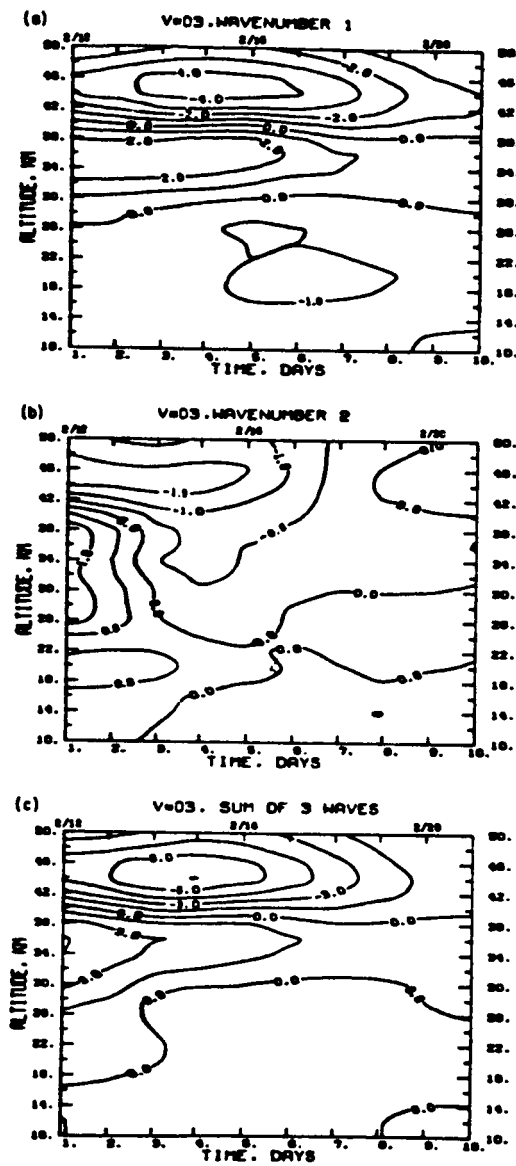


Figure 5.8. Time variations of eddy ozone flux ( $\text{ppm ms}^{-1}$ ). Due to  
(a) wavenumber 1, contour interval  $1 \text{ ppm ms}^{-1}$ , and  
(b) wavenumber 2, contour interval  $0.5 \text{ ppm ms}^{-1}$ . The sum  
of the first three waves is given in (c), contour interval  
 $1.5 \text{ ppm ms}^{-1}$ . (+ poleward, - equatorward.)

km in the first 2 to 3 days (Figure 5.8b). Later, the equatorward transport system in the upper stratosphere is observed to increase slightly reaching a peak value of  $3 \text{ ppmv ms}^{-1}$  at 46 km on February 15, 1981. On February 14, 1984 (Figure 5.8b), a change in transport direction is observed within the layer between approximately 24 km and 38 km from poleward to equatorward. After February 15, the wavenumber 2 eddy ozone transport in the entire layer is observed to decay. From Figures 5.8a and 5.8b, it is evident that the wavenumber 2 eddy ozone transports are generally weaker than wavenumber 1 in this particular warming. The sum of the eddy ozone transport due to the first three wave components is given in Figure 5.8c. Since the transport due to wavenumber 1 is relatively strong, the transport shown in Figure 5.8c exhibits features similar to those shown in Figure 5.8a. By comparing Figure 5.8c with the corresponding results presented in Wang, McCormick and Chu (1983), one will notice that they exhibit generally similar features. In both cases, the ozone mixing ratio transports exhibit three distinct layers, namely, two equatorward transport layers, one in the upper stratosphere, and one in the lower stratosphere, and a poleward transport layer in the middle stratosphere. There are, however, slight differences in the vertical extension and the center altitude of these layers for the two warming cases.

Since eddy ozone mass transport is directly related to changes in total ozone amount, the contribution of the first two wave components to this transport during the mid-February 1981 warming are analyzed (Figures 5.9a and 5.9b). Below about 26 km, the development of an intense equatorward wavenumber 1 transport is observed (Figure 5.9a). This transport reached a peak intensity of  $2.7 \times 10^{12} \text{ molecules cm}^{-3} \text{ ms}^{-1}$  at 16 km about February 17, 1981. Above 26 km, the wavenumber 1 transport is relatively weaker than that below. Nevertheless, a layer of poleward mass transport between 26 km and 38

ORIGINAL PAGE IS  
OF POOR QUALITY

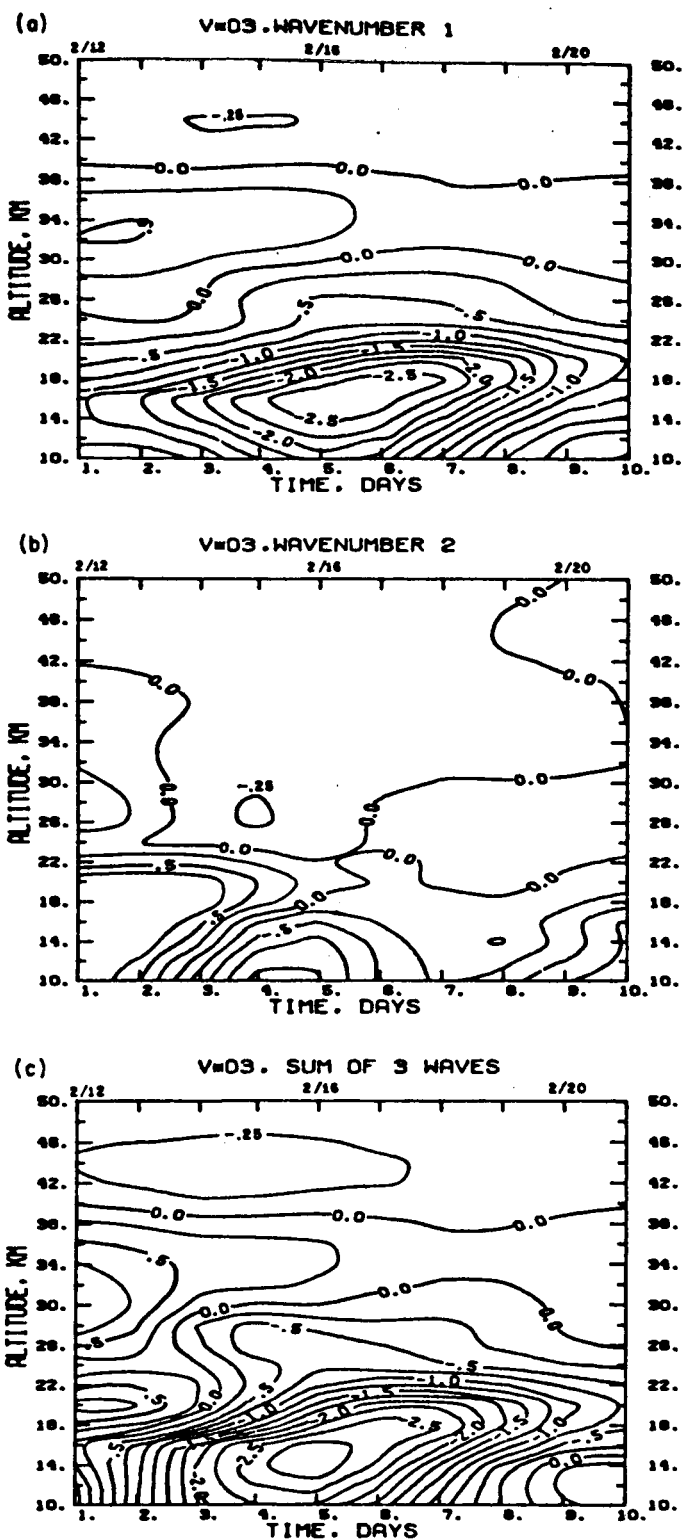


Figure 5.9. Time variations of eddy ozone mass transport ( $\text{molecule cm}^{-3} \text{ms}^{-1}$ ). Due to (a) wavenumber 1; and (b) wavenumber 2, contour interval 0.25 molecule  $\text{cm}^{-3} \text{ms}^{-1}$ . The sum of the first three waves is given in (c) contour interval 1 molecule  $\text{cm}^{-3}$ . Scaled by  $10^{-12}$  (+ poleward, - equatorward.)

km and also a layer of equatorward transport above 38 km are noticeable (Figure 5.9a). The calculated results of wavenumber 2 ozone mass transport indicates a contribution that is generally much smaller than that of wavenumber 1 except in regions below 22 km during the first 2 to 3 days (Figure 5.9b). In these regions, poleward eddy transport is observed during those days. The sum of the first 3 components of eddy ozone mass transports is displayed in Figure 5.9c. It is obvious that an intense equatorward transport developed below approximately 26 km. This development seems to be associated with the decaying of a poleward eddy ozone mass transport in the layer between 26 km and 40 km as revealed from the first 3 days of this data period. Although this poleward transport became rather weak by the third day, a thin layer of poleward transport centered at altitude 34 km is still noticeable in the rest of the data period. From Figure 5.9, it is clear that the wavenumber 1 component plays a dominant role in the eddy ozone mass transport in this mid-February 1981 warming. As indicated in Figure 5.9c, the peak of the equatorward transport occurred around February 16, 1981 at ~16 km. The vertical integrated mass flux of ozone (10-30 km altitude) on this day is found to be  $(3.2 \pm 0.08) \times 10^{20}$  (molecules/cm<sup>-2</sup>)(cm/sec) to the south.

In Wang, McCormick and Chu (1983), the ozone and temperature eddy transports in the upper stratosphere (above 35 km) were shown acting in opposite directions in both wavenumber 1 and 2 components. Of particular interest is that both the wavenumber 1 ozone and temperature eddy transports show a change in their direction on about the same day. To see whether such a feature exists in the middle February 1981 warming, the eddy transports of temperature have been calculated. The results are shown in Figure 5.10. The most distinct feature of the temperature wavenumber 1 transport (Figure

ORIGINAL PAGE IS  
OF POOR QUALITY

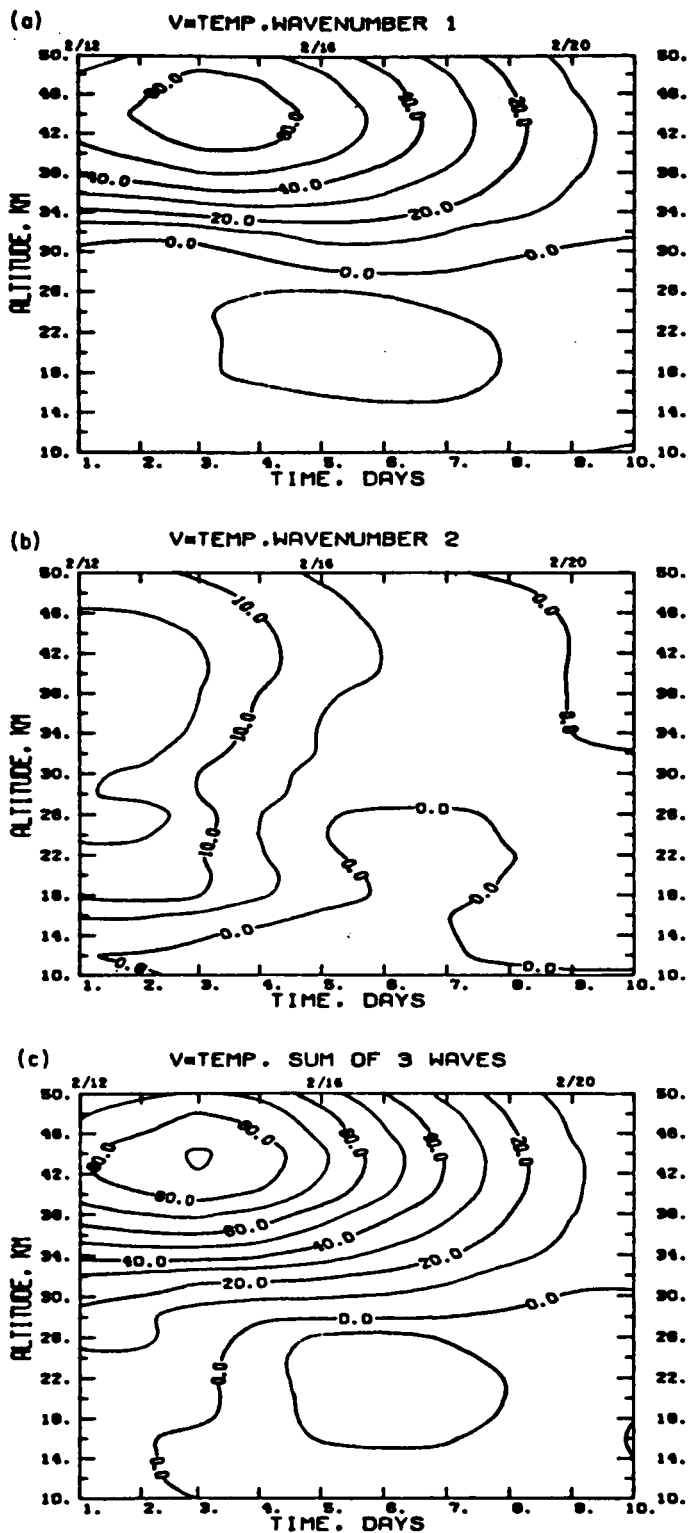


Figure 5.10. Time variation of eddy heat flux ( $\text{k m s}^{-1}$ ). Due to (a) wavenumber 1, contour interval  $20^{\circ}\text{C ms}^{-1}$ ; (b) wavenumber 2, contour interval  $5^{\circ}\text{C ms}^{-1}$ , and (c) the sum of the first three waves, contour interval  $20^{\circ}\text{C ms}^{-1}$ . (— poleward, --- equatorward.)

5.10a) is the development of a poleward transport above about 30 km with the peak at about 44 km. This peak reached its maximum intensity ( $\sim 67$  km/sec) on approximately February 14, and decreased steadily thereafter. Below about 30 km, only mild equatorward eddy heat transports are observed (Figure 5.10a). In the case of wavenumber 2, a decrease of the poleward heat transport is generally observed throughout most of the altitude range of this study during this middle February 1981 warming (Figure 5.10b). The net eddy heat transports (shown in Figure 5.10c) exhibit a rather similar time variation as that of wavenumber 1, with a distinct layer of poleward eddy heat transport above 30 km centered at about 40 km, particularly on February 14. It should be noted that the daily values of the temperature difference between  $80^{\circ}\text{N}$  and  $50^{\circ}\text{N}$  at 30 mb pressure level exhibit the second peak of the temperature reversal on about February 14, 1980 (Labitzke, 1982). This peak occurs about the same time at which the eddy heat transports began to change its direction from poleward to equatorward. As mentioned earlier, the wavenumber 1 ozone transport during the period of the data set in this study shows the peak of equatorward transport at an altitude of 44 km. In addition, this peak reached its maximum intensity on February 14. Thus, the observed wavenumber 1 of ozone and temperature transports are negatively correlated during this mid-February 1981 warming. In the case of wavenumber 2, the behavior of ozone and temperature transports showed similar negative correlation above 40 km. In particular, in this altitude region, they both changed their transport directions sometime between February 20 and 21.

#### 5.3.3.4 Phase relationships between the eddy fields

The phase relationship between ozone, temperature, and meridional velocity waves of wavenumber 1 component on February 13, 1981, is shown in Figure 5.11a. The horizontal bars, as in Wang, McCormick and Chu (1983), are

ORIGINAL PAGE IS  
OF POOR QUALITY

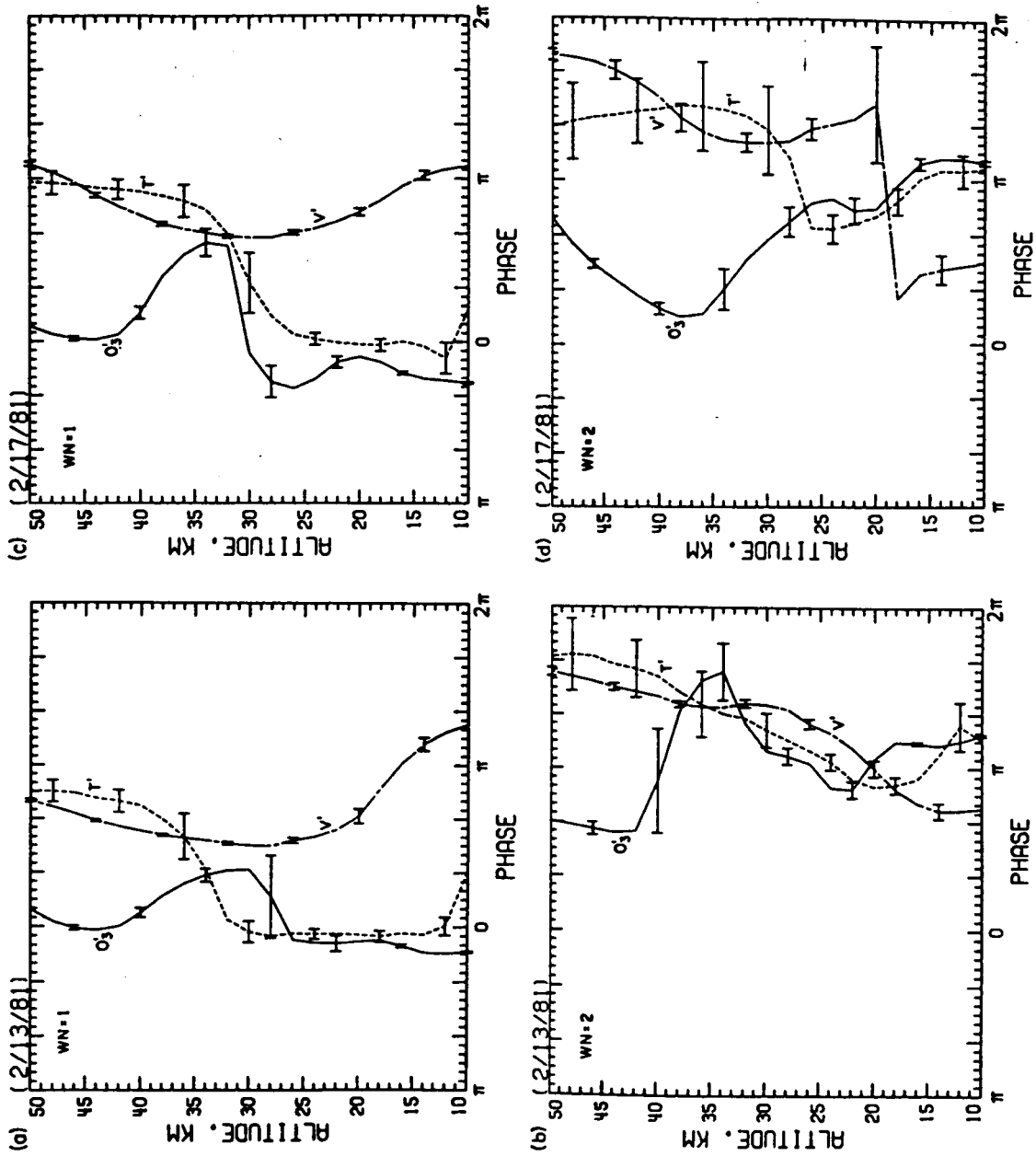


Figure 5.11. Phase relationship between ozone mixing ratio (solid line), temperature (dashed line), and eddy meridional velocity (solid and dashed line) waves during the middle February 1981 warming ( $\sim 52^\circ\text{N}$ ). Phase increases westward: (a) wavenumber 1, February 13, 1981; (b) wavenumber 2, February 13, 1981; (c) wavenumber 1, February 17, 1981; and (d) wavenumber 2, February 17, 1981.

Figure 5.11.

the computed uncertainty of the calculated phase based on the given uncertainty of the SAGE and meteorological data. On the one hand, Figure 5.11a shows that the ozone and temperature waves are nearly out-of-phase above approximately 42 km. Below about 27 km, on the other hand, they are closely in-phase. In the region between approximately 27 km and 42 km, a change from the in-phase relationship below 27 km to an out-of-phase one about 42 km takes place. As to the phase relationship between ozone and meridional waves, it is observed that they are generally out-of-phase below about 25 km and above approximately 43 km (Figure 5.11a). They become closely in-phase at altitudes centered at 30 km. This phase relationship explains the vertical variation of the wavenumber 1 ozone transport which was observed on February 13, 1981 (Figure 5.8a). The phase relationship between temperature and meridional waves can also be seen in Figure 5.10a. In the region above 32 km, their phase difference is less than  $\pi/2$ , and is greater than  $\pi/2$  in the region below. This feature explains the two distinct regions of different heat transport directions which was observed on the corresponding day (Figure 5.10a). The phase relationship of wavenumber 2 components on February 13, 1981 is shown in Figure 5.11b. The ozone and temperature waves are observed to be out-of-phase above 42 km. Below 38 km, they are generally in-phase. A similar phase relationship also can be found to exist between ozone and meridional velocity waves. The wavenumber 2 component of the temperature and meridional velocity waves are observed to be closely in-phase throughout the entire altitude range of this study on February 13, 1981. This phase relationship between temperature and meridional waves accounts for the poleward heat transport at all altitudes on this particular date. The phase relationship between ozone, temperature, and meridional velocity waves on February 17, 1981 are shown in Figures 5.11c and 5.11d, for wavenumber 1 and wavenumber 2, respectively. As can be seen, the

phase relationships are generally similar to those on February 13, between the corresponding wave components.

The detailed time variation of the wavenumber 1 phase relationship over the period of the data set at altitudes 44 km and 26 km are shown in Figures 5.12a and 5.12b, respectively. The former shows the typical phase relationship in the upper stratosphere and the latter depicts that in the lower stratosphere. It is evident that an out-of-phase relationship between ozone and temperature waves in the upper stratosphere and a nearly in-phase relationship in the lower stratosphere occurred throughout during this mid-February 1981 warming. Similar phase relationships can also be found for the wavenumber 2 components (Figures 5.12c and 5.12d). The evolutions of the phase of meridional velocity waves are also shown in Figures 5.12a to 5.12d for comparison.

#### 5.3.4 Summary

We have analyzed the planetary waves of ozone mixing ratio, temperature and meridional velocity near  $52^{\circ}\text{N}$  during the middle February 1981 stratospheric warming by utilizing SAGE ozone data and the associated meteorological information. In addition, the eddy ozone and temperature fluxes during this warming were also examined. The result large temperature wavenumber 1 developments in the upper stratosphere centered at altitude 44 km and also in the lower stratosphere with a peak at about 22 km. The maximum intensities of about  $12^{\circ}\text{C}$  and  $10^{\circ}\text{C}$  in the upper and lower stratosphere, respectively, occurred on approximately February 15, 1981. Comparatively, the corresponding wavenumber 2 component is much weaker in intensity, especially in the upper stratosphere. Nevertheless, the wavenumber 2 activities in the lower stratosphere, centered at 22 km, are clearly visible in the computed results

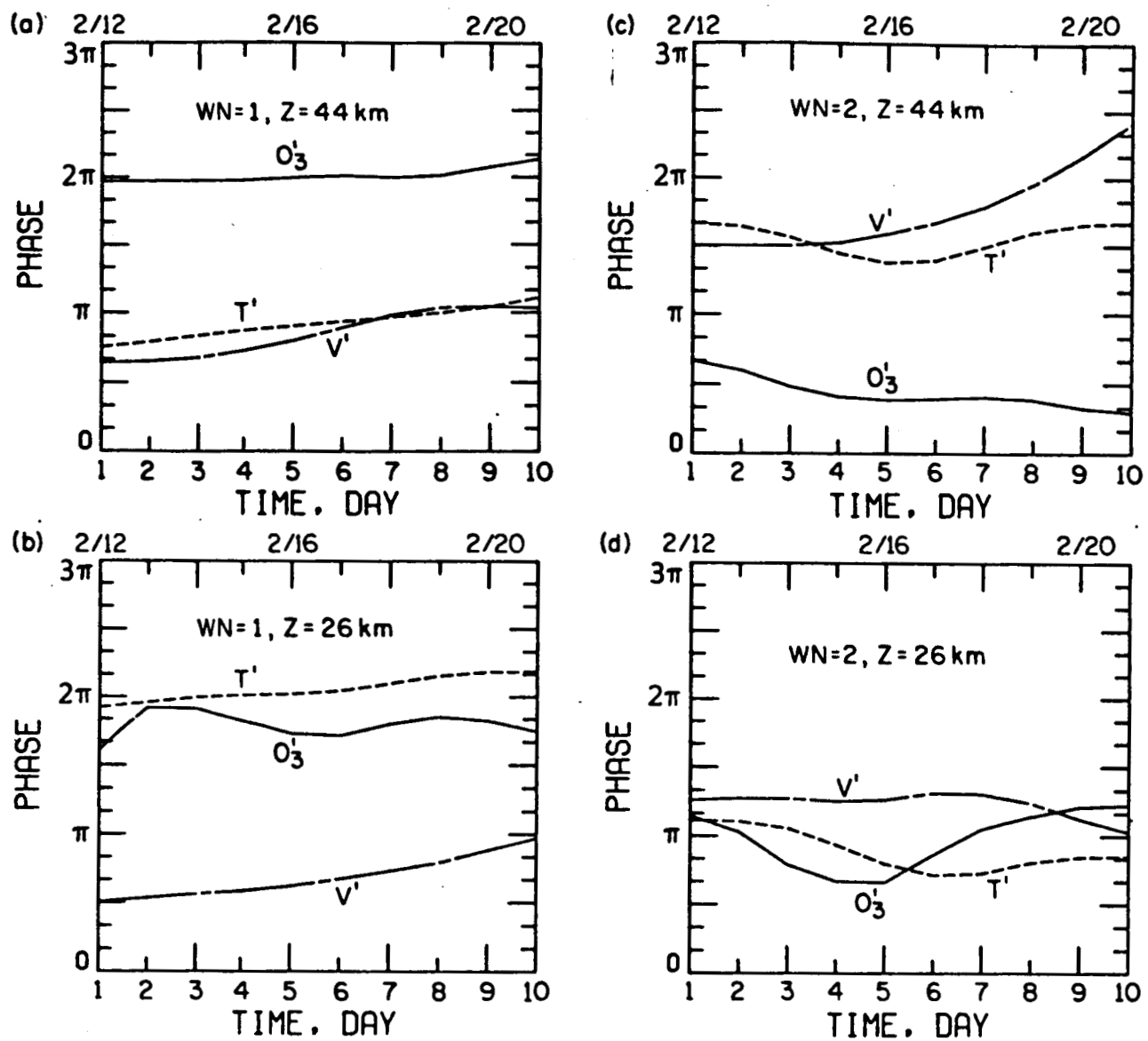


Figure 5.12. Time variation of the phase relationship between ozone mixing ratio (solid line), temperature (dashed line), and eddy meridional velocity (solid and dashed line) waves during the middle February 1981 warming ( $\sim 52^\circ\text{N}$ ). Phase increases westward:  
 (a) wavenumber 1, 44 km altitude; (b) wavenumber 1, 26 km;  
 (c) wavenumber 2, 44 km; (d) wavenumber 2, 26 km.

and were observed to decrease during almost the entire data period of this study. With respect to the meridional velocity waves, the peak intensity of the wavenumber 1 component occurred at an altitude about 37 km on February 14, 1981. In contrast, the corresponding wavenumber 2 component exhibited an overall decline of the wave amplitude during this middle February 1981 warming. The analysis of the ozone mixing ratio wave during this period exhibits a distinct development of wavenumber 1 in the upper stratosphere centered at 44 km with the peak intensity occurring on February 15, 1981. In the lower stratosphere, the ozone wavenumber 1 was much less active and remained rather steady throughout the entire period of this middle February warming. This trend also seems to be the case for the wavenumber 2 ozone mixing ratio waves. With respect to ozone eddy transports, the results show a layer with poleward transport between approximately 30 km and 40 km. This transport was found to be decreasing during this warming period. Above 40 km, ozone was being transported equatorward with the peak intensity occurring on February 15 at 44 km. The results also indicate that the wavenumber 1 activity is the dominant component in this ozone transport. In the case of eddy temperature transport, the results show large poleward fluxes above about 30 km. The peak of the fluxes occurred on February 14, 1981 at altitude 44 km. Similar to the case of ozone transport, wavenumber 1 component is found to be primarily responsible for the temperature transport.

Furthermore, the results of this warming have also been compared with those of the late February 1979 warming. For completeness, the synoptic aspects of the large scale disturbances during the Winter 1980-1981 were discussed. Similar discussions on that of the Winter 1978-1979 were also included for comparison purpose. It is interesting to note that, in contrast

to the late February 1979 warming which involves disturbances with an outstanding wavenumber 2 component, this middle February 1979 warming is associated primarily with large amplifying wavenumber 1 disturbances (Figures 5.2c and 5.3c). Despite this distinct difference in the planetary wave activities between these two warming events, many common features are clearly evident. First of all, the results show that the development of ozone wavenumber 1 component in the upper stratosphere was closely associated with that of corresponding temperature waves. More specifically, they are negatively correlated. This feature is also noticeable in the case of wavenumber 2 component although it is not as predominant as wavenumber 1. Furthermore, in both warmings, there was rapid increase in the zonally-averaged ozone column abundance. This increase was shown to be a response to the increases of the zonal mean ozone number density in the lower stratosphere centered at altitude 20 km. With respect to the ozone mixing ratio transports associated with the waves, the results generally show the equatorward transports in the upper stratosphere and poleward transports in the middle stratosphere. In the lower stratosphere, the transport is much less intense. The equatorward ozone transport in the upper stratosphere is found to be accompanied by poleward heat transport during both warming events. As to the phase relationship between ozone and temperature waves, the computed results of this warming event also show three distinct layers, i.e., an out-of-phase relationship in the upper stratosphere and an in-phase relationship in the lower stratosphere with a transition layer in between.

Finally, in contrast to the warming case studied by Wang, McCormick and Chu (1983), which involves an outstanding wavenumber 2 activity, this analysis was devoted to a warming dominated by wavenumber 1 development. Although the data period covers only 10 days, it includes the second half

part of the major midwinter warming according to Labitzke and Goretzki (1982). Furthermore, like the analysis of Wang, McCormick and Chu (1983), the results of this investigation can be useful for modeling the winter circulation in the northern high latitude stratosphere and for simulating the planetary wave development and their transport effects.

6. TASK 5--TO INVESTIGATE THE FORMATION AND EVOLUTION OF AEROSOLS INCLUDING  
THE STUDY OF PHYSICAL AND CHEMICAL PROCESSES

6.1 Post-Volcanic Decay Rates

6.1.1 Introduction

Stratospheric aerosol concentrations are strongly dependent upon volcanic injection of sulfur dioxide followed by chemical conversion into sulphate and growth of sulfuric acid aerosols. Theoretical simulations and experimental measurements of aerosol optical properties show two distinct phases (Deirmendjian 1973; Deepak 1982). There is an initial growth phase lasting 3-6 months, followed by a slower quasi-exponential decay over a somewhat longer time period. Comparison of theoretical models and direct measurements have suffered in the past from the fact that the experimental observations are usually made from a single location on the ground or, if from an airborne platform, are limited to a relatively short time period. In both cases, the experimental results are strongly affected by poorly known aerosol movements and may not represent well the global variation in stratospheric aerosol concentration.

The advent of the SAM II and SAGE satellite systems with global capability for measuring stratospheric aerosol extinction (McCormick et al. 1979) has enabled a much more accurate picture to be obtained of the aerosol mass variation following volcanic injection (Kent 1982; Kent and McCormick 1984). It is thus of interest to make a more detailed comparison of these new experimental results with the predictions of the theoretical models and to use this comparison to determine the principal contents of the aerosol growth and decay. The approach used in this paper has been to search for a simple

empirical function that provides a good fit to an available theoretical model (Turco et al. 1982). This function, containing adjustable constants has then been fitted to the global optical depth time sequence as obtained from the SAGE/SAM II measurements between February 1979 and November 1981. The use of a fitted function, rather than an apparently simpler direct measurement from the optical depth sequence, is made necessary by the fact that five eruptions of significance occurred during this time period with overlapping and superimposed stratospheric effects.

#### 6.1.2 Derivation of empirical function and fitting to theoretical curves

A recent theoretical study, showing the predicted long-term variation in stratospheric aerosol optical depth following volcanic injection, is that of Turco et al., 1982. This study simulates the physical and chemical processes associated with the stratospheric aerosol following the eruption of Mt. St. Helens in May 1980. The resultant optical depth variations (at wavelength of 0.55  $\mu\text{m}$ ) were determined as a function of time after the eruption for different injected quantities of  $\text{SO}_2$  and  $\text{H}_2\text{O}$ . These variations are shown by the solid lines in Figure 6.1. An empirical analytic function, providing a good fit to these theoretical curves, was searched for subject to the following criteria:

1. It should not contain more than two or three floating parameters.
2. It should fit both the rising and falling portions of the growth curves.

3. It should be subject to easy computation and give unambiguous figures for the time between the eruption and the maximum optical depth and the initial rate of decay following the maximum.

The functional form adopted was

$$f(t) = A + B t^n e^{-t/t_0} \quad (1)$$

where

$t$  = time after the eruption

$f(t)$  = optical depth

$A$  = a constant (background level prior to eruption)

and  $B$ ,  $n$  and  $t_0$  are empirical constants to be determined from the fitting.

Examination of this equation shows that the time between the eruption and maximum optical depth is given by

$$t_m = n t_0 \quad (2)$$

and that the maximum optical depth

$$f_m = A + B t_m^n e^{-t_m/t_0} \quad (3)$$

The time,  $t_d$ , taken for the increase in optical depth to decay by a factor  $1/e$  from its maximum value is given by the equation

$$\left(\frac{t_d}{t_m}\right) - \ln\left(\frac{t_d}{t_m}\right) = 1 + 1/n \quad (4)$$

For large  $t$ , the decay becomes quasi-exponential with time constant  $t_o$ .

Equation (1) has been fitted to both the theoretical and experimental data using the Levenberg-Marquardt algorithm (Brown and Dennis, 1972) for a non-linear least squares approximation, the calculations being carried out on the Control Data computer system at NASA/LaRC. In the case of fitting to the theoretical model, Turco et al.'s theoretical curves have been read at 0.75-month intervals from 0 to 9 months, 1.5-month intervals from 9 to 12 months and 3-month intervals from 12 to 27 months. The resultant curves for the fitted empirical function are shown by the dashed lines in Figure 6.1, the derived parameters being listed in Table 6.1. From inspection of Figure 6.1, it can be seen that the theoretical models and the fitted analytic functions agree very well. Table 6.1(b) shows the difference between the three main parameters,  $f_m$ ,  $t_m$  and  $t_d$ , derived from the fitted functions and directly measured from the theoretical curves. With the exception of the time delays for Model (1), where there is a three-week error in the determination of time of maximum, the errors are extremely low. Taking into consideration that the purpose of using an analytical model function is to derive these parameters from experimental data which itself will contain considerable uncertainties, these differences are considered acceptable. It should be noticed that the empirical formula has been chosen to fit the first two years variation after an eruption and is not necessarily representative of the behavior over a longer time period.

#### 6.1.3 Fitting to experimental data

The experimental data set used is that obtained by the SAGE and SAM II satellite systems between February 1979 and November 1981. The data set has been used by Kent and McCormick (1984), to derive the global mean

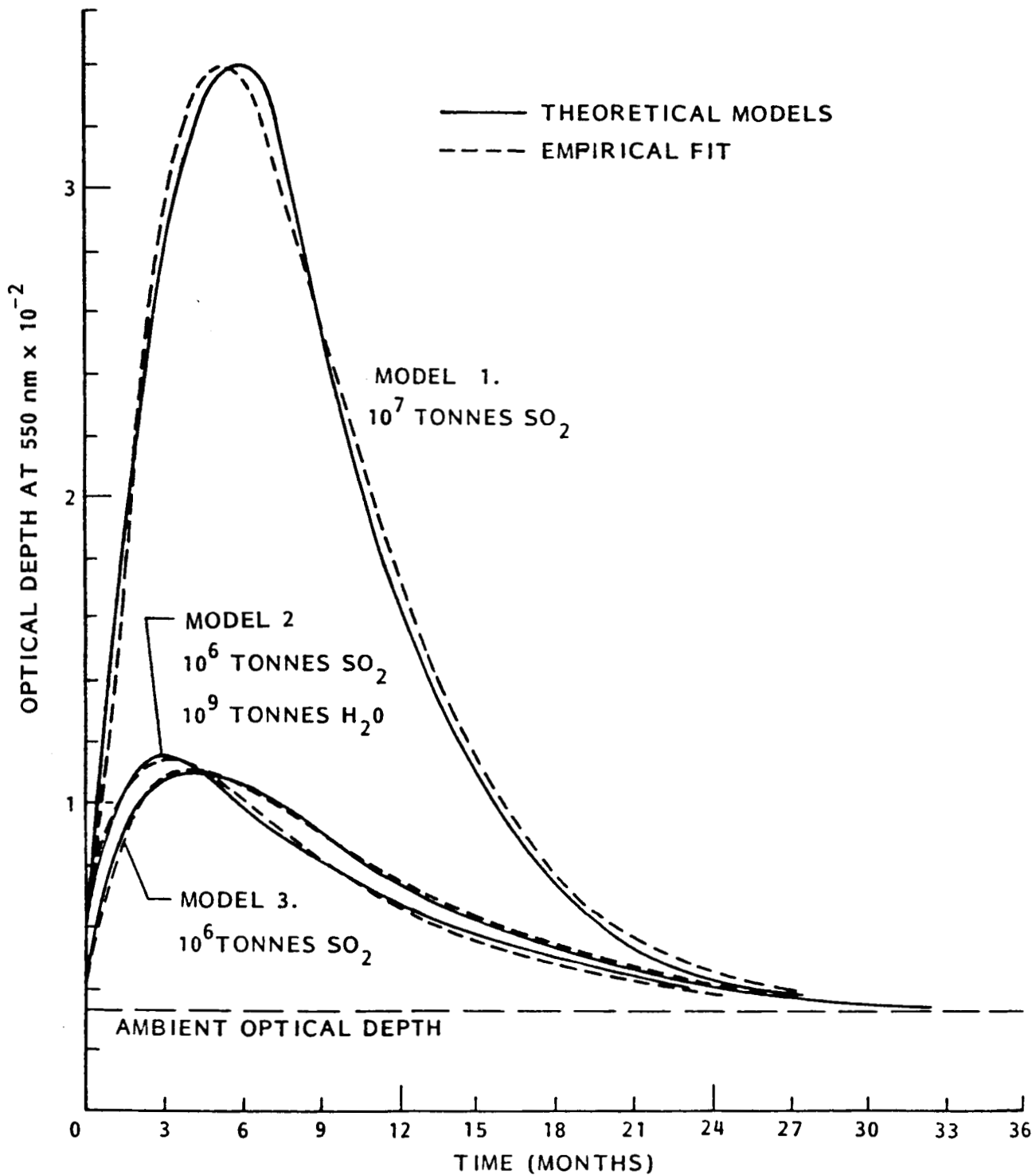


Figure 6.1. Modeled variations in stratospheric aerosol layer optical depth (at  $0.55 \mu\text{m}$ ) following volcanic eruptions with different amounts of injected material (Turco et al., 1982). Solid curves show results of theoretical calculations, dashed curves the fitted empirical functions.

TABLE 6.1(a). Constants Derived from Empirical Fitting to Theoretical Models in Figure 1.

Theoretical Model No.	$A$ ( $10^{-2}$ )	$B$ ( $10^{-2}$ )	$n$	$t_0$ (months)	$f_m$ ( $10^{-2}$ )	$t_m$ (months)	$t_d$ (months)
1	.338	1.406	1.365	3.52	3.39	4.80	8.36
2	.337	.779	.509	5.59	1.13	2.85	9.85
3	.321	.611	.657	6.01	1.10	3.95	11.40

TABLE 6.1(b). Comparison of Constants Shown in Table 1(a) with Those Determined Directly from the Theoretical Models.

Theoretical Model No.	Maximum Optical Depth, $f_m$ ( $10^{-2}$ )			Time Delay to Maximum, Optical Depth, $t_m$ (months)			$1/e$ Decay Time, $t_d$ (months)		
	Empirical Fit	Model	Error (%)	Empirical Fit	Model	Error (%)	Empirical Fit	Model	Error (%)
1	3.39	3.40	1	4.80	5.6	-14	8.36	7.1	+12
2	1.13	1.15	-2	2.85	2.9	-2	9.85	10.3	-4
3	1.10	1.09	+1	3.95	4.1	-4	11.40	11.3	+1

stratospheric aerosol optical depth at 1.0  $\mu\text{m}$  measured from 2 km above the tropopause for the Northern and Southern Hemispheres over this time period and is fully described by them. Large variations in optical depth were observed which were attributed to one or the other of five volcanic eruptions which affected the stratosphere during this period. Figure 6.2 shows the mean global optical depth as a function of time and also shows the times of eruption of these five significant eruptions. Prior to the first eruption, that of Sierra Negra in November 1979, the mean global optical depth is almost constant. Following each eruption, the optical depth increases to a maximum after 4-5 months, following which a decrease is observed. The eruptions have occurred sufficiently close together in time that the stratospheric effects overlap. This is particularly true for Alaid and Pagan which we shall not be able to separate analytically and for St. Helens and Ulawun which are separable. In two places, just after the eruptions of St. Helens and Ulawun, double values are shown for the optical depth. One of these corresponds to the total global average. The other has been obtained by averaging over a hemisphere (extending from the North to South Poles), which, because of the still localized nature of the stratospheric injection from the recent eruption, is unaffected by that eruption. Error bars representing the uncertainty in the mean optical depth are shown in the figure; the sources of error have been discussed in detail by Kent and McCormick (1984).

The maximum optical depth, the time between each volcanic eruption and that of the corresponding maximum optical depth and the decay time for the injected aerosol has been derived for each eruption by fitting a function of

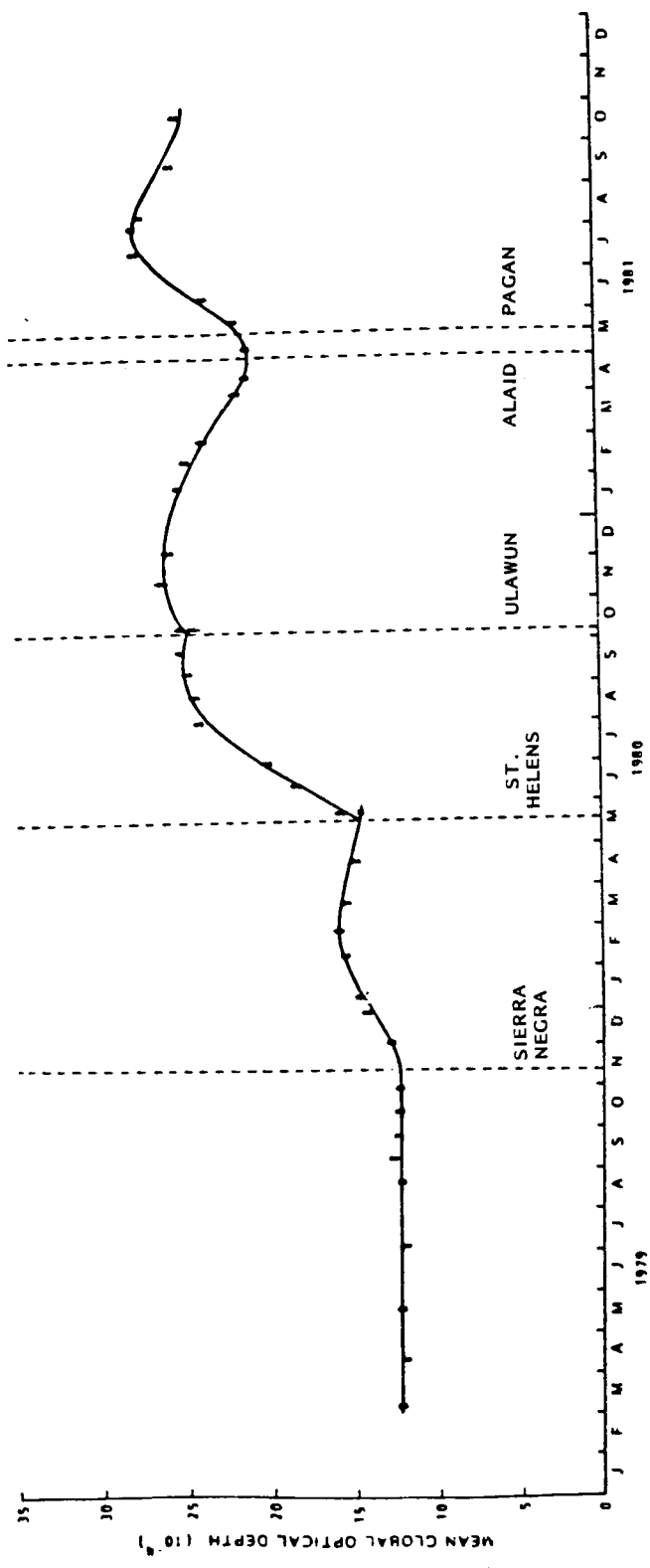


Figure 6.2. SAM II/SAGE measurements of mean global stratospheric aerosol layer optical depth (at 1.0  $\mu\text{m}$ ). Crosses indicate experimental values, the solid curve the best fit empirical function.

TABLE 6.2. Key Background and Volcanic Parameters Determined from Empirical Fitting.

Aerosol Source	Maximum Optical Depth, $f_m$ ( $10^{-4}$ )	Time Delay to Maximum Optical Depth, $t_m$ (months)	1/e Decay time, $t_d$ (months)
Background	$12.4 \pm .1$ (1%)	—	—
Sierra Negra	$3.5 \pm .2$ (6%)	$3.5 \pm .2$ (6%)	$5.1 \pm .5$ (10%)
St. Helens	$11.9 \pm .3$ (3%)	$4.5 \pm .4$ (9%)	$8.4 \pm 1.2$ (14%)
Ulawun	$3.9 \pm 1.1$ (28%)	$3.7 \pm .5$ (14%)	$6.7 \pm 2.7$ (40%)
Alaid & Pagan (Average)	$5.4 \pm 3$ (6%)	$3.8 \pm .1$ (3%)	$6.3 \pm .5$ (7%)
Weighted Mean	—	$3.8 \pm .1$ (3%)	$5.9 \pm .3$ (5%)

the form

$$f(t) = A + \sum_{i=1}^{i=5} B_i (t - t_i)^{n_i} e^{-(t - t_i)/t_{oi}} \quad (5)$$

to the data points shown in Figure 6.1. In this equation, A is constant representing the prevolcanic background condition and the suffix i refers in sequence to each of the five volcanic eruptions.  $t_i$  refers to the time of the ith eruption and  $n_i$  and  $t_{oi}$  have the meanings defined earlier in relation to the ith eruption. It is, in addition, assumed that the contribution to the total optical depth of any volcano, prior to its eruption, is zero. Because of the impossibility of separating the effects of Alaid and Pagan within a global average, it has been necessary to set  $B_4 = B_5$ ,  $n_4 = n_5$  and  $t_{o4} = t_{o5}$  in order to stabilize the solution. Equation 5 thus contains 13 unknown parameters representing the background and the various eruptions. Despite this, a unique solution was readily obtained which has been used to derive the peak optical depth and appropriate time constants for each eruption. Data for the peak optical depths and their use to estimate the mass loading for each volcano has been presented by Kent and McCormick (1984) and will not be discussed in any detail here.

Although use of Equation (5) permits the derivation of a unique set of parameters, it is not obvious how the errors in the values for optical depths shown in Figure 6.2 should be used to derive corresponding errors in the derived parameters. This problem was handled by a statistical approach. The optical depth errors were used, in conjunction with a random number generator, to randomly increase or decrease each measured optical depth value from its mean value by an amount equal to its standard error. Each set of new optical depth values thus obtained was used in conjunction with Equation

(5) to determine a set of parameters for each volcanic eruption. This process was repeated a large number of times (approximately two hundred) using different sets of random numbers and the mean and standard deviation found for the total set of values for each parameter. These are shown in Table 6.2. The best estimate of  $f(t)$  [Equation (5) is shown by the solid line in Figure 6.2.]

The fit between the analytic curve and the experimental data shown in Figure 6.2 is seen to be extremely good, the curve lying within the limits of the error bars for most data points. This fit indicates that there is a close relationship between the theoretical and experimental results and that both are well simulated by Equation (1). In noting this fact, it should be remembered that the theoretical optical depth curves were calculated for a wavelength of  $0.55 \mu\text{m}$  whereas the experimental measurements were made at a wavelength of  $1.0 \mu\text{m}$ . The two are not equivalent and their relationship depends on the aerosol size distribution and composition of the volcanic aerosol, which will certainly change during the months following an eruption. Thus, even though the analytic forms used for the growth and decay curves are the same, the parameters of the curves might be expected to differ somewhat in the two cases.

Values for  $t_m$  and  $t_d$  in Table 6.2 may be compared with each other and also with the theoretical values in Table 6.1. The errors in Table 6.2 may be compared with those shown in Table 6.1. The main conclusions to be shown are:

1. With the exception of the Ulawun eruption, whose effects are difficult to separate from those of St. Helens, errors in the calculated parameters are less than about 10%.

2. The time between the eruption of each volcano and its maximum effect on the stratosphere,  $t_m$  is between  $3-1/2$  and  $4-1/2$  months for all the eruptions studied, agreeing quite well with the values in Table 6.1(a).

3. The  $1/e$  decay time,  $t_d$  shows more variability and more error than  $t_m$  with its average value being about 6 months. This is somewhat smaller than the values in Table 6.1(a).

4. Errors in  $f_m$ ,  $t_m$  and  $t_d$  in Table 6.2 are, in general, somewhat larger than those in Table 6.1(b) and are, therefore, not greatly effected by the inaccuracies in the empirical model.

#### 6.1.4 Comparison with other observations and conclusions

Many observations have been made of the remote optical and in situ changes produced in the stratosphere by volcanic eruptions. These measurements and the subsequent estimates of the aerosol mass loading and its rate of change suffer from the disadvantage of having only limited sampling in either space or time or both. This can effect very strongly the observed time delay,  $t_m$  to maximum stratospheric change, as the maximum effect observed from a single point on the ground may be produced by the passing of a single intense cloud of material which is unrepresentative of the global distribution. To a lesser extent, the decay rate is also effected, being strongly dependent upon the closeness of the observing point to any stratospheric aerosol reservoirs and to the seasonal movements within and between the hemispheres. Data comparisons may thus be regarded as semi-quantitative rather than exact. While general conclusions may be drawn regarding the behavior of the stratosphere following an eruption, any exact study, such as distinguishing the characteristics of one eruption from another, must be regarded as difficult.

TABLE 6.3. Estimates of Stratospheric Time Constants for Volcanic Injection  
Made by Other Workers.

Authors	Eruption	Observational Technique	Maximum Effect (Months)	Time Delay to 1/e Decay Time (Months)
Deirmendjian (1973)	Krakatoa (1883, 6°S) Katmai (1912, 58°N) Agung (1963, 8°S)	Atmospheric Optical Anomalies (various locations) Turbidity measurement (34°N) Turbidity measurement (29°S)	4-5	Effects lasted 2-1/2 years
Lazarus et al. (1979)	Fuego (1974, 15°N)	In situ sampling by aircraft (75°N - 10°S)	~5	~12 (mass loading)
McCormick et al. (1978)	Fuego (1974, 15°N)	Lidar backscattering (37°N)	~3	4.9 (initial rate for integrated backscattering) 3.4 (initial rate for peak backscattering)
Cadle et al. (1977)	Fuego (1974, 15°N)	Lidar peak backscattering (40°N)	~2	~9
Hofmann et al. (1983)	Sierra Negra (1979, 1°S)	Lidar peak backscatter (48°N) and equivalent from in situ balloon (41°N)	~2	~6
	St. Helens (1980, 46°N)	Lidar peak backscatter (48°N) and equivalent from in situ balloon (41°N)	~1-1/2	~10
	Alaid (1981, 51°N)	Lidar peak backscatter (48°N) and equivalent from in situ balloon (41°N)	~1-1/2	5
Hofmann and Rosen (1983, 1984)	El Chichón (1982, 17°N)	In situ balloon (28°N and 51°N)	~1-1/2 (mass loading, 28°N)	~8 (mass loading, 28°N)
			~12 (mass loading, 41°N)	~12 (mass loading, 41°N)
			~4 (particle radius, 20-25 km, 28°N and 41°N)	~4 (particle radius, 20-25 km, 28°N and 41°N)
			>12 (particle radius, 20 km, 28°N and 41°N)	>12 (particle radius, 17- 20 km, 28°N and 41°N)

Table 6.3 lists some of the observations made of stratospheric effects following volcanic injection, together with estimates of the relevant time constants. The list is not exhaustive, but includes both observations made on earlier eruptions and observations made by other workers on the eruptions discussed in the present paper. Latitudes at which the observations were made, as well as those of the eruptions, are shown in the table. In general, quantitative terms, the values for the two major time constants, are consistent with each other and with the values shown in Table 6.2. In detail, the agreement is not good and illustrates the comments made above concerning the problems of determining volcanic time constants from a single or a small number of ground observation points. Thus, the low values of 1-1/2 to 2 months, observed for the time delay to maximum effect at some stations, are almost certainly due to the passage of single intense volcanic clouds over those stations. The range of values observed by Hofmann and Rosen (1983, 1984) for El Chichon arises from the different height ranges and different parameters measured. This list illustrates the difficulty of extrapolating from local to global terms.

The main conclusion to be drawn from the analysis presented in this paper is that it is now possible, given the global coverage of satellites, such as SAM II and SAGE, to establish fairly precisely the rates of change in the stratospheric aerosol concentration following a significant volcanic eruption. The empirical model used here represents a useful technique for doing this particularly when several eruptions occur within a limited time frame, such that their atmospheric effects overlap.

7. TASK 6--TO INVESTIGATE THE DETERMINATION OF STRATOSPHERIC MOLECULAR AND AEROSOL OPTICAL PROPERTIES USING MULTIWAVELENGTH EXTINCTION AND BACKSCATTER DATA

7.1 Retrieval of Aerosol Properties from Aerosol Extinction Ratios at 0.45  $\mu\text{m}$  and 1.0  $\mu\text{m}$

The possibility of retrieving the size distribution of aerosol particles in the stratosphere by measuring the extinction of solar radiation traversing the aerosol medium at wavelengths 0.45  $\mu\text{m}$  and 1.0  $\mu\text{m}$  has been explored in this study. The aerosol size distributions used consisted of nine analytical expressions, including most stratospheric aerosol models used by investigators. The aerosol compositions used were supercooled sulfuric acid droplets, with different weight percentage of  $\text{H}_2\text{SO}_4$  in the aerosol.

In each aerosol size expression used, there are two unknowns, namely, the constant  $N$ , which determines the number concentration of aerosol particles and the variable parameter,  $r_g$ , which determines the mode radius of the aerosol size distribution. To eliminate one unknown, we calculated  $R$ , the ratio of the volume extinction coefficient of solar radiation by aerosol particles at wavelength  $\lambda = 0.45 \mu\text{m}$  to the volume extinction coefficient at wavelength  $\lambda = 1.0 \mu\text{m}$ . Results of this parametric study showed that  $R$  was not very sensitive to either the composition or the radii limits of stratospheric aerosol under consideration, but was quite sensitive to the value of the variable parameter governing the mean radius. In addition, there was a one-to-one correspondence between the extinction ratio  $R$  and the variable parameter in all nine aerosol size distributions. Consequently, the experimental value for  $R$  could be utilized to retrieve the variable parameter from the plotted curves generated in this study. After the variable

parameter had been retrieved, the expected aerosol extinction coefficient for N=1 could be calculated using Mie scattering theory and the true value of N for aerosol particles in the atmosphere was then given by the ratio of the measured aerosol extinction coefficient to the expected aerosol extinction coefficient for N=1.

This work has been published in Applied Optics (Yue and Deepak, 1983). The abstract is included in Appendix J.

## 7.2 Multiwavelength Aerosol Extinction Models

Between 1979 and 1982, there were several volcanic eruptions that injected material into the stratosphere. This series culminated in the very large eruption of El Chichon whose effects are only now disappearing (in 1986). In view of the great changes to the stratospheric aerosol layer that were observed during this period, it is of interest to ask in what manner these changes have affected the multiwavelength extinction characteristics of the aerosol. A preliminary study was made of these changes, using the seven wavelengths listed in Table 7.1 (SAGE II wavelengths) and three stratospheric models. The models are as follows:

MOD 4: A prevolcanic model (based on measurements by Gras and Michael, 1979)

MOD 5: A post Mt. St. Helens model (based on measurements by Hofmann and Rosen, 1982)

MOD 6: A post El Chichon model (based on measurements by Hofmann and Rosen, 1984)

TABLE 7.1. Modeled Stratospheric Aerosol Extinction.

$\lambda$ ( $\mu\text{m}$ )	MOD 4	MOD 5	MOD 6
	EXT, $\text{m}^{-1}$	EXT, $\text{m}^{-1}$	EXT, $\text{m}^{-1}$
.385	$.314 \times 10^{-6}$	$1.95 \times 10^{-6}$	$8.86 \times 10^{-6}$
.448	$.292 \times 10^{-6}$	$1.66 \times 10^{-6}$	$8.69 \times 10^{-6}$
.453	$.291 \times 10^{-6}$	$1.65 \times 10^{-6}$	$8.71 \times 10^{-6}$
.525	$.200 \times 10^{-6}$	$1.43 \times 10^{-6}$	$9.06 \times 10^{-6}$
.600	$.226 \times 10^{-6}$	$1.248 \times 10^{-6}$	$9.20 \times 10^{-6}$
.940	$.107 \times 10^{-6}$	$.715 \times 10^{-6}$	$7.82 \times 10^{-6}$
1.02	$.089 \times 10^{-6}$	$.631 \times 10^{-6}$	$7.40 \times 10^{-6}$
m ( $\text{kg m}^{-3}$ )	$6.5 \times 10^{-11}$	$5.01 \times 10^{-10}$	$4.09 \times 10^{-9}$
N ( $\text{m}^{-3}$ )	$.117 \times 10^7$	$.273 \times 10^8$	$.155 \times 10^8$

The results of this analysis are shown in Table 7.1, together with the aerosol mass density ( $N$ ) and particle concentration ( $n$ ). Points to note are:

1. The large effect on the extinction caused by the volcanic eruptions, particularly at the longer wavelengths;
2. The strong wavelength variation in extinction for the prevolcanic model and the lack of variation in the post El Chichon model.

Both these results reflect the effects of the larger aerosols present after the eruptions, particularly after that of El Chichon.

### 7.3 High-Altitude Lidar Modeling

Recent flights of the NASA Shuttle spacecraft have shown that the re-entry region between 70 and 100 km altitude is one in which large molecular density fluctuations occur (e.g., Price 1983). These fluctuations, which may be as great as -30% to +60% of the ambient density, are probably associated with the passage through this region of atmospheric gravity waves. The potential value of being able to study these fluctuations from the ground has led to an investigation of the possibility of upgrading and using the NASA-LaRC 48" lidar system for this purpose. Modeling studies of the theoretical performance of such an upgraded system have been carried out. Some of the results of this modeling are given in Tables 7.2, 7.3, and 7.4 which show the expected percentage uncertainty in the molecular backscattered signal from different altitudes for a 10-minute observational period. In all the cases shown here, it has been assumed that photon counting techniques are used and that the noise depends only upon signal fluctuations and background lighting conditions. Reasonable figures are used

TABLE 7.2. Theoretical Performance Figures for 48" Lidar  
System--Nighttime, Interference Filter

(A) SYSTEM PARAMETERS

Receiving Mirror Area ~ 1.00 m<sup>2</sup>  
 Full Angle Beam Divergence - 0.200E-03 r  
 Wavelength - 0.5300E-06 m  
 Overall Efficiency - 0.08  
 Pulse Energy - 0.4 J  
 Firing Rate - 10 Hz  
 Filter Bandwidth - 0.100E-08m

(B) ATMOSPHERIC PARAMETERS

Atmospheric Transmission - 0.70  
 Sky Brightness - 0.70E+00 R.A.<sup>-1</sup>

(C) OPERATIONAL PARAMETERS

Height Increment - 2.0 km  
 Integration Time - 600 S

System Constant - 8.36E+19

<u>Height</u> <u>(km)</u>	<u>Signal</u> <u>Count</u>	<u>Noise</u> <u>Count</u>	<u>% Uncertainty</u> <u>(10 Minutes Integration)</u>
65	4.26	$1.85 \times 10^{-4}$	0.63%
70	1.90	$1.85 \times 10^{-4}$	0.94%
75	0.815	$1.85 \times 10^{-4}$	1.43%
80	0.331	$1.85 \times 10^{-4}$	2.24%
85	0.121	$1.85 \times 10^{-4}$	3.72%
90	0.0428	$1.85 \times 10^{-4}$	6.25%
95	0.0150	$1.85 \times 10^{-4}$	10.59%
100	0.0057	$1.85 \times 10^{-4}$	17.40%
105	0.0022	$1.85 \times 10^{-4}$	28.56%
110	0.0009	$1.85 \times 10^{-4}$	45.93%

10 min - 10% Uncertainty Altitude = 94 km

TABLE 7.3. Theoretical Performance Figures for  
48" Lidar System--Daytime, Interference  
Filter

---

(A) SYSTEM PARAMETERS

Receiving Mirror Area - 1.00 m<sup>2</sup>  
 Full Angle Beam Divergence - 0.200E-03 r  
 Wavelength - 0.5300E-06 m  
 Overall Efficiency - 0.08  
 Pulse Energy - 0.4 J  
 Firing Rate - 10 Hz  
 Filter Bandwidth - 0.100E-08 m

(B) ATMOSPHERIC PARAMETERS

Atmospheric Transmission - 0.70  
 Sky Brightness - 8.0E+6

(C) OPERATIONAL PARAMETERS

Height Increment - 2.0 km  
 Integration Time - 600 S

System Constant - 8.36 E+19

<u>Height (km)</u>	<u>Signal Count</u>	<u>Noise Count</u>	<u>% Uncertainty (10 Minutes Integration)</u>
65	4.26	2119	13.9%
70	1.90	2119	31.2%
75	0.82	2119	72.9%
80	0.33	2119	179.6%
85			
90			
95			
100			
105			
110			

10 min - 10% Uncertainty Altitude = 63 km

---

TABLE 7.4. Theoretical Performance Figures for  
48" Lidar System--Daytime, Interference  
Filter Plus Fabry-Perot Etalon

(A) SYSTEM PARAMETERS

Receiving Mirror Area - 1.00 m<sup>2</sup>  
 Full Angle Beam Divergence - 0.200E-03 r  
 Wavelength - 0.5300E-06 m  
 Overall Efficiency - 0.04  
 Pulse Energy - 0.4 J  
 Firing Rate - 10 Hz  
 Filter Bandwidth - 1.0E-11 m (0.1 Å)

(B) ATMOSPHERIC PARAMETERS

Atmospheric Transmission - 0.70  
 Sky Brightness - 8.0E+6 R.A<sup>-1</sup>

(C) OPERATIONAL PARAMETERS

Height Increment - 2.0 km  
 Integration Time - 600 S

System Constant - 4.18E+19

<u>Height (km)</u>	<u>Signal Count</u>	<u>Noise Count</u>	<u>% Uncertainty (10 Minutes Integration)</u>
65	2.13	10.66	2.17%
70	0.95	10.66	4.83%
75	0.407	10.66	10.55%
80	0.166	10.66	25.67%
85	0.0603	10.66	70.13%
90			
95			
100			
105			
110			

10 min - 10% Uncertainty Altitude - 75 km

for angular beam-widths, system efficiencies and sky brightness; no allowance has been made for any post-detector noise or signal loss.

The conditions assumed in the tables are:

Table 7.2. Night-time with 10 Å interference filter

Table 7.3. Day-time with 10 Å interference filter

Table 7.4. Day-time with Fabry-Perot Etalon

In Table 7.2, the signal-to-noise ratio is determined mainly by signal fluctuations and useful measurements are obtainable up to about 90 km. In Table 7.3, for day-time, the sky brightness is approximately  $10^7$  greater than at night and this severely limits the system performance for altitudes above 65 km. Table 7.4 shows the improvement that may be expected if a 0.1 Å Fabry-Perot Etalon is used in conjunction with the interference filter. Considerable improvement in system performance occurs; it now being possible to obtain useful information up to about 75 km.

Results of further calculations, including modeling frequency doubled Nd-YAG, and ruby laser transmitters with different laser output energy levels have been presented in the final report to NASA, Contract NAS1-17959 (Kent and Wang, 1986). The latter report has also included an examination of the science requirements for possible density fluctuation studies.

## 8. CONCLUSIONS

A detailed study has been made of the SAM II data set from October 1978 to February 1983 and of the entire SAGE I data set from February 1979 to November 1981. The emphasis of this study has been on the validation of these data sets by their use in various analyses of the dynamical, physical and chemical processes taking place in the stratosphere. Much of the analysis has been climatological; this has included studies of the statistics of polar stratospheric clouds and of the global scale changes taking place in the stratosphere following volcanic injection. Related analyses have included the preparation of plots, tables and films showing these climatologies in as direct and simple a manner as possible. In the course of this work, various anomalies and inconsistencies in the data have been noted, this information has either been given to NASA to permit updating of successive editions of the archived data or has been specifically listed for user application (e.g., Table 2-6).

The SAGE I and SAM II data have also been used for the study of atmospheric phenomena, such as the changes in aerosol and ozone concentrations taking place in the vicinity of the north polar vortex. The SAGE I multiwavelength data have been used to investigate changes in the aerosol size distribution and the ozone data to study winter-time eddy fluxes in relation to planetary wave activity. As part of the direct data validation program, SAGE I and SAM II, 1.0 um aerosol data have been intercompared wherever the satellite events have occurred close together in space and time.

These studies have shown the quality of the data to be excellent. Results of the scientific analyses have been presented at scientific

conferences and have been published in relevant journals. The data, now archived, will represent an invaluable information source for many years, the analyses described in this report representing only a fraction of its possible uses.

## 9. REFERENCES

- Barnett, J. J., J. T. Houghton, and J. A. Pyle, 1975: The temperature dependence of the ozone concentration near the stratopause, Quart. J. Roy. Meteor. Soc., 101, 245-257.
- Bigg, E. K., 1976: Size distributions of stratospheric aerosols and their variations with altitude and time, J. Atmos. Sci., 33, 1080-1086.
- Brown, K. M., and J. E. Dennis, 1972: Derivative free analogues of the Levenberg-Marquardt and Gauss algorithms for non-linear least squares approximations," Numerische Mathematik, 18, 289-297.
- Cadle, R. D., F. G. Fernald, and C. L. Frush, 1977: Combined use of lidar and numerical diffusion models to estimate the quantity and dispersion of volcanic eruption clouds in the stratosphere: Volcan Fuego, 1974 and Augustine, 1976, J. Geophys. Res., 82, 1783-1786.
- Chu, W. P., and M. P. McCormick, 1979: Inversion of stratospheric aerosol and gaseous constituents from spacecraft solar extinction data in the 0.38-1.0 um wavelength region, Appl. Opt., 18, 1404-1413.
- Craig, R. A., 1965: The Upper Atmosphere and Physics, Academic Press, New York, 509 pp.
- Deepak, A. (Ed.), 1982: Atmospheric Effects and Potential Climatic Impact of the 1980 Eruptions of Mt. St. Helens. NASA Conference Publication 2240, 303 pp.
- Deirmendjian, D., 1973: On volcanic and other particulate turbidity anomalies, Advan. Geophys., 16, 267-296.
- Farlow, N. H., G. V. Ferry, H. Y. Lem, and D. M. Hayes, 1979: Latitudinal variations of stratospheric aerosols, J. Geophys. Res., 84, 733-743.
- Farrukh, U.O. 1986: Polar Stratospheric Cloud Sightings by SAM II: 1978-1982, NASA Contractor Report 117995 (March).
- Garcia, R. R. and D. L. Hartmann, 1980: The role of planetary waves in the maintenance of the zonally averaged ozone distribution of the upper atmosphere, J. Atmos. Sci., 37, 2248-2264.
- Gille, J. C., P. L. Bailey, and J. M. Russell III, 1980: Temperature and composition measurements from the l.r.i.r. and l.i.m.s. experiments on Nimbus 6 and 7, Phil. Trans. Roy. Soc., London, A296, 205-218.
- Gras, J. L., and C. G. Michael, 1979: Measurement of the stratospheric aerosol particle size distribution, J. Appl. Meteor., 18, 855-860.
- Hamill, P., and L. R. McMaster (Eds.), 1984: Polar Stratospheric Clouds, Their Role in Atmospheric Processes, NASA Conference Publication 2318.
- Hartmann, D. L., and R. R. Garcia, 1979: A mechanistic model of ozone transport by planetary waves in the stratosphere, J. Atmos. Sci., 36, 350-364.

Hofmann, D. J., and J. M. Rosen, 1982: Balloon-based observations of stratospheric aerosol and condensation nuclei during the year following the Mt. St. Helen's eruption, J. Geophys. Res., 87, 11039-11061.

Hofmann, D. J., and J. M. Rosen, 1983: Stratospheric sulfuric acid fraction and mass estimate for the 1982 volcanic eruption of El Chichon, Geophys. Res. Lett., 10, 313-316.

Hofmann, D. J., and J. M. Rosen, 1984: On the temporal variation of stratospheric aerosol size and mass during the first 18 months following the 1982 eruptions of El Chichon, J. Geophys. Res., 89, 4883-4890.

Hofmann, D. J., J. M. Rosen, R. Reiter, and H. Jager, 1983: Lidar and Balloon-borne particle counter comparisons following recent volcanic eruptions, J. Geophys. Res., 88, 3777-3782.

Holton, J. R., 1975: The Dynamic Meteorology of the Stratosphere and Mesosphere, Meteor. Monogr., No. 37, Amer. Meteor. Soc., 261 pp.

Holton, J. R., and W. M. Wehrbein, 1980: A numerical model of the zonal mean circulation of the middle atmosphere, Pure Appl. Geophys., 11, 284-306.

Kawahira, K., 1982: A quasi-one-dimensional model of the ozone transport by planetary waves in the winter stratosphere, J. Meteor. Soc. Japan, 60, 831-848.

Kent, G. S., 1982: SAGE Measurements of Mount St. Helens Volcanic Aerosols, in Atmospheric Effects and Potential Climatic Impact of the 1980 Eruptions of Mount St. Helens, NASA Conference Publication 2240, 109-116, A. Deepak (Ed.).

Kent, G. S., and M. P. McCormick, 1984: SAGE and SAM II measurements of global stratospheric aerosol optical depth and mass loading, J. Geophys. Res., 89, 5303-5314.

Kent, G. S., C. R. Trepte, U. O. Farrukh, and M. P. McCormick, 1985a: Variation in the stratospheric aerosol associated with the north cyclonic polar vortex as measured by the SAM II satellite sensor, J. Atmos. Sci., 42, 1536-1551.

Kent, G. S., P-H. Wang, U. O. Farrukh, A. Deepak, and E. M. Patterson, 1985b: Development of a Global Model for Atmospheric Backscatter at CO<sub>2</sub> Wavelengths, Final Report on NASA Contract NAS8-35594. (NASA Contractor Report 3959.)

Kent, G. S., and P-H. Wang, 1986: SAGE II Satellite Data Set Validation, NASA CR-178189.

Kurziga, R. J., K. V. Haggard, and W. L. Grose, 1984: Numerical experiments with a general circulation model concerning the distribution of ozone in the stratosphere, J. Atmos. Sci., 41, 2029-2051.

Labitzke, K., 1981: The amplification of height wave 1 in January 1979: A characteristic precondition for the major warming in February, Mon. Wea. Rev., 109, 985-989.

- Labitzke, K., 1982: On the interannual variability of the middle stratosphere during the northern winters, J. Met. Soc. Japan, 60, 124-139.
- Labitzke, K., and B. Goretzki, 1982: A catalogue of dynamic parameters describing the variability of the middle stratosphere during the northern winters, in Handbook for MAP., Vol. 5, Middle Atmosphere Program, SCOSTEP, University of Illinois, Urbana.
- Lazarus, A. L., R. D. Cadle, B. W. Gandrud, J. P. Greenberg, B. J. Huebert, and W. I. Rose, Jr., 1979: Sulphur and halogen chemistry of the stratosphere and of volcanic eruption plumes, J. Geophys. Res., 84, 7869-7875.
- Leovy, L., 1964: Simple models of thermally driven mesospheric circulation, J. Atmos. Sci., 21, 327-341.
- McCormick, M. P., 1985: SAGE Aerosol Measurements, Volume 1--February 21, 1979 to December 31, 1979. NASA Reference Publication 1144.
- McCormick, M. P., 1986: SAGE Aerosol Measurements, Volume 2--January 1, 1980 to December 31, 1980. NASA Ref. Publication 1149.
- McCormick, M. P., P. Hamill, T. J. Pepin, W. P. Chu, T. J. Swissler, and L. R. McMaster, 1979: Satellite studies of the stratospheric aerosol, Bull. Am. Meteor. Soc., 60, 1038-1046.
- McCormick, M. P., W. P. Chu, G. W. Grams, P. Hamill, B. M. Hennan, L. R. McMaster, T. J. Pepin, P.B. Russell, H. M. Steele, and T. J. Swissler, 1981: High-latitude stratospheric aerosols measured by the SAM II Satellite System in 1978 and 1979, Science, 214, 328-331.
- McCormick, M. P., H. M. Steele, P. Hamill, W. P. Chu and T. J. Swissler, 1982: Polar stratospheric cloud sightings by SAM II, J. Atmos. Sci., 39, 1387-1397.
- McCormick, M. P., T. J. Swissler, W. P. Chu, and W. H. Fuller, Jr., 1978: Post-volcanic stratospheric aerosol decay as measured by lidar, J. Atmos. Sci., 35, 1296-1303.
- McCormick, M. P., C. R. Trepte, and G. S. Kent, 1983: Spatial changes in the stratospheric aerosol associated with the North Pole vortex, Geophys. Res. Lett., 10, 941-944.
- McCormick, M. P., P. Hamill and U. O. Farrukh, 1985: Characteristics of polar stratospheric clouds as observed by SAM II, SAGE, and Lidar, Journal of the Meteorological Society of Japan, 63, 267-276.
- Nagatani, R. M., and A. J. Miller, 1984: Stratospheric ozone changes during the first year of SBUV observations, J. Geophys. Res., 89, 5191-5198.
- Noxon, J. F., E. Marovich, and R. B. Norton, Effect of a major warming upon stratospheric NO<sub>2</sub>, J. Geophys. Res., 84 (C12), 7884
- Oberbeck, V. R., N. H. Farlow, G. V. Ferry, H. Y. Lem, and D. M. Hayes, 1981: A study of stratospheric aerosol maturity, Geophys. Res. Lett., 8, 18-20.

- Price, J. M., 1983: Atmospheric definition for shuttle aerodynamic investigations, J. Spacecraft, 20, 133-140.
- Quiroz, R. S., Tropospheric-stratospheric interaction in the major warming event of January-February 1979, Geophys. Res. Lett., 6, 645-648, 1979.
- Rood, R. B., and M. R. Schoeberl, 1983a: A mechanistic model of Eulerian, Lagrangian-mean, and Lagrangian ozone transport by steady planetary waves, J. Geophys. Res., 88, 5208-5218.
- Rood, R. B., and M. R. Schoeberl, 1983b: Ozone transport by diabatic and planetary wave circulations on a ..plane, J. Geophys. Res., 88, C13, 8491-8504.
- Schoeberl, M. R., 1978: Stratospheric warmings: Observations and theory, Space Phys., 16, 521-538.
- Steele, H. M., P. Hamill, M. P. McCormick, and T. J. Swissler, 1983: The formation of polar stratospheric clouds, J. Atmos. Sci., 40, 2055-2067.
- Syed, M. Q., and A. W. Harrison, Behavior of stratospheric NO<sub>2</sub> during stratospheric warming of January-February 1979, Atmos. Ocean, 19, 216-235, 1981.
- Turco, R. P., P. Hamill, O. B. Toon, R. C. Whitten, and C. S. Kiang, 1979: A one-dimensional model describing aerosol formation and evolution in the stratosphere, I. Physical processes and mathematical analog, J. Atmos. Sci., 69, 699-717.
- Turco, R. P., O. B. Toon, R. G. Whitten, R. G. Keese, and P. Hamill, 1982: Simulation studies of the physical and chemical processes occurring in the stratospheric clouds of the Mount St. Helens eruptions of May and June 1980, in Atmospheric Effects and Potential Climatic Impact of the 1980 Eruptions of Mount St. Helens, NASA Conference Publication 2240, 161-190, A. Deepak (Ed.).
- Wang, P-H., and M. P. McCormick, 1985: Behavior of zonal mean aerosol extinction ratio and its relationship with zonal mean temperature during the winter 1978-1979 stratospheric warming, J. Geophys. Res., 90, 2360-2364.
- Wang, P-H., and M. P. McCormick, 1985a: Variations in stratospheric aerosol optional depth during northern warmings, J. Geophys. Res., 90, 10597-10606.
- Wang, P-H., M. P. McCormick, and W. Chu, 1983b: A study on the planetary wave transport of ozone during the late February 1979 stratospheric warming using the SAGE ozone observation and meteorological information, J. Atmos. Sci., 40, 2419-2431.
- Wu, M-F., M. A. Geller, J. G. Olson, A. J. Miller, and R. M. Nagatani, 1985: Computations of zone transport using Nimbus 7 solar backscatter ultraviolet and NOAA/National Meteorological Center data, J. Geophys. Res., 90, 5745-5755.

Yue, G. K., and A. Deepak, 1984: Latitudinal and altitudinal variation of size distribution of stratospheric aerosols inferred from SAGE aerosol extinction coefficient measurements at two wavelengths, Geophys. Res. Lett., 11, 999-1002.

Yue, G. K., M. P. McCormick, and W. P. Chu, 1984: A comparative study of aerosol extinction measurements made by the SAM II and SAGE satellite experiments, J. Geophys. Res., 89, 5321-5327.

Yue, G. K., and A. Deepak, 1983: Retrieval of stratospheric aerosol size distribution from atmospheric extinction of solar radiation at two wavelengths, Appl. Opt., 22, 1639-1645.

## APPENDIX A

### A COMPARATIVE STUDY OF AEROSOL EXTINCTION MEASUREMENTS MADE BY THE SAM II AND SAGE SATELLITE EXPERIMENTS

by

Glenn K. Yue<sup>1</sup>  
Institute for Atmospheric Optics and Remote Sensing (IAFORS)

M. P. McCormick and W. P. Chu  
NASA Langley Research Center

#### Abstract

SAM II and SAGE are two satellite experiments designed to measure stratospheric aerosol extinction using the technique of solar occultation or limb extinction. Although each sensor is mounted aboard a different satellite, there are occasions when their measurement locations are nearly coincident, thereby providing opportunities for a measurement comparison. In this paper, the aerosol extinction profiles and daily contour plots for some of these events in 1979 are reported. The comparisons shown in this paper demonstrate that SAM II and SAGE are producing similar aerosol extinction profiles within their measurement errors and that since SAM II has been previously validated, these results show the validity of the SAGE aerosol measurements.

(From J. of Geophy. Res., 89, 1984, 5321-5327.)

<sup>1</sup>Present affiliation: NASA Langley Research Center, Hampton, Virginia.

## APPENDIX B

### POLAR STRATOSPHERIC CLOUD SIGHTINGS BY SAM II: 1978-1982

by

U. O. Farrukh<sup>1</sup>

Institute for Atmospheric Optics and Remote Sensing,  
Hampton, Virginia 23666

#### Abstract

Satellite data sets, obtained by the SAM II experiment, are analyzed to study the characteristics and distribution of Polar Stratospheric Clouds (PSC). Mappings and tables were made of their distribution and probability of formation. A 50% probability of formation was found to exist around a minimum stratospheric temperature of 193°K. The highest probability of cloud formation was found to be close to 0° longitude. However, some differences in clouds altitude distribution were found to exist between the northern and southern polar regions. Satellite observations inside and outside the boundaries of the asymmetric northern polar night jet are made daily. It was possible to conclude that these clouds are formed only inside the polar jet boundaries in the northern hemisphere. In general, the number of PSC events that were observed in the southern hemisphere were three to four times the ones observed in the northern one.

(From NASA Contractor Report 177995, March 1986.)

<sup>1</sup>Present affiliation: Hampton University, Hampton, Virginia.

PREVIOUS PAGE BLANK NOT FILMED

## APPENDIX C

### CHARACTERISTICS OF POLAR STRATOSPHERIC CLOUDS

AS OBSERVED BY SAM II, SAGE, AND LIDAR

by

M. P. McCormick  
NASA Langley Research Center Hampton, Virginia

Patrick Hamill  
Systems and Applied Sciences Corporation Palo Alto, California

and

U. O. Farrukh  
Institute for Atmospheric Optics and Remote Sensing (IAFORS)  
Hampton, Virginia

#### Abstract

The discovery of polar stratospheric clouds (PSC's) in the Arctic and Antarctic stratosphere during winter is described, and the directly observed and implied properties of these clouds are discussed. It is proposed that the more familiar "mother-of-pearl" or "nacreous" clouds are a special subset of PSC's. The size, location, prevalence and temperature dependence of the clouds as measured by the SAM II and SAGE satellite systems are outlined. Airborne lidar measurements have recently demonstrated that the PSC phenomenon is most probably associated with an extended stratospheric cloud bank existing within the cold polar vortex region during the winter period with the PSC's bounded by a 188° temperature isotherm. The PSC's probably exist at a 50 percent frequency within the 193 K isotherm. Using the observed information on the cloud extinction and change in location with time we consider possible formation mechanisms, the size of the cloud particles, and show the descending motion of the cloud during wintertime.

(Reproduced from the Journal of the Meteorological Society of Japan, 1985,  
63, 267-276.)

PRECEDING PAGE BLANK NOT FILMED

APPENDIX D

SPATIAL CHANGES IN THE STRATOSPHERIC AEROSOL ASSOCIATED WITH THE  
NORTH POLAR VORTEX

by

M. P. McCormick  
NASA Langley Research Center

C. R. Trepte  
SASC Technologies, Inc.,

and

G. S. Kent  
Institute for Atmospheric Optics and Remote Sensing (IAFORS)  
Hampton, Virginia

Abstract

In late January and early February 1983, observations made by the Stratospheric Aerosol Measurement (SAM II) satellite system showed that aerosol extinction profiles measured within the northern polar vortex differed significantly above 18 km from those measured outside the vortex. Values of the calculated optical depths above 18 km for February 1, 1983, are lower by approximately one order of magnitude within the polar vortex than those outside. Similar differences were found in the aerosol back-scattering profiles obtained using an airborne lidar system when crossing the polar vortex. Since potential vorticity at a constant altitude is not conserved across the polar vortex, horizontal adiabatic transport does not occur.

(Reproduced from Geophys. Res. Lett., 1983, 941-944.)

PRECEDING PAGE BLANK NOT FILMED

APPENDIX E

VARIATION IN THE STRATOSPHERIC AEROSOL ASSOCIATED WITH  
THE NORTH CYCLONIC POLAR VORTEX AS MEASURED  
BY THE SAM II SATELLITE SENSOR

by

G. S. Kent  
Institute for Atmospheric Optics and Remote Sensing (IAFORS)  
Hampton, Virginia

C. R. Trepte  
SASC Technologies, Inc., Hampton, Virginia 23666

U. O. Farrukh  
Institute for Atmospheric Optics and Remote Sensing (IAFORS)  
Hampton, Virginia

and

M. P. McCormick  
NASA Langley Research Center, Hampton, Virginia

Abstract

Aerosol extinction data obtained by the Stratospheric Aerosol Measurement II (SAM II) satellite instrument during the 1979/1980 Northern Hemisphere winter season have been analyzed in relation to the cyclonic polar vortex. A Synoptic approach has been employed to study the behavior of aerosol extinction ratio and optical depth between altitudes of 8 and 30 km as a tracer of mean atmospheric motions in and near the polar vortex. As the polar vortex intensifies, a gradient of extinction ratio is established across the polar-night jet stream, which is associated with subsidence within the vortex. Maximum subsidence occurs at the center of the vortex. Calculated descent rates relative to isentropic surfaces are of the order of  $8 \times 10^{-4} \text{ m s}^{-1}$  near 20 km, at the center of the vortex between September and December. Below an altitude of 14 km, taken as the base of the vortex, and outside the vortex, horizontal movements occur freely, masking any systematic vertical motions. Extinction enhancements by polar stratospheric clouds and changes produced by sudden warmings in the second half of winter have prevented a similar study for this period. An estimate of the aerosol mass transferred downward through the base of the vortex for the entire season is 7000 tonnes. Comparison of the inferred stratospheric motions with earlier studies using radioactive tracers show good agreement.

(Reproduced from J. Atmos. Sci., 42, 1985, 1536-1551.)

APPENDIX F

LATITUDINAL AND ALTITUDINAL VARIATION OF SIZE DISTRIBUTION  
OF STRATOSPHERIC AEROSOLS INFERRED FROM SAGE AEROSOL  
EXTINCTION COEFFICIENT MEASUREMENTS AT TWO WAVELENGTHS

by

Glenn K. Yue<sup>1</sup> and Adarsh Deepak  
Institute for Atmospheric Optics and Remote Sensing (IAFORS)  
Hampton, Virginia

Abstract

A method of retrieving aerosol size distribution from the measured extinction of solar radiation at wavelengths 0.45  $\mu\text{m}$  and 1.0  $\mu\text{m}$  has recently been proposed. This method is utilized to obtain latitudinal and altitudinal variations of size distributions of stratospheric aerosols from the SAGE data for March 1979. Small particles are found in the lower stratosphere of the tropical region, and large particles are found at higher altitudes and latitudes in both hemispheres. Results of this study are consistent with the suggestion that the upper troposphere in tropical regions is a source of condensation nuclei in the stratosphere, and they become mature as they move to higher altitudes and latitudes.

(From Geophys. Res. Lett., 11, 1984, 999-1002.)

PRECEDING PAGE BLANK NOT FILMED

---

<sup>1</sup>Present affiliation: NASA Langley Research Center, Hampton, Virginia.

## APPENDIX G

### SAGE AND SAM II MEASUREMENTS OF GLOBAL STRATOSPHERIC AEROSOL OPTICAL DEPTH AND MASS LOADING

by

G. S. Kent  
Science and Technology Corporation  
Hampton, Virginia

and

M. P. McCormick  
NASA Langley Research Center  
Hampton, Virginia

#### Abstract

Several volcanic eruptions between November 1979 and April 1981 have injected material into the stratosphere. The SAGE and SAM II satellite systems have measured, with global coverage, the 1- $\mu\text{m}$  extinction produced by this material and examples of the data product are shown in the form of global maps of stratospheric optical depth and altitude-latitude plots of zonal mean extinction. These data, and that for the volcanically quiet period in early 1979, have been used to determine the changes in the total stratospheric mass loading. Estimates have also been made of the contribution to the total aerosol mass from each eruption. It has been found that between early 1979 and mid-1981, the total stratospheric aerosol mass increased from a background level of approximately 570,000 metric tons to a peak of approximately 1,300,000 metric tons.

(From J. Geophys. Res., 89, 1984, 5303-5314.)

PRECEDING PAGE BLANK NOT FILMED

## APPENDIX H

### BEHAVIOR OF ZONAL MEAN AEROSOL EXTINCTION RATIO AND ITS RELATIONSHIP WITH ZONAL MEAN TEMPERATURE DURING THE WINTER 1978-1979 STRATOSPHERIC WARMING

by

Pi-Huan Wang  
Institute for Atmospheric Optics and Remote Sensing (IAFORS)  
Hampton, Virginia

and

M. P. McCormick  
NASA Langley Research Center  
Hampton, Virginia

#### Abstract

The behavior of the zonal mean extinction ratio in the lower stratosphere near 75°N and its relationship with the zonal mean temperature during the January–February 1979 stratospheric sudden warming have been investigated based on the satellite sensor SAM II (Stratospheric Aerosol Measurement) and auxiliary meteorological measurements. The results indicate that distinct changes in the zonal mean aerosol extinction ratio occurred during this stratospheric sudden warming. It is also found that horizontal eddy transport due to planetary waves may have played a significant role in determining the distribution of the zonal mean aerosol extinction ratio.

(From J. of Geophys. Res., 90, 1985, 2360-2364.)

PRECEDING PAGE BLANK NOT FILMED

## APPENDIX I

### VARIATIONS IN STRATOSPHERIC AEROSOL OPTICAL DEPTH DURING NORTHERN WARMINGS

by

Pi-Huan Wang  
Institute for Atmospheric Optics and Remote Sensing (IAFORS)  
Hampton, Virginia

and

M. P. McCormick  
NASA Langley Research Center  
Hampton, Virginia

#### Abstract

In this paper the properties of the stratospheric aerosol optical depth (above 50 mbar) have been studied by using aerosol extinction profiles (at 1  $\mu\text{m}$ ) derived from the Stratospheric Aerosol Measurement (SAM II) and Stratospheric Aerosol and Gas Experiment (SAGE) during warming periods in the northern hemisphere. It is shown that, during the disturbed periods in winter, low values of aerosol optical depth ( $<0.2 \times 10^{-3}$ ) are found within the low-pressure system(s) (at the 30-mbar pressure surface), while high values are found outside. Similar characteristics are found to exist for the simultaneously observed SAGE O<sub>3</sub> and NO<sub>2</sub> columnar density distributions. Strong longitudinal gradients are shown with the low values within and wherever the vortex exists. This characteristics is maintained during and after the circumpolar vortex is disturbed, even after breakdown, indicating an isolation of the material within the vortex.

(From J. Geophys. Res., 90, 1985, 10,597-10,606.)

PRECEDING PAGE BLANK NOT FILMED

## APPENDIX J

### RETRIEVAL OF STRATOSPHERIC AEROSOL SIZE DISTRIBUTION FROM ATMOSPHERIC EXTINCTION OF SOLAR RADIATION AT TWO WAVELENGTHS

by

Glenn K. Yue and Adarsh Deepak  
Institute for Atmospheric Optics and Remote Sensing (IAFORS)

#### Abstract

The possibility of retrieving size distribution of aerosol particles in the stratosphere by measuring the extinction of solar radiation traversing the aerosol medium at two different wavelengths is explored in this work. This paper presents a parametric study of the effects of size distribution and composition of stratospheric aerosols on the value  $R$ , the ratio of extinction of solar radiation at wavelength  $0.45 \mu\text{m}$  to the extinction at wavelength  $1.0 \mu\text{m}$ . The aerosol size distributions under study are nine analytical expressions including most stratospheric aerosol models used by investigators. The aerosol compositions under study are the supercooled sulfuric-acid droplets, with different weight percentages of  $\text{H}_2\text{SO}_4$  in the aerosol. It is found that  $R$  is not very sensitive to either the composition or the radii limits of stratospheric aerosols under consideration but is quite sensitive to the value of the variable parameter governing the mode radius of the size distribution of aerosol particles. Based on the results of this parametric study, a method of retrieving the size distribution of aerosol particles in the stratosphere from the experimental results of the extinction of solar radiation at two wavelengths is proposed.

(From Appl. Opt., 22, 1983, 1639-1645.)

PRECEDING PAGE BLANK NOT FILMED

**Standard Bibliographic Page**

1. Report No. NASA CR-178256	2. Government Accession No.	3. Recipient's Catalog No.	
4. Title and Subtitle  Validation of SAM II and SAGE Satellite Data		5. Report Date April 1986	
7. Author(s) G.S. Kent, P.-H. Wang, U.O. Farrukh, and G.K. Yue		6. Performing Organization Code	
9. Performing Organization Name and Address  Institute for Atmospheric Optics and Remote Sensing 101 Research Drive Hampton, Virginia 23666		8. Performing Organization Report No. IFAORS TR 248	
12. Sponsoring Agency Name and Address  National Aeronautics and Space Administration Washington, DC 20546		10. Work Unit No.	
		11. Contract or Grant No. NAS1-17032	
		13. Type of Report and Period Covered Contractor Report	
		14. Sponsoring Agency Code 665-10-40-04	
15. Supplementary Notes  Technical Monitor: Leonard R. McMaster, Langley Research Center, Hampton, Virginia Final Report			
16. Abstract  This report presents the results of a validation study of data obtained by the Stratospheric Aerosol and Gas Experiment I (SAGE I) and Stratospheric Aerosol Measurement II (SAM II) satellite experiments. The study includes the entire SAGE I data set (February 1979 - November 1981) and the first four and one-half years of SAM II data (October 1978 - February 1983). These data sets have been validated by their use in the analysis of dynamical, physical and chemical processes in the stratosphere. They have been compared with other existing data sets and the SAGE I and SAM II data sets intercompared where possible. The study has shown the data to be of great value in the study of the climatological behavior of stratospheric aerosols and ozone. Several scientific publications and user-oriented data summaries have appeared as a result of the work carried out under this contract.			
17. Key Words (Suggested by Author(s))  SAGE I SAM II Satellite radiometry Validation Stratosphere Aerosols                      Ozone	18. Distribution Statement  Unclassified - Unlimited		
		Subject Category 46	
19. Security Classif.(of this report) Unclassified	20. Security Classif.(of this page) Unclassified	21. No. of Pages 161	22. Price A08

For sale by the National Technical Information Service, Springfield, Virginia 22161

NASA Langley Form 63 (June 1985)